UC Santa Cruz

UC Santa Cruz Electronic Theses and Dissertations

Title

Supersymmetric Electroweak Baryogenesis Beyond the MSSM in the LHC Era

Permalink

https://escholarship.org/uc/item/9356v2s4

Author

Kozaczuk, Jonathan Anthony

Publication Date

2013

Peer reviewed|Thesis/dissertation

UNIVERSITY OF CALIFORNIA

SANTA CRUZ

**SUPERSYMMETRIC ELECTROWEAK BARYOGENESIS
BEYOND THE MSSM IN THE LHC ERA**

A dissertation submitted in partial satisfaction of the
requirements for the degree of

DOCTOR OF PHILOSOPHY

in

PHYSICS

by

Jonathan A. Kozaczuk

June 2013

The Dissertation of Jonathan A. Kozaczuk
is approved:

_____

Professor Stefano Profumo, Chair

_____

Professor Anthony Aguirre

_____

Professor Michael Dine

_____

Tyrus Miller
Vice Provost and Dean of Graduate Studies

Table of Contents

Abstract

Supersymmetric Electroweak Baryogenesis

Beyond the MSSM in the LHC Era

by

Jonathan A. Kozaczuk

In this dissertation, I explore the theory and prospects for generating the baryon asymmetry of the universe at the electroweak phase transition. Models of electroweak baryogenesis stand out among the possible explanations of the baryon asymmetry in that they can be conclusively probed by current experiments, such as collider, dark matter, and electric dipole moment (EDM) searches. After reviewing the mechanism of electroweak baryogenesis in superymmetric theories, I show that EWB is tightly constrained in the minimal supersymmetric extension of the Standard Model (MSSM) due to the apparent absence of light superpartners at the Large Hadron Collider (LHC), the non-observation of electric dipole moments, dark matter search results, and the discovery of a 125 GeV Standard Model-like Higgs. This suggests that electroweak baryogenesis, if realized in our universe, may require a non-minimal incarnation of supersymmetry. With this in mind, I then present a scenario for electroweak baryogenesis with an MSSM-like spectrum embedded in a Randall-Sundrum space-time. This model can accommodate a strongly first-order electroweak phase transition provided by the dynamics of the radion without light stops. In this case, CP-violating sources in the higgsino-gaugino sector can give rise to the observed baryon asymmetry and still be in agreement with

constraints from dark matter and electric dipole moment searches. Finally, in the next-to-MSSM (NMSSM), I show that one can obtain a 125 GeV Higgs, a viable dark matter candidate with a 130 GeV gamma-ray line from the galactic center (as observed by the Fermi space telescope), and successful electroweak baryogenesis while satisfying all other relevant phenomenological constraints. A strongly first order electroweak phase transition can be realized in this case without a light stop. These novel possibilities are well-motivated and will be effectively probed by increased sensitivity in current experiments.

To my soon-to-be wife, Cynthia, and my parents, Tony and Ester:

I owe it all to you guys.

Acknowledgments

I would like to thank Stefano Profumo for being an excellent mentor and providing constant support throughout the course of this work. His guidance has been invaluable in shaping my intuition and skills as a researcher. I am also very grateful to my advisor, Anthony Aguirre, for getting me on my feet as a grad student and teaching me how to approach difficult questions with a fresh perspective and patience. Both have served as an inspiration and I look forward to many more projects together. I am also thankful to my collaborators, Max Wainwright and Michael Ramsey-Musolf, both of whom are very deep thinkers and excellent physicists. They have provided valuable insight on many occasions and have raised the bar for me in my work. Their contributions to the projects that comprise this dissertation are detailed below. I am grateful to all my classmates and the faculty at UCSC, who have taught me a great deal and provided much support (and good times) over the years. I also owe many thanks to my parents, Tony and Ester, who have been behind me from elementary school until now, as well as my fiancée Cynthia, who has stood by my side and been my best friend through it all. Without their love and support this work would not have been possible.

Summary of Graduate Work

The text of this dissertation contains reprints from the following previously published material:

1. J. Kozaczuk and S. Profumo, JCAP **1111**, 031 (2011) [arXiv:1108.0393 [hep-ph]].

2. J. Kozaczuk, S. Profumo, M. J. Ramsey-Musolf and C. L. Wainwright, Phys. Rev. D **86**, 096001 (2012) [arXiv:1206.4100 [hep-ph]].

3. J. Kozaczuk, S. Profumo and C. L. Wainwright, JCAP **1301**, 027 (2013) [arXiv:1208.5166 [hep-ph]].

4. J. Kozaczuk, S. Profumo and C. L. Wainwright, Phys. Rev. D **87**,075011 (2013) [arXiv:1302.4781 [hep-ph]].

Stefano Profumo supervised and directed the research which comprises this dissertation. On the second paper listed, Michael Ramsey-Musolf also supervised both Carroll (a.k.a. Max) Wainwright and myself as we were visiting the University of Wisconsin, Madison. Max Wainwright contributed a significant amount of original research to papers 2–4. In these projects, Max was responsible for computing the bounds from electric dipole moment searches, as well as producing the plots in paper 3 and calculating the electroweak phase transition properties in paper 4. I was responsible for the rest of the work.

There are several past and ongoing projects I have worked on as a graduate student that do not appear in this dissertation. Under the direction and supervision of Anthony Aguirre, I explored cosmic bubble collisions in the early universe and their observational impact on the microwave background. In particular, we considered observers whose past light cones contain many bubble collisions. We were able to analytically calculate the expected signal using cosmological perturbation theory and found that multiple collisions generally produce a dramatic increase in low-multipole power in the

CMB temperature power spectrum. We were able to place bounds on the multi-bubble model parameters in our universe using WMAP observations of the CMB sky. These results have been published in Ref. [1]. Also, my work as an undergraduate on the Gravity Probe B collaboration at Stanford University resulted in two other publications as a graduate student [2, 3], related to the mapping of trapped flux on the surface of the gyroscope rotors. I developed a non-linear minimization routine, based on a Nelder-Mead simplex algorithm, to accurately determine the time evolution of the gyroscope spin phases.

Currently, I am working with Anthony Aguirre on a project related to closed systems and horizons in cosmology. I am also working with Stefano Profumo, Max Wainwright, and Laurel Stephenson-Haskins on a more systematic study of phase transitions in the NMSSM, as well as the time-evolution of electroweak bubble walls after nucleating in the plasma. I am also working with Stefano on a project related to light supersymmetric dark matter in view of the recent Higgs discovery.

1

Introduction: Where did it all come from?

> "*Principium cuius hinc nobis exordia sumet, nullam rem e nihilo gigni divinitus umquam.*"
>
> – Lucretius, *De Rerum Natura, Book 1*

The Universe is a very big place and, for the most part, quite empty. Measurements of the Cosmic Microwave Background (CMB), relic photons left over from the early universe, tell us that the density of atoms is roughly equivalent to 1 proton per 4 cubic meters [4]. Although this number is staggeringly small relative to the scales we encounter every day, it is surprisingly *large* from the standpoint of particle physics.

The mid- to late-20th century saw the development of the Standard Model (SM) of particle physics, an enormously successful paradigm explaining nearly all interactions known to us. It is based on *symmetry principles*: specifying the symmetries

obeyed by the different particles (for example, requiring the outcome of any experiment to be the same in all inertial reference frames) determines the possible interactions that can exist in the world we observe. In fact, as you go back further in time, the Standard Model suggests that the laws of physics begin to look even more symmetric - interactions that appear different to us now may in fact have been one and the same in the early universe. This high level of symmetry is the theoretical underpinning of he Standard Model, and the cornerstone of modern particle physics.

Although a tiny number, the symmetries of the Standard Model make it difficult to explain the observed density of matter in the universe. The SM is formulated as a *quantum field theory*, whereby each particle is described as a *field*, an object with an infinite number of degrees of freedom corresponding to the different allowed states of the particle. For every particle, the symmetries of the SM dictate that there must exist an *antiparticle*, a field with the same mass but opposite charge. Symmetries also dictate that the laws governing these antimatter particles are very nearly the same as those for ordinary matter. For example, the Standard Model allows an anti-proton and a positron (the antiparticle of the electron) to form anti-Hydrogen atoms, which would have properties almost identical to those of ordinary Hydrogen. This suggests that whatever matter was produced in the Big Bang should have been accompanied by an equal amount of antimatter. However, matter and antimatter tend to *annihilate* each other. If there was no matter–antimatter asymmetry, the quarks, electrons, and other particles produced in the early universe should have been met and destroyed by

2

anti-quarks, anti-electrons, and other antiparticles shortly thereafter[1]. The annihilation of matter and antimatter would have left behind a universe filled mostly with relic radiation and neutrinos, but not much else - no galaxies, solar systems, stars, planets, and no life. Since this is not the case, we know that there must be an asymmetry between matter and antimatter. Just how might this asymmetry come about? This dissertation is aimed at providing insight into this very question.

Let us be a bit more rigorous about our definitions. Nearly all visible matter in the universe is made up of *baryons*, particles consisting of three quarks each. Protons and neutrons are examples of baryons. Thus, when we speak of the "matter–antimatter asymmetry", we are primarily referring to a *baryon asymmetry* [2]. We can quantify this asymmetry by introducing *baryon number*, B, which is equal to $1/3$ for quarks, $-1/3$ for anti-quarks, and 0 for all other fundamental particles. Then the net baryon number density n_B, can be defined as

$$n_B \equiv \frac{n_{\text{quarks}} - n_{\text{antiquarks}}}{3} \qquad (1.1)$$

We can do better than this. n_B tells us the number of baryons per unit volume; however, the universe is expanding (and has been since the Big Bang) and so the number density of baryons is not a constant. We can instead consider the ratio of baryon number density

---

[1]There are would-be caveats to this story. For example, there could have been regions of matter and antimatter produced in the early universe but separated by large distances. However, this possibility is ruled out because it would have resulted in radiation originating from the boundaries of these regions from annihilations, which is not seen [5].

[2]There is also a *lepton asymmetry*, which is often to be assumed to be related to the baryon asymmetry. The process of generating an excess of leptons over anti-leptons is known as *leptogenesis*; see e.g. Ref. [6] for a review.

to entropy, s, which remains constant with the expansion of the universe:

$$Y_B \equiv \frac{n_B}{s} \tag{1.2}$$

Observations of the CMB dictate $Y_B \sim 10^{-10}$ so this will be the number we try to account for throughout this dissertation.

To explain why Y_B is not zero requires some particle physics mechanism. Even if we tried to explain Y_B as an initial condition of the universe, we would run into trouble because of *inflation*, a period right after the Big Bang during which the universe expanded faster than light. Inflation is a cornerstone of modern cosmology, providing answers to several difficult questions that had puzzled many brilliant people for decades. One of inflation's key successes is being able to explain why why we don't observe relics like magnetic monopoles that are often predicted by theories beyond the Standard Model. However, the success in diluting away monopoles and relics means that any existing baryon asymmetry will also have been diluted away by inflation. Thus, we need some microphysical mechanism for generating the baryon asymmetry, a process known as *baryogenesis*.

One can write down the general criteria that need to be met in order for a model to accommodate successful baryogenesis. This was first realized by Russian physicist (and Nobel Peace Prize winner) Andrei Sakharov in 1967, and so these reuqirements are known collectively as the "Sakharov Conditions"[7]. They can be formulated as follows:

1. To generate a baryon asymmetry requires **baryon number violation**. This is obvious: if all processes conserve B then Y_B cannot change.

4

2. Both **charge (C) and charge-parity (CP) symmetry must be violated**. Charge conjugation acts on a particle by transforming it to its antiparticle. If all processes respect a charge symmetry, then particles and their antiparticles will be produced at the same rate, resulting in no net baryon asymmetry. Parity, P, can be thought of as transforming a particle to its mirror image. In the Standard Model, fermions and anti-fermions come in two varieties, categorized as being either *left-* or *right-handed* depending on the direction of the quantum mechanical spin angular momentum. P then transforms between left- and right-handed particles, just as looking in a mirror causes your right hand to appear on your left hand side in the image and the left to appear on your right. Consequently, CP transforms a left-handed (right-handed) particle to a right-handed (left-handed) antiparticle, and vice versa. The baryon density can be split up into a contribution from left-handed (right-handed) fermions and right-handed (left-handed) anti-fermions, which subtract against each other. If CP is conserved, then any process generating a net density of e.g. left-handed baryons will be accompanied by a process generating the same number of right-handed anti-baryons. Since these number densities enter with opposite signs in n_B, they will cancel each other, and so to get a non-zero n_B requires CP-violation.

3. Baryogenesis requires a **departure from equilibrium**, or, more generally, some macroscopic time reversal violation. In a state of equilibrium, the rate for any process (like one producing baryon number) will be the same as the rate of the

inverse process (like one reducing baryon number). Thus, in order to produce a net baryon density, the universe had to have gone through a period during which such processes did not proceed at the same rate and wash each other out. In other words, the flow forward in time (processes producing more baryons) must be favored over the flow backwards in time (processes destroying those baryons).

If a model satisfies all three of the conditions listed above, it has a chance to achieve successful baryogenesis, although it is not guaranteed. As we will see, the Standard Model contains the necessary ingredients to satisfy all three of Sakharov's conditions, however it falls well short of explaining $Y_B \sim 10^{-10}$. Thus, to have any hope of generating the observed baryon asymmetry, we must go beyond the Standard Model.

Throughout this dissertation, my aim will be to explain the baryon asymmetry through processes at the *electroweak scale*, which can be thought of as the temperature in the early universe at which the Standard Model particles acquired mass through the Higgs mechanism. This process is detailed in Chapter 2 and is known as *electroweak baryogenesis*. I will investigate this mechanism in the context of *supersymmetry*, which provides a theoretically well-motivated and phenomenologically rich extension beyond the Standard Model, also discussed in the following Chapter.

It is also worth mentioning that there is another, more mysterious, component of the universe, *dark matter* (DM), which will enter frequently into the investigation of baryogenesis. Dark matter is so called precisely because it is dark: it does not carry charge, and so does not interact with photons. Its density is roughly five times that of

baryonic matter. Its existence is inferred from its gravitational effects. Additionally, DM might interact with the SM through weak interactions. Unlike baryonic matter, dark matter may have been generated thermally, since its abundance does not have to be an asymmetry. Explaining the abundance of dark matter still requires a departure from thermal equilibrium, but this can simply be supplied by the expansion of the universe: once dark matter particles cannot efficiently find each other to annihilate, the relic density is frozen in. Most of the efforts to explain the observed value of Y_B explored in the subsequent Chapters will also come with an explanation of the observed relic abundance of dark matter. This connection is detailed further in Chapter 2. Thus, if any of the ideas presented here turn out to be realized in nature, we will have made an enormous and crucial step forward in understanding our world.

The remainder of this dissertation is structured as follows: Chapter 2 provides a brief introduction to electroweak baryogenesis and supersymmetry. In Chapter 3, I show how recent experimental progress has tightly constrained the parameter space of the minimal supersymmetric extension of the Standard Model (MSSM) suitable for electroweak baryogenesis. As a result, in the next two Chapters I put forward two novel scenarios for electroweak baryogenesis beyond the MSSM and satisfying all relevant phenomenological constraints: Chapter 4 considers dark matter and baryogenesis in the case of the MSSM embedded in a Randall-Sundrum model of warped extra dimensions, while Chapter 5 details the possibility of achieving successful electroweak baryogenesis along with a dark matter candidate consistent with the 130 GeV gamma-ray line as observed by the Fermi space telescope. Finally, Chapter 6 provides a brief summary

7

and conclusion to this work.

2

Electroweak Baryogenesis and

Supersymmetry

Over the past several decades, many different mechanisms have been put forward to satisfy the Sakharov conditions outlined in Chapter 1, each associated with different mass scales. One intriguing possibility, and the most conclusively testable, is the mechanism of "electroweak baryogenesis" (EWB). In EWB, all processes relevant for generating Y_B occur around the electroweak scale, $m_{\mathrm{EW}} \sim 100$ GeV. As I will discuss in more depth in Chapter 3, this implies that the degrees of freedom responsible for EWB should be accessible to present-day experiments. In this Chapter I briefly recount how electroweak processes can be responsible for baryogenesis, particularly within the context of supersymmetry. Parts of this Chapter draw on arguments from the reviews of EWB found in Refs. [5, 8, 9, 10], to which I refer the Reader for a more in-depth account of electroweak baryogenesis.

2.1 Satisfying the Sakharov Conditions at the Electroweak Scale

As mentioned in Chapter 1, all of the ingredients necessary for baryogenesis can be found within the Standard Model. B-violation can arise in anomalous transitions between vacua of the SM $SU(2)$ gauge sector, C and CP-violation are known to arise in the fermionic sector of the SM Lagrangian, and the breaking of electroweak symmetry at the electroweak phase transition may provide a departure from equilibrium. We describe each of these ingredients below.

2.1.1 $SU(2)$ Sphalerons

Baryon number (B) and lepton number (L) are not conserved in the SM, but suffer from an axial anomaly. The continuity equation for the $B + L$ current can be written as [9]

$$\partial_\mu j^\mu_{B+L} = \frac{N_f}{16\pi^2} \left[-g_1^2 B_{\mu\nu} \widetilde{B}^{\mu\nu} + g_2^2 \, \mathrm{Tr} \left(F_{\mu\nu} \widetilde{F}^{\mu\nu} \right) \right] \tag{2.1}$$

while the *difference* $B - L$ has no anomaly. In the above expression, N_f is the number of generations, $g_{1,2}$ are the $U(1)_Y$ and $SU(2)$ gauge couplings, respectively, $F_{\mu\nu}$ and $B_{\mu\nu}$ are the field strength tensors corresponding to the $SU(2)$ and $U(1)_Y$ gauge fields A_μ, B_μ, respectively and where the trace is over the $SU(2)$ indices. Integrating the continuity equation from time t_i to t_f yields a change in baryon number ΔB proportional to Chern-Simons number N_{CS}

$$\Delta B = N_f \left[N_{CS}(t_f) - N_{CS}(t_i) \right] \tag{2.2}$$

where

$$N_{CS}(t) \equiv \frac{1}{32\pi^2} \int d^3 s \epsilon_{ijk} \left[g_2^2 \operatorname{Tr}\left(F_{ij} A_k - \frac{2}{3} g_2 A_i A_j A_k \right) - g_1^2 B_{ij} B_k \right]_t . \qquad (2.3)$$

For a pure-gauge configuration $F_{ij} = B_{ij} = 0$, N_{CS} is an integer[1], and the vacua of the $SU(2)$ gauge sector each correspond to a different value of N_{CS}. Thus, transitions between vacua of different Chern-Simons number correspond to changes in baryon number and could potentially satisfy the first of Sakharov's conditions.

At zero temperature, the amplitude for these vacuum-to-vacuum transitions which change N_{CS} by one unit (in some gauge) are dominated by *instantons*, field configurations which are solutions to the classical Euclidean equations of motion with finite Euclidean action. The instanton transition probability is suppressed by the factor $e^{-S_{inst}}$, which is vanishingly small in the SM. Therefore, at low energies there is no possibility for these vacuum transitions to provide the necessary B-violation. However, finite temperature effects can allow for a large transition amplitude, through the existence of the *sphaleron*, a saddle-point configuration corresponding to the top of the barrier separating vacua differing in N_{CS} by one unit. The sphaleron is a static (but unstable) solution to the classical equations of motion with finite energy E_{sph} at zero temperature. At finite temperature (but below the electroweak phase transition where the Higgs fields acquire a vacuum expectation value, or VEV), the sphaleron energy (corresponding to the barrier height) scales approximately as [9]

$$E_{sph}(T) \simeq \frac{v(T)}{v(0)} E_{sph} \qquad (2.4)$$

---

[1]Note that N_{CS} is gauge-dependent, but the difference in Eq. 2.2 is independent of the choice of gauge.

where v is the VEV of the $SU(2)$ Higgs.

At high temperatures, transitions between vacua can occur through thermal fluctuations (rather than tunneling, which is highly suppressed). The amplitude for such transitions will be dominated by configurations passing close to the sphaleron, since it corresponds to the lowest possible energy configuration not falling beneath the barrier. These sphaleron solutions carry a Boltzmann suppression factor $\sim e^{-E_{sph}(T)/T}$ and so the transition rate between vacua is still suppressed. However, around the EW phase transition temperature T_c, the barrier height vanishes, and so the transition amplitude can be of order unity. For $T > T_c$ this means that there is in fact no sphaleron solution, and thermal fluctuations can efficiently transition between vacuum configurations in a random-walk fashion, hence changing N_{CS} and violating baryon number, as required for baryogenesis by the Sakharov conditions. These transitions with $|\Delta N_{CS}| = 1$ are still dubbed "sphaleron transitions", despite the vanishing of E_{sph} at $T \gtrsim T_c$; they proceed with rate Γ_{sph}.

2.1.2 CP-Violation

Since they correspond to transitions between $SU(2)$ configurations, the sphaleron-dominated solutions are sensitive to the left-handed (LH) fermion chiral density n_L, as the right-handed (RH) degrees of freedom transform as singlets under $SU(2)$. Thus for sphaleron transitions to effectively source the baryon asymmetry, there must be a net left-handed charge density to bias the sphalerons towards producing a net baryon number; otherwise, if both the $\Delta B > 0$ and $\Delta B < 0$ processes were in equilibrium, no

net baryon number would arise. A net left-handed charge density n_L will result in a non-zero chemical potential for LH baryon number μ_B, which will bias the sphalerons towards $|\Delta B| > 0$. This can be seen by considering the relationship between the rates of a process that changes B by ± 1 unit:

$$\frac{\Gamma_{B \to B+1}}{\Gamma_{B \to B-1}} \simeq e^{-\frac{\mu_B}{T}}. \tag{2.5}$$

Applied to sphaleron transitions, this results in the following expression for the evolution of the baryon density in the symmetric phase [9]:

$$\dot{n}_B \simeq -\frac{\Gamma_{sph}}{T} \mu_B. \tag{2.6}$$

The chemical potential μ_B provides a departure from chemical equilibrium, ensuring that the baryon production by sphalerons is not washed out by the inverse process. A LH chiral current in the symmetric phase will thus be converted efficiently to a baryon density, provided Γ_{sph} is faster than the expansion rate of the universe.

Generating a net n_L requires both C and CP violation. This can be seen simply as follows: both the LH fermion, f_L and the antifermion counterpart[2] to f_R, denoted as $\bar{f}_R$, transform in doublets under $SU(2)$, while a RH fermion f_R and the antifermion $\bar{f}_L$ transform as singlets. These operators transform under C- and CP-conjugation as follows:

$$\begin{aligned} C &: f_L \to \bar{f}_L, & CP &: f_L \to \bar{f}_R \\ C &: f_R \to \bar{f}_R, & CP &: f_R \to \bar{f}_L \end{aligned} \tag{2.7}$$

---

[2]Note that in this notation, the Weyl spinor $\bar{f}_R$ is a left-handed object.

The relevant charge density for sphaleron transitions is that of the $SU(2)$ doublet fermions,

$$n_L \equiv \sum \left(n_{f_{iL}} - n_{\bar{f}_{iR}} \right) \tag{2.8}$$

which will vanish if C and CP are conserved, as discussed in Chapter 1.

Once again, the Standard Model contains the necessary ingredients, coming equipped with C-violation and a source of CP-violation: the complex phases in the Cabbibo-Kobayashi-Maskawa (CKM) matrix which determines the quark mixing in the broken electroweak phase. This mixing originates in the Yukawa sector of the SM once the Higgs field acquires a vacuum expectation value. In principle, then, the SM can also satisfy the second Sakharov condition with physics associated with the electroweak symmetry breaking.

2.1.3 The Electroweak Phase Transition

Finally, in the Standard Model, the electroweak phase transition might provide the out-of-equilibrium scenario required for successful baryogenesis. At the EWPT, the universe transitions between a symmetric phase, with $v(T) = 0$, to a broken phase, with $v(T) \neq 0$. This transition is governed by the Higgs effective potential and can proceed in two qualitatively different ways. In the first, the Higgs VEV at high temperatures starts off at the origin in field space, which is metastable, and transitions to $v \neq 0$ by tunneling to a nearby lower vacuum, separated from the origin by a finite barrier at non-zero temperature. This process is known as a *first-order* transition, and proceeds via bubble nucleation: inside the bubble, electroweak symmetry is broken, while outside

$SU(2) \times U(1)_Y$ is unbroken. Because the interiors of the bubbles correspond to higher pressure regions, the bubbles of broken phase expand through the plasma and collide with each other, after which the universe is found everywhere to be in the broken electroweak phase. A second possibility for the transition is that no barrier forms between the two phases and the transition occurs without tunneling: this is known as a *second-order* phase transition. In this case, no bubbles are formed and the Higgs VEV varies continuously.

As mentioned previously, after electroweak symmetry breaking the $SU(2)$ sphaleron transition rate will be suppressed. Therefore, the EWPT might be able to freeze in whatever baryon asymmetry was produced by these anomalous processes around the phase transition. However, if the transition is second-order, this freeze-out process proceeds too slowly and whatever excess baryons might have been produced around the transition will be efficiently washed out by the reverse processes, since right after the transition the sphalerons will still be active and tend to restore chemical equilibrium between baryons and anti-baryons. Additionally, since the Higgs VEVs vary continuously in this case, it is difficult to generate a large enough deviation from equilibrium to bias the sphalerons towards $|\Delta N_{CS} > 0|$ in the first place. Thus, in general, a first-order transition is needed to realize baryogenesis via $SU(2)$ sphalerons.

Provided a first-order electroweak phase transition, the sphalerons sourcing the baryon asymmetry can be biased toward $|\Delta N_{CS}| > 0$ by the injection of (LH) baryon number into the symmetric phase from CP-violating interactions of the various

particle species with the bubble wall[3] For example, in the SM case of CP-violation in the quark sector, the phase in the Yukawa couplings and the spacetime variation of the Higgs VEV in the bubble wall will lead to different rates for the reflection of LH quarks and RH anti-quarks off of the wall and into the symmetric phase. Thus, CP-violating interactions with the bubble wall (possible because of the first-order nature of the transition) can generate a net n_L and bias the sphalerons to produce a net baryon number. Furthermore, if the Higgs vev after the transition $v(T_c)$, is large, then the sphaleron energy will jump very quickly to large values inside the bubble by Eq. 2.4, de-activating the sphalerons very soon after the transition. In practice, this condition is realized for

$$\frac{v(T_n)}{T_n} \gtrsim 1, \tag{2.9}$$

where T_n is the bubble nucleation temperature which is at or below T_c. A phase transition satisfying $v(T_n)/T_n \gtrsim 1$ is usually referred to as a *strongly first order* transition. Thus, provided that Eq. 2.9 is satisfied, the anomalous B-violating transitions will be quenched inside the bubble before inverse processes can wash out the asymmetry; the baryon asymmetry will then be frozen in in the broken phase and baryogenesis will be complete.

2.1.4   Elctroweak Baryogenesis

The above process, involving the generation of a CP-asymmetry at the electroweak phase transition with sphalerons sourcing B-violation in the symmetric phase

---

[3]This is known as the "charge transport" scenario [11] and will be the primary n_L-generating mechanism throughout this work.

and quenched in the broken phase, is known as *electroweak baryogenesis*. It is the only known model of baryogenesis which can in principle satisfy all the Sakharov conditions without going beyond the Standard Model [4]. However, as we will see in the following section, the SM falls short of realizing successful electroweak baryogenesis in practice.

2.2 The Standard Model Is Not Enough

Despite having the necessary ingredients for electroweak baryogenesis, the Standard Model alone falls short of producing $Y_B \sim 10^{-10}$. First of all, there is not enough CP-violation in the Standard Model to account for the baryon asymmetry. This can be appreciated by considering the so-called "Jarlskog invariant" [12], which provides a parametrization of the physical CP-violating phase in the CKM matrix invariant under field rotations:

$$J \equiv \det \left[m_u^2, m_d^2 \right] \tag{2.10}$$

where $m_{u,d}$ are the mass-matrices for the up- and down-type quarks respectively. A dimensionless measure of the strength of the CP-violation around the temperature of the electroweak phase transition (when sphalerons are active) would then be

$$\frac{J}{(T_c)^{12}} \sim 10^{-20} \tag{2.11}$$

for $T_c \sim 100$ GeV, which is much too small to explain $Y_B \sim 10^{-10}$. There has been some debate on whether J/T^{12} is a sufficiently robust measure of CP-violation in the

---

[4]Models of leptogenesis come close, relying only on the addition of a heavy right-handed neutrino sector. See e.g. Ref. [6] for a review.

SM (see e.g.Ref. [5] and references therein), but in any case it seems very difficult to accommodate a sufficient amount of CP-violation in the Standard Model alone.

Perhaps more concerning is that the effective potential of the Standard Model does not give rise to a first order phase transition. This is a consequence of the recently measured value of the Higgs mass, $m_H \simeq 126$ GeV, which can be explained by the following argument. At finite temperature, the one-loop effective potential receives contributions from all degrees of freedom coupled to the Higgs sector, given by [10]

$$\Delta V_1(T > 0) = \frac{T^4}{2\pi^2} \sum_i n_i J_\pm \left(\frac{m_i(\phi)^2}{T^2} \right) \tag{2.12}$$

where the upper (lower) sign corresponds to bosons (fermions), $\langle H^0 \rangle \equiv \phi/\sqrt{2}$, $m_i(\phi)$ are the field-dependent masses of all the relevant degrees of freedom, and the loop functions $J_\pm(x^2)$ can be expanded for small x as [13]

$$
\begin{aligned}
J_+(x^2) &= -\frac{\pi^4}{45} + \frac{\pi^2}{12}x^2 - \frac{\pi}{6}x^3 - \frac{1}{32}x^4 \log\left(x^2/\alpha_+\right) + \mathcal{O}(x^3) \\
J_-(x^2) &= -\frac{7\pi^4}{360} - \frac{\pi^2}{24}x^2 - \frac{1}{32}x^4 \log\left(x^2/\alpha_-\right) + \mathcal{O}(x^3)
\end{aligned}
\tag{2.13}
$$

where $\log(\alpha_+) \simeq 5.4$ and $\log(\alpha_-) \simeq 2.6$. From these expansions, we see that bosons can contribute a cubic term to the 1-loop finite temperature effective potential, corresponding to a barrier between the symmetric and broken phases, and can thus result in a first-order transition. This can be seen more clearly by rewriting the effective potential in the high-temperature approximation, which yields[13]

$$V(\phi, T) \simeq D\left(T^2 - T_0^2\right)\phi^2 - ET\phi^3 + \frac{\bar{\lambda}}{4}\phi^4 \tag{2.14}$$

where D, $\bar{\lambda}$ are slowly varying T-dependent functions independent of ϕ and T_0 is a constant that would correspond to the transition temperature in the limit that the

cubic term $E \to 0$. The effective potential in Eq. 2.14 will support a first-order EWPT for $E > 0$, with critical temperature T_c (defined as the temperature for which the minima are degenerate) given by the solution to

$$T_c = \frac{T_0}{\sqrt{1 - E^2/(\bar{\lambda}(T_c)D(T_c))}}. \tag{2.15}$$

At $T = T_c$, the minimum corresponding to the broken EW phase is located at

$$\phi_c = \frac{2ET_c}{\bar{\lambda}(T_c)} \tag{2.16}$$

and so given $D(T_c)$, $\bar{\lambda}(T_c)$, and E, one can evaluate the order parameter $\phi(T_c)/T_c$. Plugging in the SM values, it turns out that the requirement $\phi(T_c)/T_c \gtrsim 1$ can only be realized for a SM Higgs mass $m_H \lesssim 45$ GeV, which is clearly not possible in light of the 125 GeV Higgs discovery [14, 15] (in fact, this mass range has been ruled out for quite some time). As the Higgs mass is increased, the quartic coupling λ increases, which in turn increases $\bar{\lambda}$ in this approximation, thereby lowering the order parameter. Thus, the observed value of the Higgs mass rules out a strongly first-order electroweak phase transition in the Standard Model.

The fact that the Standard Model falls short of the level of CP-violation required for electroweak baryogenesis and does not possess a strongly first-order EWPT may be somewhat disappointing, but it is not very surprising. It has been known for some time that the Standard Model in very likely not the end of the story for various other reasons. Thus, one might hope that physics beyond the Standard Model (BSM) might shore up the SM where it is lacking from the standpoint of electroweak baryogenesis. This is the avenue pursued in the remainder of this work.

19

2.3 Supersymmetry

A major theoretical shortfall of the Standard Model is the inability to explain the large hierarchy between the electroweak scale ($m_{EW} \sim 100$ GeV) and the Planck scale ($M_{Pl} \sim 10^{19}$ GeV). All particles receive quantum corrections to their masses, which can be computed by looking at the poles of the relevant self-energies. For example, the Higgs mass at one loop receives a correction from top quarks, which is quadratically divergent:

$$\left(\delta m_H^2\right)_{top} = -\frac{y_t^2}{8\pi^2}\Lambda^2 \tag{2.17}$$

where y_t is the top Yukawa coupling and Λ is the UV-cutoff of the theory. If the SM were the whole story, there is no reason why Λ should not be of order M_{Pl}, thereby driving m_H^2 to the Planck scale. Since $m_H \simeq 126$ GeV, this would require finely-tuning a counterterm to very nearly cancel the divergence. This is known as the *hierarchy problem*. If, on the other hand, there is new physics that enters above the electroweak scale, then m_H^2 will generally receive contributions from the new particles running in the loop as well. However, in this case, there must again be a dramatic cancellation of the contributions to m_H^2 from the various loop diagrams, which again would correspond to an enormous amount of fine-tuning, unless the cancellation was ensured by a new symmetry. *Supersymmetry* (SUSY) is one such possibility.

Clearly, a comprehensive review (or even introduction) to supersymmetry is beyond the scope of the present work. For a good introduction, see e.g. Refs. [16, 17]. Let us briefly recall the essentials. Supersymmetry, in its minimal incarnation, postu-

lates the existence of a new boson corresponding to each SM fermion (and new fermion corresponding to each SM boson), with the same masses, couplings, and quantum numbers (besides spin) as their SM counterparts. The generator[5] Q_α of such a symmetry must carry spin-1/2 to transform between bosons and fermions, and be in the doublet representation of the Lorentz group, i.e. a two-component spinor. The supersymmetry algebra is then specified by the relations [16, 17]

$$\left\{Q_\alpha, Q_{\dot\alpha}^\dagger\right\} = -2\sigma_{\alpha\dot\alpha}^\mu P_\mu, \quad \{Q_\alpha, Q_\beta\} = \left\{Q_{\dot\alpha}^\dagger, Q_{\dot\beta}^\dagger\right\} = 0 \qquad (2.18)$$

where P_μ is the spacetime momentum operator. The simplest irreducible representations of the $N = 1$ supersymmetry algebra are [17]:

1. Chiral superfields, (ϕ, ψ_α), where ϕ is a scalar and ψ a chiral fermion (a "sfermion")

2. Vector superfields, (λ, A_μ), where λ is a chiral fermion and A_μ a vector boson, both in the adjoint representation of the gauge group. If A_μ is a gauge boson, λ is known as a "gaugino". After EW symmetry breaking, the gauginos and the superpartners of the Higgs doublets, the *Higgsinos*, mix to form neutral and charged mass eigenstates, known as "neutralinos" and "charginos", respectively.

3. Gravity multiplet, $(\psi_{\mu,\alpha}, g_{\mu,\nu})$, where $\psi_{\mu,\alpha}$ is a spin-3/2 gravitino and $g_{\mu,\nu}$ the spin-2 graviton.

From these representations, one can construct supersymmetry-invariant Lagrangians

---

[5]A SUSY algebra with one central charge is known as $N = 1$ supersymmetry. In four dimensions, one can also consider SUSY with $N = 2$, 4, or 8, however we will consider only the minimal $N = 1$ case, of which the MSSM and NMSSM are examples.

and work out the features of the spectrum allowed by the algebra in Eq. 2.18; see e.g. Section 3 of Ref. [16] and Chapter 9 of Ref. [17].

As promised, the contributions of superpartners to the SM particle masses cancel the quadratic divergences of the Standard Model. For example, SUSY postulates a scalar partner of the top quark, the *stop squark*, with the same couplings to the Higgs as the top quark. In the limit that supersymmetry is unbroken, the stops provide a contribution to m_H^2 with *opposite sign* with respect to the top loop given by

$$\left(\delta m_H^2\right)_{stop} = 2\frac{y_t^2}{16\pi^2}\Lambda^2 \tag{2.19}$$

where the factor of two comes from the fact that there are two diagrams contributed by the stops. The extra bosonic degree of freedom exactly cancels the divergent contributions from the top order-by-order in perturbation theory. The same holds true for the contributions from the other Standard Model fields. In this way, SUSY provides an elegant solution to the hierarchy problem without a large amount of fine-tuning.

Supersymmetry has many other virtues. Two of the most important are gauge coupling unification, made possible by the contributions of the superpartners to the various β-functions, and the possibility of a viable dark matter candidate. The latter is achieved by imposing a discrete symmetry, known as R-parity, defined by the quantum number

$$P_R \equiv (-1)^{3(B-L)+2s} \tag{2.20}$$

where s is the particle's spin. Requiring that the Lagrangian be invariant under P_R prohibits dangerous B and L-violating operators which would lead to unacceptable

phenomenological consequences, such as proton decay, but also results in the lightest supersymmetric particle (LSP) being *absolutely stable*. If the LSP is electrically neutral, it will interact only weakly with the SM fields, and hence can be a viable weakly interacting massive particle (WIMP) dark matter candidate. In fact, the dominant sources of CP-violation in supersymmetric EWB are often associated with the gaugino sector, in which the LSP often resides (as an admixture) after EW symmetry breaking. Thus, electroweak baryogenesis and dark matter in SUSY are often closely related, as we will see in the subsequent Chapters. This is a major theme throughout this work.

Finally, note that the non-observation of the superpartners of the SM particles means that SUSY must actually be *broken*, so that the masses of the superpartners are not degenerate with those of their SM counterparts. There are several different mechanisms for breaking supersymmetry, but it is often most useful to parametrize the effects of the SUSY breaking mechanism by including mass terms in the Lagrangian that explicitly break supersymmetry softly (i.e. by introducing terms with positive mass dimension in the Lagrangian). Then a renormalizable[6] supersymmetric field theory is fully determined by specifying a *superpotential*, W, which is an analytic function of the chiral superfields treated as complex variables, the soft SUSY-breaking Lagrangian, and the gauge-transformation properties of the various fields. For example, the minimal supersymmetric extension of the Standard Model (MSSM) is specified by requiring that all fundamental particles transform in either a chiral or vector multiplet, with no additional matter content and with the Lagrangian invariant under P_R. In terms of

---

[6]For non-renormalizable theories, one must also specify the *Kahler potential* and the *gauge-kinetic function* [16]

23

chiral superfields, the superpotential is then

$$W_{MSSM} = \bar{u}y_u Q H_u - \bar{d}y_d Q H_d - \bar{e}y_e L H_d + \mu H_u H_d, \qquad (2.21)$$

while the gauge properties are specified as in the SM and the soft-breaking Lagrangian gives rise to masses for the various superpartners. The soft-breaking masses are generally related to one another in a given scheme of SUSY breaking, but I will typically employ a bottom-up approach and treat them as free parameters.

2.3.1 Looking Ahead: SUSY and EWB

Since supersymmetry postulates many new degrees of freedom, one might imagine that the shortcomings of the SM from the standpoint of EWB might be alleviated even in minimal SUSY BSM scenarios. For example, the MSSM adds several scalar degrees of freedom which will contribute to the cubic term in the finite temperature effective potential. The largest contribution will come from the stop sector, since it has the largest coupling to the Higgs sector. If the stop mass is light enough, a strongly first-order electroweak phase transition can be realized in the MSSM [18]. Also, the MSSM contains 40 new physical CP-violating phases, which can potentially source n_L by the interactions of the various (s)particles with the EW bubble wall. Thus, although put forward to settle a number of distinct theoretical and phenomenological shortcomings of the SM, supersymmetry can provide an attractive and well-motivated framework to address the generation of the baryon asymmetry at the electroweak phase transition. The remainder of this work will be devoted to considering different SUSY

scenarios in which successful EWB might be realized in our universe.

3

Closing the Baryogenesis Window in the MSSM

A thorough exploration of the electroweak scale is currently underway, not only at colliders (such as the LHC), but in dark matter searches and precision tests as well. Results from these observational efforts can provide us with guidance towards the correct supersymmetric EWB scenario, if realized in our universe. In this Chapter, I discuss some of the observational constraints on supersymmetric electroweak baryogenesis. As an informative example, I investigate the available parameter space for the various CP-violating sources in the MSSM, setting aside for the moment the consideration of the phase transition, which is also highly constrained due to the apparent absence of a light stop [19, 20]. I will show that Dark Matter searches are placing strong constraints on the MSSM parameter space for CP-violating sources arising in the Higgsino-gaugino sector, while electric dipole moment searches are closing the window for sferiomic CP-violating

sources. The requirement of a 125 GeV Higgs and the non-observation of SUSY partners at the LHC also significantly tighten the parameter space in both cases. These strong constraints will motivate us to consider two supersymmetric models of EWB beyond the MSSM in the subsequent Chapters.

3.0.2 CP-Violating Sources in the MSSM

In the framework of supersymmetric EWB, the baryon asymmetry of the universe is produced by $SU(2)$ sphalerons acting on a charge density of left-handed fermions, generated by CP-violating sources S_i^{CPV} associated with the electroweak phase transition. As bubbles of broken electroweak symmetry nucleate and expand, the CP-violating phases between the supersymmetric particles and the background Higgs fields lead to the production of net charge densities when (s)particles scatter off of the EWPT bubble wall. These CP-violating sources can be computed using the framework of non-equilibrium quantum field theory from a given Lagrangian. In the MSSM, the particle species with potential CP-violating phases in their mass matrices and a non-trivial dependence on the (spacetime-varying) Higgs vevs are the Higgsinos, gauginos, and sfermions. There is then a potential CP-violating source in the Higgsino-gaugino sector, corresponding to Higgsino-gaugino-VEV interactions governed by the Lagrangian

$$\mathcal{L} \supset - g_2 \bar{\Psi}_{\widetilde{H}^+} \left[v_d(x) P_L + e^{i\phi_2} v_u(x) P_R \right] \Psi_{\widetilde{W}^+} - \frac{g_2}{\sqrt{2}} \bar{\Psi}_{\widetilde{H}^0} \left[v_d(x) P_L + e^{i\phi_2} v_u(x) P_R \right] \Psi_{\widetilde{W}^0}$$

$$+ \frac{g_1}{\sqrt{2}} \bar{\Psi}_{\widetilde{H}^0} \left[v_d(x) P_L + e^{i\phi_1} v_u(x) P_R \right] \Psi_{\widetilde{B}^0} + h.c.,$$

$$(3.1)$$

where $\phi_{1,2}$ are the complex phases between μ and $M_{1,2}$, as well as CP-violating sources involving sfermion-sfermion-VEV interactions in the bubble wall, stemming from

$$\mathcal{L} \supset \quad y_t \tilde{t}_L \tilde{t}_R^* \left[A_t v_u(x) - \mu^* v_d(x) \right] + y_b \tilde{b}_L \tilde{b}_R^* \left[A_b v_d(x) - \mu^* v_u(x) \right] \qquad (3.2)$$

$$+ y_\tau \tilde{\tau}_L \tilde{\tau}_R^* \left[A_\tau v_d(x) - \mu^* v_u(x) \right] + h.c.,$$

where we consider only the third generation scalars, as their couplings to the Higgs doublets are largest. CP-violating phases can arise between the gaugino masses $M_{1,2}$, μ, and the Higgs soft mass parameter b for the Higgsino-gaugino case, and between the various triscalar couplings A_f, μ, b for the scalar sources. Thus, the relevant phases will be $\phi_{1,2} \equiv \mathrm{Arg}(\mu M_{1,2} b^*)$ and $\phi_f \equiv \mathrm{Arg}(\mu A_f b^*)$ where f is the particular sfermion under consideration. Without loss of generality, we will assume b to be real. The CPV sources for species i will be denoted as S_i^{SPV}.

In addition to the CP-violating sources, there are several CP-conserving processes arising from Eqs. (3.1), (3.2) that affect particle number n_i for the relevant species in the MSSM. There are relaxation terms associated with chirality-changing particle scattering off of the Higgs vevs, with corresponding thermally-averaged rates Γ_i^M. There are triscalar and supersymmetric Yukawa interactions given by Eqs. (3.1), (3.2) without replacing $H_{u,d}^0$ by their vevs; as discussed below, supergauge equilibrium typically allows us to combine the rates for both types of processes which we write as Γ_{yi}. For the squarks, there are also $SU(3)$ sphalerons, with rate Γ_{ss}, that produce 1st- and 2nd-generation squarks from a 3rd-generation density and vice-versa. Finally, weak sphalerons ultimately convert the left-handed particle density n_L to a net baryon asym-

metry with rate Γ_{ws}. A complete set of expressions for these various sources can be found in Refs. [21, 22], to which I refer the Reader for additional details of the calculational framework.

We will follow Refs. [21, 22, 23, 24, 25] and work in the Higgs vev-insertion approximation, in which it is assumed that the sources in the bubble wall are strongest near the unbroken phase and where one uses a basis of $SU(2)$ gauge eigenstates, expanding about flavor-diagonal states in the bubble wall. This approximation tends to overestimate the resulting baryon asymmetry and clearly breaks down farther inside the wall where flavor mixing cannot be neglected. However the vev-insertion approximation is expected to characterize the production of the BAU to order unity accuracy [22]. Recent studies have worked out the flavor oscillations in the bubble wall beyond the vev-insertion approximation for a toy model [26], and found qualitatively similar results to those obtained in the vev-insertion approximation, including a resonance in the various sources. Although a treatment beyond the vev-insertion approximation is desirable for an accurate assessment of EWB in the MSSM, since we will be looking at the baryon asymmetry across a wide range of parameter space with other inherent uncertainties, we will content ourselves with the vev-insertion approximation, deferring a more detailed analysis including flavor-mixing effects to future study. Our results can thus be interpreted as a "best case scenario" for EWB in the MSSM, albeit we also show results that would correspond to a factor 10 smaller net BAU, to guide the reader to a more conservative interpretation.

Proceeding within the outlined framework for computing the baryon-to-entropy

ratio Y_B, the weak sphaleron rate Γ_{ws} is typically much slower than the rates for the creation and diffusion of the left-handed charge density n_L ahead of the EWPT bubble wall. This allows us to consider separately the diffusion equations for the various (s)particle densities and the creation of the baryon density n_B, which is given, in terms of Γ_{ws}, n_L, and the bubble wall velocity v_w as [27]:

$$ n_B = \frac{-3\Gamma_{ws}}{v_w} \int_{-\infty}^{0} dz \ n_L(z) e^{\frac{15\Gamma_{ws}}{4v_w}z}, \tag{3.3} $$

where z is the distance from the bubble wall in the wall rest frame (neglecting the wall curvature) and where the unbroken EW phase corresponds to $z < 0$. The left handed charge density n_L is given by the sum of the charge densities of the various left-handed quarks and leptons $n_L = \sum(q_i + l_i)$ where the sum runs over all colors and generations and q_i, l_i denote the difference of particle and antiparticle densities for each species. The charge densities entering into the expression for n_L are obtained from a set of coupled quantum Boltzmann equations (described below) which, once solved, allow one to compute n_B via Eq. (5.34).

Detailed derivations of the quantum Boltzmann equations (QBEs) governing the generation of the BAU have been discussed at length in the existing literature (see e.g. Ref. [22] for a full treatment) so we do not reproduce them here; in what follows we use the simplified form of the QBEs discussed in Ref. [21], with some modifications. For each particle species we can define a corresponding chemical potential μ_i, which is the fundamental quantity entering into the Boltzmann equations, related to its

corresponding charge density by

$$n_i = \frac{T^2}{6} k_i \mu_i + \mathcal{O}\left(\frac{\mu_i}{T}\right)^3, \tag{3.4}$$

where we have expanded in μ/T and the statistical weight for the density k_i is given by

$$k_i = g_i \frac{6}{\pi^2} \int_{m_i/T}^{\infty} dx \frac{x e^x}{(e^x \pm 1)^2} \sqrt{x^2 - m_i^2/T^2}. \tag{3.5}$$

Additionally, as we will see in the following sections, for the cases we consider, the so-called supergauge rates, which drive chemical equilibrium between particles and their superpartners $\mu_i \leftrightarrow \mu_{\tilde{i}}$, are typically faster than the corresponding diffusion timescale τ_{diff}, defined in terms of the various diffusion constants and k-factors in Ref. [22]. As a result of this "superequilibrium" condition, one can define common charge densities for the various particles and their corresponding superpartners: U_i for right-handed up-type (s)quarks, D_i for left-handed down-type (s)quarks, Q_i for left-handed (s)quarks, H for the combined Higgs-Higgsino density, R_i for the right handed (s)leptons, and L_i for left-handed (s)leptons (here i is a generational index). We also use the notation $Q \equiv Q_3$, $T \equiv U_3$, $B \equiv D_3$, $L \equiv L_3$, and $R \equiv R_3$, while the k-factors for these densities are defined by $k_I = k_i + k_{\tilde{i}}$. In terms of these definitions, the fermionic part of the density I (the quantity entering the weak sphaleron equation for the LH densities) is given by

$$n_i = \frac{k_i}{k_I} I \tag{3.6}$$

and the LH fermionic charge density n_L is

$$n_L = \sum_{i=1}^{3} \frac{k_{q_i}}{k_{Q_i}} Q_i + \sum_{i=1}^{3} \frac{k_{l_i}}{k_{L_i}} L_i. \tag{3.7}$$

31

Two more observations allow us to reduce the number of equations needed to solve for the various densities. First, since weak sphalerons are decoupled from the Boltzmann equations, baryon and lepton number are approximately locally conserved, so that the sum of all the densities vanishes at a given spacetime point. Second, since the first and second generation Yukawa couplings are negligible compared to corresponding couplings for the third generation, a first and second generation quark charge can arise only through strong sphalerons, and thus all corresponding charges will be produced in equal number, i.e. $Q_1 = Q_2 = -2U_1 = -2U_2 = -2D_1 = -2D_2$. Combined, these two relations imply $B = -(T + Q)$ so that we can eliminate the set of equations governing the B density as well as all of the other first and second generation (s)quark densities besides Q_1.

Given the above assumptions, the relevant set of Boltzmann equations to consider are:

$$\partial_\mu Q^\mu = - \Gamma_{yt} \left(\frac{Q}{k_Q} - \frac{T}{k_T} + \frac{H}{k_H} \right) - \Gamma_{yb} \left(\frac{Q}{k_Q} + \frac{T+Q}{k_B} - \frac{H}{k_H} \right)$$
$$- \Gamma_{mt} \left(\frac{Q}{k_Q} - \frac{T}{k_T} \right) - \Gamma_{mb} \left(\frac{Q}{k_Q} + \frac{T+Q}{k_B} \right) - S_{\tilde{t}}^{CPV} - S_{\tilde{b}}^{CPV} \qquad (3.8)$$
$$- 2\Gamma_{ss} \left(2\frac{Q}{k_Q} - \frac{T}{k_T} + \frac{Q+T}{k_B} + \frac{1}{2} \sum_{i=1}^{2} \left[4\frac{1}{k_{Q_i}} + \frac{1}{k_{U_i}} + \frac{1}{k_{D_i}} \right] Q_1 \right)$$

$$\partial_\mu T^\mu = \Gamma_{yt} \left(\frac{Q}{k_Q} - \frac{T}{k_T} + \frac{H}{k_H} \right) + \Gamma_{mt} \left(\frac{Q}{k_Q} - \frac{T}{k_T} \right) + S_{\tilde{t}}^{CPV}$$
$$+ \Gamma_{ss} \left(2\frac{Q}{k_Q} - \frac{T}{k_T} + \frac{Q+T}{k_B} + \frac{1}{2} \sum_{i=1}^{2} \left[4\frac{1}{k_{Q_i}} + \frac{1}{k_{U_i}} + \frac{1}{k_{D_i}} \right] Q_1 \right) \qquad (3.9)$$

$$\partial_\mu Q_1^\mu = - 2\Gamma_{ss} \left(2\frac{Q}{k_Q} - \frac{T}{k_T} + \frac{Q+T}{k_B} + \frac{1}{2} \sum_{i=1}^{2} \left[4\frac{1}{k_{Q_i}} + \frac{1}{k_{U_i}} + \frac{1}{k_{D_i}} \right] Q_1 \right) \qquad (3.10)$$

$$\partial_\mu H^\mu = -\,\Gamma_{yt}\left(\frac{Q}{k_Q} - \frac{T}{k_T} + \frac{H}{k_H}\right) + \Gamma_{yb}\left(\frac{Q}{k_Q} + \frac{T+Q}{k_B} - \frac{H}{k_H}\right)$$
$$+\,\Gamma_{y\tau}\left(\frac{L}{k_L} - \frac{R}{k_R} - \frac{H}{k_H}\right) - \Gamma_h\frac{H}{k_H} + S^{CPV}_{\widetilde{H}} \tag{3.11}$$

$$\partial_\mu L^\mu = -\Gamma_{y\tau}\left(\frac{L}{k_L} - \frac{R}{k_R} - \frac{H}{k_H}\right) - \Gamma_{m\tau}\left(\frac{L}{k_L} - \frac{R}{k_R}\right) - S^{CPV}_{\widetilde{\tau}} \tag{3.12}$$

$$\partial_\mu R^\mu = \Gamma_{y\tau}\left(\frac{L}{k_L} - \frac{R}{k_R} - \frac{H}{k_H}\right) + \Gamma_{m\tau}\left(\frac{L}{k_L} - \frac{R}{k_R}\right) + S^{CPV}_{\widetilde{\tau}} \tag{3.13}$$

We solve these equations in the so-called diffusion approximation, in which one introduces a diffusion constant for each species D_i and assumes $\mathbf{j}_i = D_i \nabla n_i$. The diffusion constants we use are those found in Ref. [22]: $D_Q = D_T = D_{Q_i} \simeq 6/T$, $D_H \simeq 100/T$, $D_L \simeq 100/T$, $D_R \simeq 380/T$ where T is the EWPT temperature, assumed to be 100 GeV. Note that the left- and right-handed (s)lepton diffusion constants are different; this is because of the $SU(2)$ interactions active in the plasma for LH-densities. We neglect this difference for the (s)quark diffusion constants since D_{Q,T,Q_i} are determined primarily by $SU(3)$ interactions which are non-chiral.

With our framework in place, we can now compute the various sources and rates based on previous work in Refs. [21, 22, 23, 24, 25] for the Higgsinos/gaugino, stop, sbottom, and stau cases and consider the constraints on each scenario. We assume the transition temperature $T_c = 100$ GeV throughout.
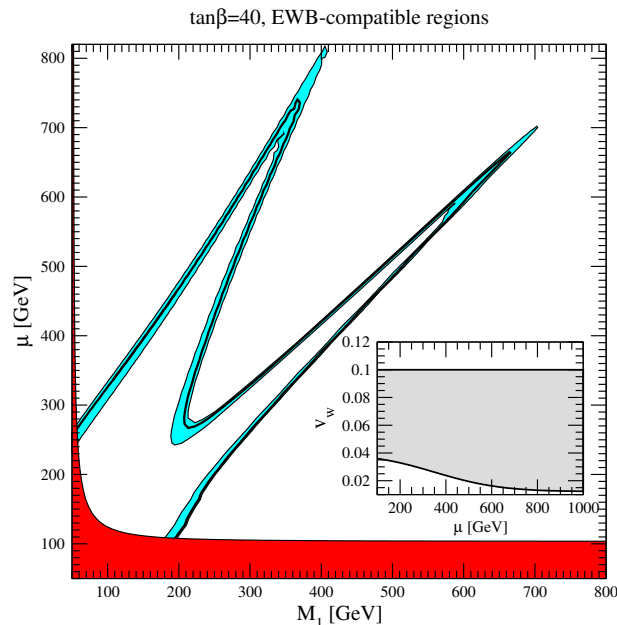
Figure 3.1: Regions compatible with resonant chargino-neutralino electroweak baryogenesis, on the (M_1, μ) plane at $\tan\beta = 40$, for maximal gaugino-higgsino CP-violating phase $\sin\phi_\mu = 1$ and for $m_A = 300$ GeV. The cyan region corresponds to the band in the wall velocity v_w shown in the inset. The red shaded region is excluded by LEP searches for light neutralinos/charginos [29]

3.1 Higgsino-Gaugino Sources

We consider first the CPV sources arising from Eq. 5.23 assuming universal CP-violating phases, so that

$$\phi \equiv \arg(M_1\mu b^*) = \arg(M_2\mu b^*). \qquad (3.14)$$

Relaxing this assumption to the case of non-universal CP-violating phases may be necessary to produce the observed baryon asymmetry if the next generation of EDM experiments yield null results, especially for large values of $\tan\beta$ [28].

For the Higgsino-gaugino sources, we can take all sfermions, other than the right-handed stops, to be heavy, $m_{sf} \sim 1 - 10$ TeV. The gaugino masses, which are

generally assumed to be unified to a common mass at some higher scale, typically organize themselves into patterns given the mechanism of supersymmetry breaking. We follow Ref. [30] and concentrate for the sake of illustration on two scenarios for our investigation, namely gravity-mediated SUSY breaking, which yields the pattern $M_1 \approx M_2/2$, and anomaly-mediated SUSY breaking models (AMSB), for which $M_2 \approx M_1/3$ [31]. These hierarchies and their implications are discussed in more detail in Sec. 3.1.2 and Sec. 3.1.3. In calculating the baryon asymmetry we typically vary the lightest gaugino mass and μ, focusing on the (M_1, μ) plane for the gravity-mediated case and the (M_2, μ) plane for the anomaly-mediated scenario.

We calculate the baryon asymmetry numerically for values of μ, $M_{1,2}$ between 100 GeV and 1 TeV to find parametric regions producing the observed[1] baryon-to-entropy ratio for a given value of the CP-violating phase ϕ_μ. Our results in the (M_1, μ) plane for $\sin \phi_\mu = 1$, $\tan \beta = 40$ are shown in Fig.3.1. As we are considering the resonant EWB scenario [23, 32], the largest contributions to the baryon asymmetry come from points near resonance for the scattering off of the VEVs in the wall. For the higgsino-gaugino-vev interactions this resonant behavior occurs for nearly degenerate gaugino, higgsino masses, $M_{1,2} \sim \mu$, leading to the two-funnel structure in Fig.3.1 as discussed in Refs. [28, 30].

Since the gauginos in this scenario are light, it was previously realized that much of the parameter space suitable for successful EWB is also that required for a neutralino lightest supersymmetric particle (LSP), thus providing a viable dark matter

---

[1]The uncertainty in Y_B^{WMAP} leads to negligible uncertainties in the higgsino-gaugino mass planes. We thus adopt the value $Y_B^{WMAP} = 9.1 \times 10^{-11}$ for consistency with previous studies.

candidate along with the baryon asymmetry (see e.g. Refs. [28, 30, 33]). As a result, one can place further constraints on the gaugino-higgsino parameter space from the results produced by various dark matter searches. In the resonant EWB scenario, however, the right-handed stop is typically also light to satisfy the requirement of a strongly first-order EWPT, and consequently to prevent the washout of the baryon asymmetry in the broken phase [34, 35, 36]. A right-handed stop mass $m_{\tilde{t}_R}$ of $\mathcal{O}(100\ \mathrm{GeV})$ would imply significant regions of the gaugino-higgsino parameter space in which the RH stop is instead the LSP. Following the strategy in Refs. [28, 30] we expand the region of the parameter space simultaneously viable for EWB and a neutralino LSP by assuming that some other mechanism is responsible for ensuring a strongly first order phase transition. Several such mechanisms have been proposed [37, 38] that are decoupled from the mechanisms driving EWB and thus allowing for a heavy RH stop with $m_{\tilde{t}_R} \gtrsim 1$ TeV while still preventing baryon number washout[2]. For example, extending the scalar sector of the theory by including (well-motivated) gauge singlets can augment the strength of the EWPT (see e.g. [38] and references therein). For increasing values of $m_{\tilde{t}_R}$, the baryon asymmetry is suppressed and our numerical results find no viable parameter space for EWB given $m_{\tilde{t}_R} \gtrsim 500$ GeV. This suppression is due to the erasure of chiral charges by strong sphaleron processes [40] as discussed in the following subsection. For heavier RH stop masses and large values of $\tan \beta$ one might circumvent this problem by taking relatively light sbottoms, staus (~ 1 TeV) , a combination of which may serve to bolster

---

[2]Such a mechanism may also be necessary in light of recent studies indicating that magnetic fields may be produced at the EWPT which might lower the sphaleron energy and thus necessitate a stronger phase transition to prevent baryon number washout [39].

the baryon asymmetry (albeit with a potential sign change) [21, 22, 24] and possibly

extend the range of $m_{\tilde{t}_R}$ consistent with the observed baryon-to-entropy ratio. For the

purposes of our numerical analysis, however, we take the RH SUSY breaking scalar

mass $m_{\tilde{U}_3} = 0$, corresponding, for the value of the tri-scalar coupling, $\tan\beta$ and range

of μ we consider, to a physical RH stop mass $m_{\tilde{t}_R} \approx 160$ GeV, and consider our results

to be a conservative outline of the gaugino-higgsino parameter space consistent with

EWB and a neutralino LSP, deferring a detailed analysis of the more realistic case with

finite sbottom and stau masses to future work.

The other MSSM parameters relevant to our analysis are chosen to satisfy

both the condition of a strongly first-order phase transition and bounds from precision

electroweak measurements [27, 41, 42]. We take the heavy Higgs mass to be set by the

common scalar soft SUSY-breaking mass at the TeV scale, while for the light Higgs we

take $m_{H_u}^2 = -(50)^2$ GeV^2. To ensure that the lightest stop is mostly right handed, as

required to prevent significant contributions to the ρ parameter [30], the mixing must

be small and we take $A_t = 200$ GeV^3. The baryon asymmetry depends sensitively on

the mass of the CP-odd Higgs, m_A, through the quantity $\Delta\beta$ (which we discuss in the

following section) and is suppressed for large values [28, 30]. We generally take $m_A = 300$

GeV and 1000 GeV as these two values bracket the interesting range for MSSM resonant

EWB; namely, the low value corresponds to contributions to, for example, the branching

ratio $b \to s\gamma$ close to the experimental limit, while the high value corresponds to a rather

large suppression of the BAU. This suppression may be alleviated by including additional

---

[3] Note that precision electroweak and Higgs constraints also require $\tan\beta \gtrsim 5$ in the resonant EWB
scenario [42]

non-resonant source terms in our analysis [19, 43], however such contributions typically require larger values of $\sin\phi$ to produce results consistent with the observed BAU and scale as $1/\tan\beta$ for large values; we do not consider such sources here. Note that for large $\tan\beta$ one may be forced to consider larger values for m_A to satisfy experimental bounds on the $B_u \to \tau\nu_\tau$ decay mode [28].

3.1.1 Dependence on Bubble Wall Parameters

The baryon asymmetry also depends on several parameters associated with the electroweak phase transition, namely the bubble wall velocity, v_w, the wall width, L_w, and the variation of the ratio of Higgs vevs across the bubble wall, $\Delta\beta$. An accurate determination of these quantities for a given choice of MSSM parameters requires solving for the exact Higgs profile in the bubble wall. We instead aim to understand how uncertainties associated with the bubble wall parameters affect our results for the baryon asymmetry. In this section we assess the various dependencies both qualitatively, by considering the analytic (approximate) solution to the QTEs discussed in detail in Refs. [21, 22, 23, 24, 25], and quantitatively by numerically solving the relevant set of QTEs while varying the relevant parameter values. We find that our results are largely insensitive to L_w, mildly dependent on v_w, and linear in $\Delta\beta$. We utilize these results to choose reasonable and, where appropriate, conservative values for the bubble wall parameters, leading to a more optimistic scenario for our results in the gaugino-higgsino mass planes, given our other assumptions about the MSSM parameter space.

The baryon density ρ_B satisfies a diffusion equation with solutions in the bro-

ken phase given in terms of $n_L(\bar{z})$ in the symmetric phase ($\bar{z} < 0$) [23], where $\bar{z}$ is the comoving distance away from the wall[4]. Early discussions (see e.g. [23, 27, 32, 44]) estimated the Yukawa rate, Γ_Y (and strong sphaleron rate Γ_{ss}) to be much faster than all other relevant particle number-changing rates, implying that the higgsino density in the unbroken phase is quickly converted to a chiral quark density in front of the bubble wall. This approximation allows one to write Q, T in terms of H and subsequently solve the QTEs by expanding in $1/\Gamma_{Y,ss}$ and rewriting the equations in terms of a single diffusion equation for H [27]

$$v_w H' - \bar{D} H'' = -\bar{\Gamma} H + \bar{S} \tag{3.15}$$

Here $\bar{D}$ is a diffusion coefficient, $\bar{\Gamma}$ is a chiral relaxation term involving Γ_Y as well as the CP–conserving stop mixing and higgsino-gaugino mixing rates, Γ_M, Γ_H, and statistical factors, $\bar{S}$ is a term proportional to the CP-violating sources, and primes denote derivatives with respect to $\bar{z}$. Under the simplifying assumptions of step function CP-violating sources constant in the wall, and step function chiral relaxation rates, $\bar{\Gamma}(\bar{z}) = \bar{\Gamma}\Theta(\bar{z})$, active only in the wall and broken phase, one obtains the lowest order solution for H in the symmetric phase,

$$H_0(\bar{z} < 0) = \frac{e^{v_w \bar{z}/\bar{D}}}{\bar{D}\kappa_+^2} \left(1 - e^{-\kappa_+ L_w}\right) \bar{S} \tag{3.16}$$

$$\kappa_\pm = \frac{v_w \pm \sqrt{v_w^2 + 4\bar{D}\bar{\Gamma}}}{2\bar{D}} \tag{3.17}$$

Using Eq. (3.16) and the relations between H and Q, T, one can obtain an analytic approximation for the baryon density in the broken phase to lowest order in $1/\Gamma_{y,ss}$

---

[4]In what follows we neglect the curvature of the wall

[23].

However, it was pointed out in Ref. [25] that although the approximation of fast Yukawa rates will generally be valid in the symmetric phase, it does not typically apply in the broken phase. Solving the diffusion equation to first non-trivial order in $1/\Gamma_{y,ss}$ yields corrections $\bar{S} \to \bar{S} + \delta\bar{S} + \mathcal{O}(1/\Gamma_y^2)$ to the generalized source term in Eq. (3.15). Additionally, the expressions for the densities Q and T, which to lowest order are proportional to H, receive corrections of $\mathcal{O}(1/\Gamma_{Y,ss})$, necessitating a full numerical solution to the set of coupled QTEs. Despite these setbacks to reliably calculating the baryon asymmetry analytically, some insight regarding the dependence of ρ_B on the various parameters can still be gained from the lowest order analytic solution and the first order corrections.

From Eqs.(3.16)-(5.12), we see that the baryon density depends nontrivially on the bubble wall velocity. The largest corrections to the lowest order solution H_0 are typically those arising from the shift in the effective source term [25], which can be written in terms of integrals over H_0 in the bubble wall. These contributions depend on the wall velocity only through the combinations $\kappa_\pm$, which, in parametric regions where the corrections are large, depend only weakly on v_w. This is because when the corrections $\delta\bar{S}/\bar{S} \sim \Gamma_M(\Gamma_H/\Gamma_Y)$ become large, $\bar{\Gamma} \sim \Gamma_M + \Gamma_H$ tends to dominate over v_w^2 in Eq. (5.12). Thus the velocity dependence of the baryon asymmetry can be reasonably approximated as that of the lowest order solution

$$\rho_B(\bar{z} > 0) \sim \frac{v_w \Delta\beta \bar{D}\mathcal{S}}{L_w \lambda_+ \kappa_+^2 (v_w - \bar{D}\lambda_-)} \left(1 - e^{-\kappa_+ L_w}\right) \left(\alpha_1 + \alpha_2 v_w^2\right) \qquad (3.18)$$

where we have defined

$$\lambda_\pm = \frac{v_w \pm \sqrt{v_w^2 + 4\mathcal{R}D_q}}{2D_q}, \qquad (3.19)$$

D_q is an effective quark diffusion constant, $\mathcal{R}$ is a relaxation term arising from weak sphaleron processes in the unbroken phase, $\alpha_{1,2}$ are known functions independent of v_w, L_w, and $\Delta\beta$, and $\mathcal{S}$ is the effective source term after scaling out the dependence on the bubble wall parameters. We have verified this approximate expression against the velocity dependence of the full numerical solution for various regions of the parameter space, both on and off resonance, and find the two to be in good agreement. The profile Eq. (3.18) reproduces well-known features of the velocity dependence of ρ_B, namely that small velocities correspond to a quasi-equilibrium situation, thereby suppressing the baryon asymmetry, while large velocities render the transport of the chiral current in front of the bubble wall inefficient, also suppressing the asymmetry, leading to a peak in ρ_B for v_w around a few $\times 10^{-2}$ [41].

A precise determination of the bubble wall velocity in the MSSM is generally difficult, as the dynamics of the wall are further complicated by friction terms arising from the interactions of the wall with the plasma. Detailed calculations of v_w in the MSSM, including various frictional contributions, have been carried out [45], suggesting a wall velocity in the range $10^{-2} < v_w < 10^{-1}$. To quantify the impact of this uncertainty on our results, we solve the QTEs numerically for wall velocities that maximize (minimize) the lowest order analytic approximation for ρ_B, Eq. (3.18), at each point in the $(M_{1,2}, \mu)$ plane. The results are shown in Fig.3.1, with the band of maximal (minimal) velocities displayed in the inset. We find that uncertainties in the wall velocity in

this range lead to $\mathcal{O}(10 \text{ GeV})$ uncertainties in the gaugino-higgsino mass plane which in turn do not significantly affect our conclusions. In what follows we thus adopt the central value $v_w = .05$ except where otherwise stated.

Turning our attention to the dependence of the baryon asymmetry on the bubble wall width, L_w, we can once again look to Eq. (3.18) for insight. To lowest order in the Yuakwa and strong sphaleron rates, the baryon asymmetry is a monotonically decreasing function of L_w. Corrections to Eq. (3.18) in general do depend on L_w, however we find that including these corrections still renders ρ_B a monotonically decreasing function of the wall width in our approximation and have verified this dependence for several choices of the relevant MSSM parameter values. This behavior matches that expected of the sources, as, to lowest non-vanishing order in the Higgs vev insertion expansion [23], the CP-violating higgsino source is proportional to the first spatial derivative of the Higgs vev in the wall and thus the baryon asymmetry becomes suppressed for larger values of L_w [41, 46]. In the analysis that follows we adopt the central value [47] $L_w = 25/T$. We find the impact of considering a much thinner bubble wall, $L_w \sim 5/T$, to be of $\mathcal{O}(1 - 10 \text{ GeV})$ in the $M_{1,2}, \mu$ plane and therefore not substantially affecting our results.

We also see from Eq. (3.18) that the baryon asymmetry is proportional to $\Delta\beta$, which is in turn a decreasing function of the CP-odd Higgs mass m_A. For the m_A dependence of $\Delta\beta$ we use the two-loop results of Ref. [47] and obtain $\Delta\beta \sim 4.5 \times 10^{-3}$ for $m_A = 300$ GeV. As mentioned above, we find the baryon asymmetry to be significantly suppressed for smaller values of $\Delta\beta$ (corresponding to larger m_A; see e.g. Fig. 3.4) and

42

we thus take this choice to represent a conservative bound on the $\Delta\beta$ dependence of Y_B, although in some cases we do consider the $m_A = 1000$ GeV scenario for illustrative purposes. The $\tan\beta$ dependence of $\Delta\beta$ has not, to our knowledge, been thoroughly explored in the literature [28], however from Eq. (3.18) its effect on Y_B would seem to simply rescale our curves by a constant multiplicative factor for a given choice for $\tan\beta$. As discussed, we do not anticipate the inclusion of such effects to greatly impact our conclusions and we defer such considerations to future work.

Finally, we note that the suppression of the net baryon density for large values of $m_{\tilde{t}_R}$ mentioned in the previous subsection is manifest in the approximate solution for the baryon density Eq. (3.18). The $\alpha_{1,2}$ depend on the RH stop mass through the statistical factor k_T, which relates the RH (s)top chemical potential to the corresponding number density. For increasing $m_{\tilde{t}_R}$, the stop contribution to k_T becomes exponentially small and $\alpha_{1,2}$ decrease to their asymptotic values for large $m_{\tilde{t}_R}$ (with all other relevant parameters fixed), while the α_2 term (which is generally positive) is proportional to $1/\Gamma_{ss}$, resulting in a suppressed baryon density for realistic strong sphaleron rates when compared to the $\Gamma_{ss} \to 0$ case for large $m_{\tilde{t}_R}$ [27, 40].

3.1.2 EWB and Bino-like Dark Matter

Having outlined the portions of the MSSM parameter space relevant for successful resonant EWB, we now direct our attention to the dark matter phenomenology associated with these regions. As mentioned earlier, the lightest neutralino in successful supersymmetric EWB models is, potentially, a viable dark matter candidate. We also
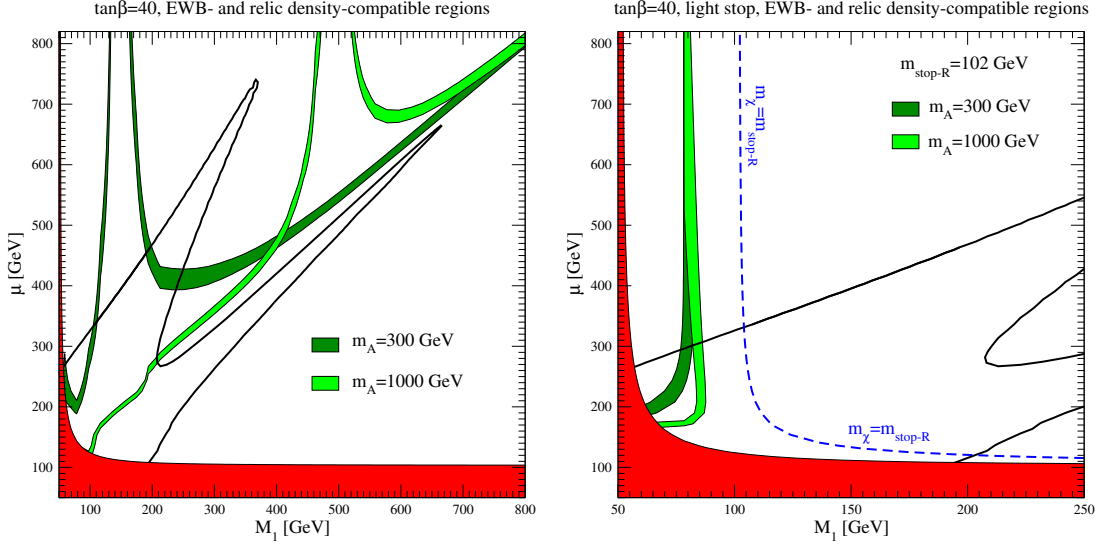
Figure 3.2: Left: Regions with a thermal relic neutralino abundance $0.095 < \Omega_\chi h^2 < 0.13$ on the (M_1, μ) plane at $\tan\beta = 40$, for maximal gaugino-higgsino CP-violating phase $\sin\phi_\mu = 1$ and for $m_A = 300$ GeV (dark green) and $m_A = 1000$ GeV (light green). The black line indicates successful electroweak baryogenesis for $\sin\phi_\mu = 1$ and $m_A = 300$ GeV, as in Fig. 3.1. Right: Regions of correct relic abundance, with a lightest stop set at a mass of 102 GeV, again for $m_A = 300$ and 1000 GeV (darker and lighter green, respectively). The dashed blue line corresponds to the parameter space where the lightest neutralino has the same mass as the lightest stop. Bounds on the density of heavy relic charged or colored particles exclude the portion of the parameter space above and to the right of the dashed blue line, where the stop would be the lightest supersymmetric particle.

pointed out above that the phenomenology of the lightest neutralino depends sensitively on the hierarchy between the masses of the hypercharge and weak gauginos, which is not fixed by EWB. In practice, EWB dictates that either $M_1 \sim \mu$ or $M_2 \sim \mu$, but it does not enforce a hierarchy between M_1 and M_2 which depends, in general, on the mechanism of supersymmetry breaking. We first consider the case where $M_1 < M_2$, which occurs for example in models where gaugino soft breaking masses are universal at the grand unification scale. Renormalization group evolution then dictates, approximately, that $M_2 \simeq \frac{3}{5} \frac{\cos^2\theta_W}{\sin^2\theta_W} M_1 \simeq 2M_1$.

Having established a relation between the soft-breaking gaugino masses, the

mass and composition of the lightest neutralino only depends on the values of M_1 and μ. We begin exploring the dark matter phenomenology on the (M_1, μ) parameter space in Fig. 3.2. In the left panel, we calculate the relic density and show regions on the parameter space where the thermal relic density of the lightest neutralino Ω_χ falls in a range consistent with the inferred dark matter density in the universe [4] (quantitatively, we highlight regions of parameter space where $0.095 < \Omega_\chi h^2 < 0.13$). We fix the mass scale of the heavy MSSM Higgs sector by setting $m_A = 300$ GeV and $m_A = 1000$ GeV - two values that bound the interesting range for MSSM EWB.

The shape of the regions where the lightest neutralino relic density matches the observed density of dark matter are qualitatively easily understood: to produce a large enough abundance, interactions of neutralinos with gauge bosons must be suppressed, enforcing a bino-like character to neutralino relics with the correct abundance; the two vertical funnels then correspond to rapid, quasi-resonant annihilation via the CP-odd Higgs A when $m_\chi \simeq m_A/2$, while away from the resonance the bino relic density is low enough only if a sufficiently large higgsino fraction is present – enforcing $M_1 \simeq \mu$. Notice that enforcing successful EWB as well as the correct relic abundance implies a bino-like neutralino and $M_2 \sim \mu$ to produce enough baryon asymmetry. The $M_1 \sim \mu$ funnel of neutralino-driven EWB [48] lies not far from, but well below, the parameter space with the correct thermal relic abundance of neutralinos. Notice also that the regions with the desired overlap of relic density and EWB depend upon the choice of the CP-violating phase, which for the black lines shown in the figure is maximal.

In the context of the minimal supersymmetric extension of the Standard Model,

the electroweak phase transition is strongly first order and compatible with collider data only for a very light right-handed stop and in a certain mass window for the Higgs mass. Ref. [19] most recently addressed this issue, in the context of an effective theory with decoupled sfermion (with the exception of the right-handed stop) and heavy-Higgs sectors [36]. The allowed region is restricted to right-handed stop masses lighter than around 115 GeV. Such a light stop has dramatic implications not only for collider phenomenology (see e.g. [49] and references therein), but also for dark matter searches: the lightest neutralino must be lighter than the stop in order for the model to be viable. As a result, the range of neutralino masses is severely restricted. In addition, stop coannihilation also occurs [33], when the masses of the lightest neutralino and stop approach each other, and the freeze-out of the two species in the early universe is correlated.

To illustrate this point, we outline on the right in Fig. 3.2 the regions in the (M_1, μ) parameter space compatible with a neutralino thermal relic abundance matching the cold dark matter density, for $m_A = 300$ and 1000 GeV (darker and lighter green, respectively) when a right-handed stop with a mass of 102 GeV is assumed. To the right of the vertical allowed bands, the relic density is driven to excessively low values via the mechanism of stop coannihilation, while for low values of M_1 coannihilations are ineffective and the bino relic density is too large. The plot also shows the boundary of the "allowed region" where the lightest neutralino is the LSP (dashed blue line), and the fact that there is an overlap between the correct relic density regions and the regions
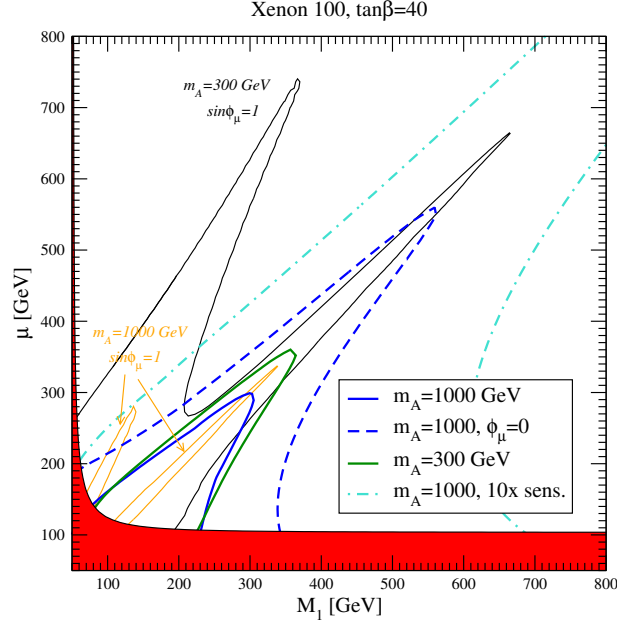
Figure 3.3: Regions excluded by the Xenon100 direct detection results, on the (M_1, μ) plane at $\tan\beta = 40$, for maximal gaugino-higgsino CP-violating phase $\sin\phi_\mu = 1$ and for $m_A = 1000$ GeV (solid blue line) and 300 GeV (green line). The dashed blue line corresponds to no CP violation, and $m_A = 1000$ GeV. Finally, the turquoise dot-dashed line indicates the region corresponding to 10 times the Xenon100 current sensitivity. The black solid line outlines the region of parameter space where successful EWB can occur, for $m_A = 300$ GeV, while the orange line corresponds to $m_A = 1000$ GeV.

with enough baryon asymmetry (black line) [5]. In the remainder of this analysis, we omit the curves corresponding to the light stop scenario, but the Reader should bear in mind that the shape indicated by the dashed blue line would appear in an analogous way in all other figures, should one resort to the light-stop minimal scenario.

Turning our attention to the various dark matter searches, we outline the impact of the recent direct detection results from the Xenon 100 collaboration [50] on the parameter space in Fig. 3.3 . For reference, we show the contours corresponding to successful EWB for both $m_A = 300$ GeV and 1000 GeV (orange solid lines). The Xenon

---

[5]Note that other non-resonant CP-violating sources not considered here might also contribute to the BAU in this scenario, especially for larger values of m_A [19]

100 constraints are calculated by computing for every point in the parameter space the spin-independent neutralino-proton cross section and comparing with the cross section limit corresponding to the given WIMP mass. As observed in Ref. [30], the relevant Higgs-neutralino coupling is sensitive to the relative bino-higgsino CP-violating phase ϕ_μ, with larger phases suppressing the spin-independent neutralino-proton cross section.

We show with a blue solid line the contours of the region excluded by the results from the Xenon 100 collaboration presented in Ref. [50] for $m_A = 1000$ GeV and $\sin \phi_\mu = 1$. Points between the red regions and the contours are excluded. Notice that almost the entire $M_1 \sim \mu$ funnel of successful EWB is ruled out by the Xenon 100 results. Turning off CP violation extends the contours significantly, to the blue dashed lines, indicating that for smaller CP-violating phases the $M_1 \sim \mu$ funnel is solidly excluded by direct detection. The green solid line encompasses the slightly larger region corresponding to $m_A = 300$ GeV: a lower value for m_A produces larger regions compatible with EWB, and the $M_1 \sim \mu$ funnel, for large enough CP violation, is still a viable option for successful EWB. Finally, for reference we show the exclusion limits that would correspond to an improvement in the Xenon 100 sensitivity by a factor of 10. Such an improvement in sensitivity is likely optimistic as a target for Xenon 100 by the end of 2012, but is well within the sensitivity expected for the XENON1T experiment, recently approved by INFN to start at the Laboratori Nazionali del Gran Sasso [51], even with a very limited time exposure. A gain in sensitivity of a factor 10 would vastly probe the entire region of $M_1 \sim \mu$ as well as the low-mass portion of the $M_2 \sim \mu$ funnel.

We move on to indirect dark matter detection in Fig. 3.4. The left panel shows
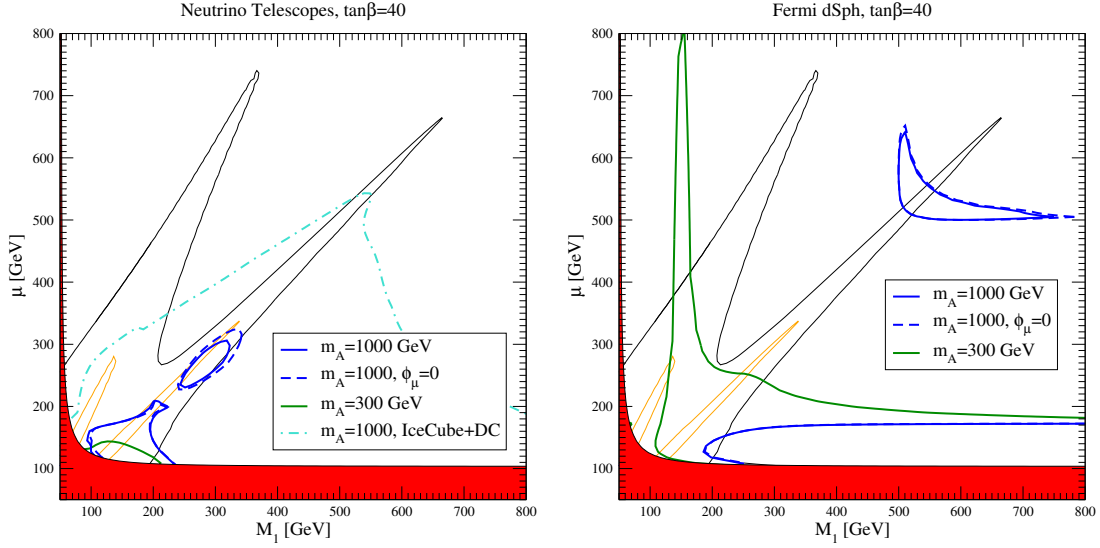
Figure 3.4: The performance of indirect dark matter searches on the (M_1, μ) plane. In the left panel, we show the current and future reach of the IceCube neutrino telescope [52], while on the right we indicate the regions of parameter space ruled out by Fermi observations of nearby dwarf spheroidal galaxies [53]

the current performance of the IceCube detector in searching for an anomalous high-energy flux of neutrinos from the Sun that might originate from the annihilation of dark matter captured and sank inside the Sun [52]. Neutrino telescope rates are sensitive primarily to the capture rate, which depends upon the vector and scalar neutralino-proton scattering cross section. In turn, the latter is maximized for maximal higgsino-gaugino mixing in the lightest neutralino. This is manifest in the shape of the parameter space regions ruled out by current IceCube data [52], primarily covering the $M_1 \sim \mu$ funnel, albeit only for relatively low masses - at most $m_\chi \lesssim 300$ GeV. We also show the effect of switching off the CP-violating phase ϕ_μ, which bears for neutrino telescope rates the opposite effect as for the spin-independent cross section (see again the detailed discussion in Ref. [30]), here enhancing – although only marginally – the telescope

49

sensitivity to the theory parameter space. This is shown by the dashed blue line. A lighter heavy-Higgs sector suppresses the reach of neutrino telescopes, as evidenced by the green line. This unusual effect is due to the bias in the annihilation final state produced by resonant annihilations via the A CP-odd Higgs boson, that produces more $b\bar{b}$ than gauge boson pairs in the final state. In turn, this yields softer neutrinos, which are harder to detect with IceCube. Finally, the dot-dashed light-blue line shows the anticipated performance of the full IceCube instrument, including DeepCore, with 180 days of data [52]. Again, large portions of the parameter space where the lightest neutralino is relatively light (less than 0.5 TeV) and with a large higgsino-bino mixing will be readily ruled out by forthcoming IceCube results.

The right panel of Fig. 3.4 shows the impact of observations of dwarf spheroidal galaxies (dSph) with the Fermi gamma-ray telescope [53]. The null result of searches for gamma-ray emission from dSph is translated into a limit on the pair-annihilation cross section, after including an appropriate normalization factor dependent upon the dark matter density distribution in the relevant dSph, and utilizing the appropriate gamma-ray spectrum (we refer the Reader to Ref. [53] for further details on this analysis). The parameter space regions that are excluded by Fermi data correspond to regions with large pair-annihilation cross section (we do not rescale here for under-abundant relic dark matter density, assuming that non-thermal production accounted for low-thermal relic abundances). Two regions are ruled out by Fermi data: in the lower right light higgsino-like neutralinos, and for $m_\chi \simeq m_A/2$ resonantly annihilating neutralinos.

We caution the Reader that the conclusions we arrive at in the present analysis
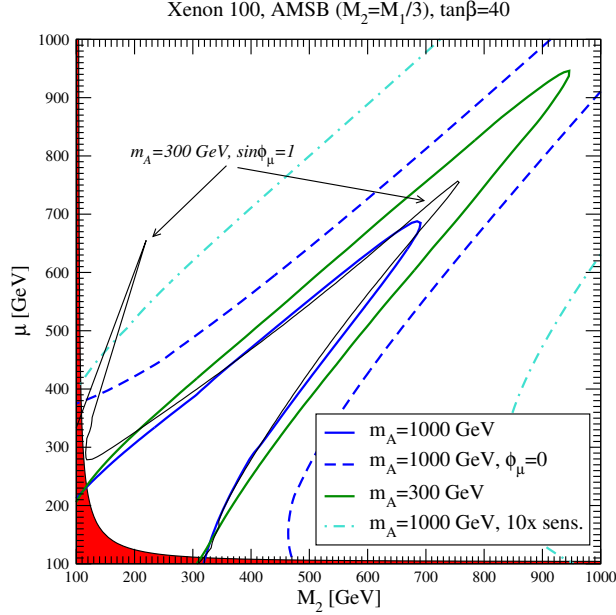
Figure 3.5: As in Fig. 3.2, right, but on the (M_2, μ) plane, and with an anomaly-mediated gaugino mass hierarchy (whereby $M_2 \simeq M_1/3$).

crucially depend on the assumption that the dominant sources at the electroweak phase transition correspond to resonant chargino-neutralino terms. Should one allow for additional source terms, such as non-resonant sources (see e.g. [19]) or sources associated with left-right stops, sbottoms or staus (see e.g. [25]), all of our conclusions would be weakened. For example, non-resonant sources allow for large values of m_A that would suppress the spin-independent dark matter direct detection rates. Losing the correlation between the μ parameter and the gaugino soft supersymmetry-breaking masses would also impact the higgsino mixing in the lightest neutralino, again affecting virtually all direct and indirect detection rates.

3.1.3 EWB and Wino-like Dark Matter

If the hierarchy between the gaugino masses at the electroweak scale is such
that $M_2 < M_1$, the phenomenology of the lightest neutralino as a dark matter particle
changes drastically from that just discussed. A prototypical scenario where the $M_2 <
M_1$ hierarchy is realized is anomaly mediated supersymmetry breaking (see e.g. [54]).
Although this class of models is unrelated to the phenomenological requirements of
EWB, we employ here for definiteness the prediction, valid at the electroweak scale,
that $M_2 \simeq M_1/3$. The lightest neutralino is here either wino-like, higgsino-like, or a
mixed wino-higgsino state, depending upon the relative size of μ versus M_2. For sub-
TeV masses, in no case is the lightest neutralino thermal relic density large enough to
produce the inferred density of cold dark matter. Requiring that the lightest neutralino
be the dark matter constituent therefore necessitates one to postulate a non-thermal
production mechanism [54] or a modified cosmological setup for example with kination
domination [55]. Here, as before, we assume that the density of neutralinos matches the
cold dark matter density by one of these mechanisms.

Fig. 3.5 illustrates, as in Fig. 3.2, the parameter space probed by the most
recent Xenon 100 results on the spin-independent neutralino-proton scattering cross
section, for a variety of choices for m_A and ϕ_μ. The black lines indicate the maximal ex-
tent of the EWB-compatible parameter space, corresponding to maximal CP violation,
i.e. $\sin \phi_\mu = 1$, within the present setup. Current direct detection results (solid blue
and green curves, for $m_A = 1000$ and 300 GeV, respectively) rule out almost the entire
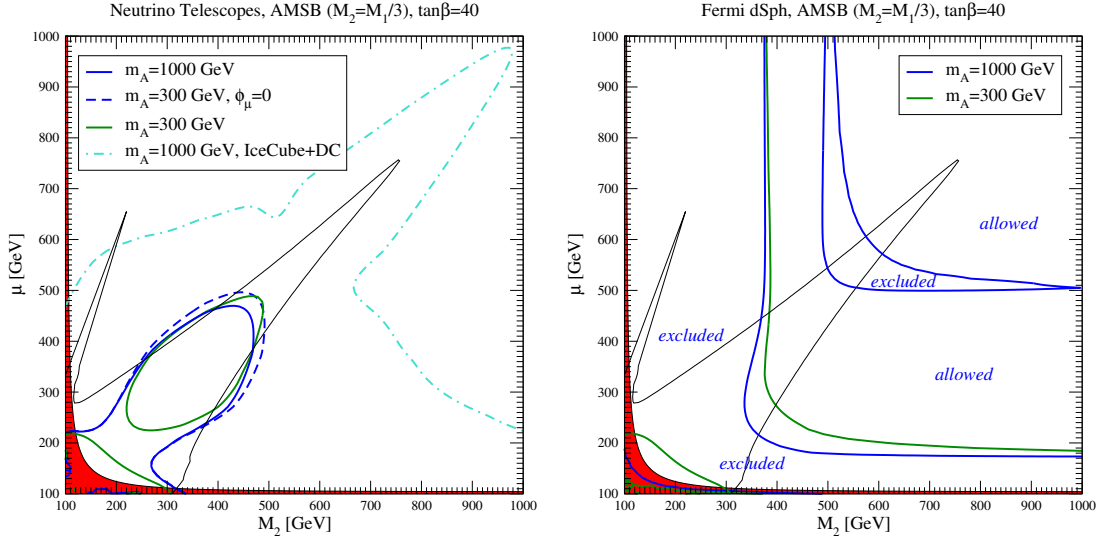
Figure 3.6: As in Fig. 3.4, but on the (M_2, μ) plane, and with an AMSB hierarchy (whereby $M_2 \simeq M_1/3$).

EWB-compatible parameter space, even for the most unfavorable case of maximal CP violation. Increasing $\sin \phi_\mu$ leads to a reduced EWB-viable region and a wider portion of parameter space ruled out by the direct detection results, as illustrated by the blue dashed line. The only region of parameter space not constrained by direct searches for dark matter is that where $M_1 \sim \mu$ (one should however bear in mind that the location of this sliver of the parameter space depends on the details of the gaugino mass hierarchy). An improvement by a factor of 10 in the direct detection sensitivity will significantly extend the parameter space excluded by dark matter searches, as illustrated by the dot-dashed light-blue line.

Neutrino telescopes also very effectively probe wino-like dark matter in the context of an MSSM realization with successful EWB, as shown by the left panel of Fig. 3.6. The effect of resonant neutralino annihilation via the CP-odd Higgs A is

shown clearly in the shape of the exclusion limits, including the the curve outlining the future performance of the full IceCube plus DeepCore detector. Current IceCube data [52] probes neutralinos as heavy as almost 0.5 TeV, but leaves both the bino-driven EWB funnel and the high-mass tip of the wino-driven EWB funnel as viable parameter space regions.

Finally, the right panel of Fig. 3.6 indicates the regions ruled out by Fermi observations of dSph. Here, similarly to the $M_1 < M_2$ case, the parameter space regions excluded by gamma-ray data mainly depend upon the size of the ratio $\langle \sigma v \rangle / m_\chi^2$. The excluded regions correspond to wino or higgsino-like light neutralinos, or to resonantly annihilating heavier neutralinos with a mass $m_\chi \simeq m_A/2$. Remarkably, we find that the $M_1 = 3M_2 \sim \mu$ funnel is entirely ruled out by gamma-ray data, as it falls in a region of light wino-like dark matter.

We thus find that MSSM EWB with an $M_2 < M_1$ gaugino mass hierarchy is essentially ruled out by dark matter searches, if the lightest neutralino is the main dark matter constituent. Also, wino-like dark matter is not compatible with EWB, as illustrated by the upper left halves of Figs. 3.5-3.6. An EWB model with $M_2 < M_1$ would thus only be phenomenologically viable if either R-parity were violated, and the lightest neutralino were not stable, or if the lightest neutralino were not the dominant dark matter constituent and some other particle were the dark matter.

We emphasize that these results (and those in the previous sections) follow largely from the relative hierarchy of the gaugino masses and do not depend sensitively on their particular values. On the one hand, the dark matter search constraints are de-

termined primarily by the lightest gaugino mass and μ and are insensitive to the precise mass of the heavier gaugino. On the other hand, regions compatible with successful EWB depend on the relation between μ and $M_{1,2}$; changing the details of the gaugino mass hierarchy affects the curves of constant Y_B in Figs. 3.1-3.6 by squeezing the upper funnel either towards the lower funnel or towards the μ-axis. If pushed downwards, larger portions of these EWB-compatible regions will typically be probed by direct detection and neutrino telescope data, which inherently constrain the lightest gaugino $\sim \mu$ funnel (this is where the LSP has maximal gaugino-higgsino mixing). If the upper funnel is pushed towards the μ-axis, portions of this region for the $M_1 < M_2$ -type hierarchy will generally still be allowed, as observations of dSph will mostly probe higgsino-like and resonantly annihilating LSPs. For the $M_2 < M_1$ case, however, gamma ray telescopes will additionally constrain the upper left half of the (M_2, μ) plane where any potentially successful bino-diven EWB will take place (this funnel is always smaller in size than the $M_2 \sim \mu$ funnel because the bino-higgsino resonance cannot occur through chargino exchange [30]), thus generally combining with the direct detection and neutrino telescope results to rule out virtually all of the parameter space viable for EWB, independent of the details of the gaugino masses.

3.1.4 EWB and the Large Hadron Collider

As the neutralinos and charginos in the resonant EWB scenario under consideration are relatively light, with masses typically in the 100 GeV-1 TeV range, one might hope to observe their production from collisions at the Large Hadron Collider
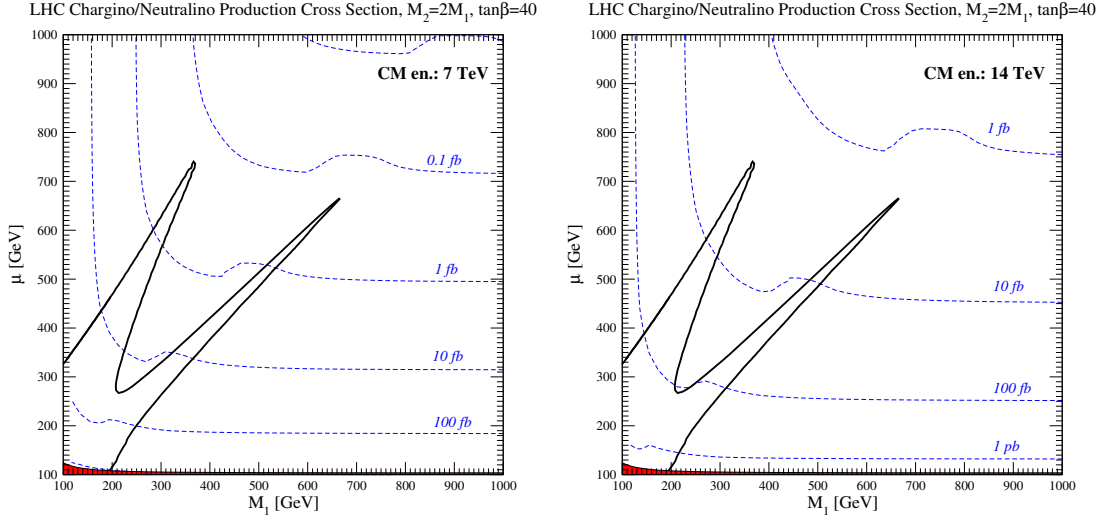
Figure 3.7: Curves of constant total -ino production cross-section at the LHC for points in the (M_1, μ) plane for the gravity-mediated supersymmetry breaking gaugino mass hierarchy, with $\sqrt{s} = 7$ TeV (left) and 14 TeV (right), and with $\tan\beta = 40$, $m_A = 300$ GeV and all other parameters as discussed in the text. Also shown are regions compatible with resonant chargino-neutralino electroweak baryogenesis, on the (M_1, μ) plane for the same values of the other parameters and maximal gaugino-higgsino CP-violating phase $\sin\phi_\mu = 1$.
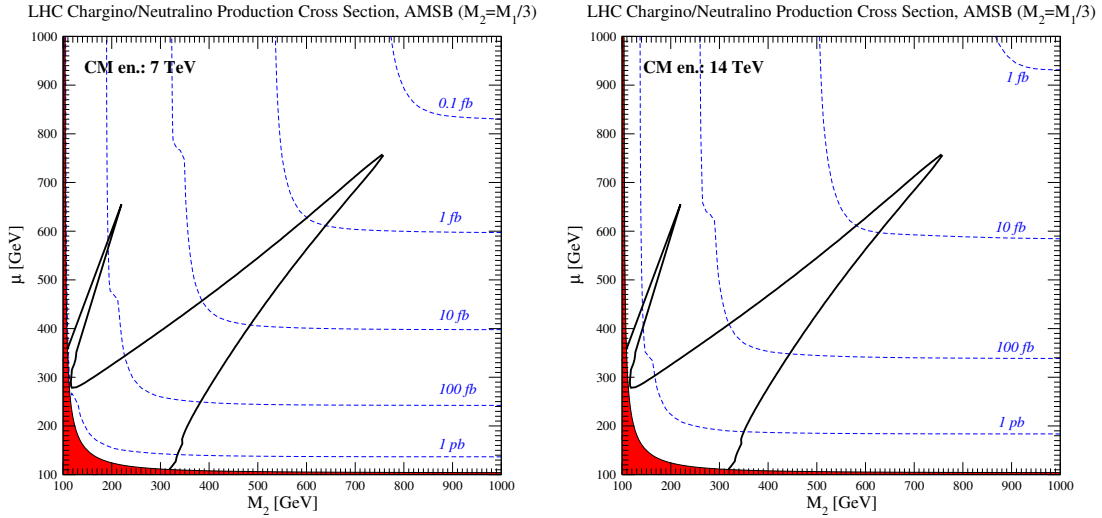
Figure 3.8: Same as Fig. 3.7 in the (M_2, μ) plane for the AMSB gaugino mass hierarchy

(LHC). All other sparticles in this picture possess masses in the multi-TeV range and are thus not expected to be produced in significant numbers at the LHC. The possible exception is the gluino, which would be naturally expected to have a mass scale comparable to that of the other two gauginos (the wino and bino). The gluino mass is, however, entirely unrelated to the phenomenology of EWB, and is thus essentially a free parameter, making it difficult to ascertain sensible predictions for the LHC based upon gluino production. We therefore only consider the electroweak -inos, i.e. charginos and neutralinos, in what follows.

We calculate here the leading order (LO) total cross-section for electroweak production of neutralinos/charginos at the LHC, with all possible pairs of -inos in the final state, for points in the gaugino-higgsino mass planes suitable for resonant EWB using a modified version of PROSPINO [56]. We do so for center-of-mass energies $\sqrt{s} = 7$ TeV and 14 TeV, and outline curves of constant total cross-section in the (M_1, μ) and (M_2, μ) planes for the gravity-mediated SUSY breaking and AMSB scenarios, respectively. Our results are displayed in Figs. 3.7 and 3.8. For the particle spectrum, we use the values for the masses and MSSM parameters discussed in the previous Sections while calculating the neutralino/chargino masses and their mixing matrices for each point in the $(M_1(M_2), \mu)$ planes.

The various -ino production cross sections approximately follow the particle spectrum, as expected e.g. from the results displayed in Figs. 15-16 of Ref. [57], which pertain to the particular slices of the (M_1, μ) parameter space with a thermal relic density matching the dark matter density. As in Ref. [57] we also find that the largest

production cross sections correspond, typically, to the next-to-lightest neutralino plus chargino ($\widetilde{\chi}_2^0 \widetilde{\chi}_{1,2}^{\pm}$), and to lightest chargino pairs ($\widetilde{\chi}_1^+ \widetilde{\chi}_1^-$); also significant are cross-sections corresponding to $\widetilde{\chi}_2^0 \widetilde{\chi}_2^0$ and $\widetilde{\chi}_2^+ \widetilde{\chi}_2^-$ final states. Ref. [57] considered in detail the so-called clean trilepton signature [58], originating from both chargino-neutralino and from neutralino-neutralino production. After imposing cuts on the lepton transverse momentum, on invariant dilepton masses and a transverse mass veto, and after considering in detail Standard Model backgrounds, Ref. [57] concluded that the 5σ discovery potential for the LHC with a center of mass energy of 14 TeV and with 100 fb^{-1} integrated luminosity corresponds to a total -ino production cross section (before cuts) of about 600 fb.

While other strategies besides the clean trilepton signature with the cuts implemented in Ref. [57] are possible and should be pursued, our predicted total -ino production cross sections indicate that the LHC reach in this channel will not exhaust the parameter space covered by dark matter searches. Specifically, we find that a cross section on the order of 600 fb for 14 TeV center of mass collisions will only probe the low-mass end of the EWB-compatible (M_1, μ) parameter space, namely values of $\mu \lesssim 200$ GeV (see Fig. 3.7). Slightly larger values of μ might be accessible if $M_2 < M_1$, but far from exhausting the EWB-compatible parameter space in the wino-resonant funnel, see Fig. 3.8.

Finally, we note that the study in Ref. [57] suggests that the 14 TeV LHC with 10 fb^{-1} of integrated luminosity accesses cross sections $\gtrsim 6$ pb via the clean trilepton channel, with the 7 TeV LHC probing only larger cross sections. Thus we see from

Figs. 3.7-3.8 that the current 7 TeV LHC run at the time of writing has so far probed very little of the relevant parameter space for $M_2 = 2M_1$ (the corresponding region has in fact already been ruled out by LEP [29]; see e.g. Fig. 3.1) and only a small sliver of the parameter space near the bottom and left edges of Fig. 3.8 for the $M_1 = 3M_2$ scenario.

3.2   Scalar Sources

Let us now turn our attention to the scalar sources. In view of the fast pace with which the LHC is exploring the electroweak scale, and especially the supersymmetric sfermion sector, evaluating the potential relevance of sfermions to produce the observed baryon asymmetry is important. In addition, the program of searches for EDMs at the "intensity frontier" is also here demonstrated to be highly synergistic to the collider "energy frontier"; searches for the EDM of multiple particle and atomic species is also crucial to testing the EW route to baryogenesis. Also, while it is too early to draw strong conclusions, LHC searches for the Higgs might indirectly point to a scenario with light staus (see e.g. [59]), potentially making the new source class we discovered all the more appealing.

The main result of this Section is that the current EDM search limits – particularly the one obtained for the Mercury atom [60] – eliminate the possibility that CP violating sources stemming from light and/or quasi-degenerate stops or sbottoms could be the main triggers for successful EWB. On the other hand, a new class of CP violat-

ing sources associated with third generation sleptons is subject to considerably weaker EDM constraints. Consequently, these sources can successfully generate the production of the net left-handed chiral charge needed to produce the observed baryon asymmetry at the EW phase transition. This "stau-mediated EWB" is possible, however, only in relatively narrow strips of parameter space where the two stau mass eigenstates are almost degenerate.

3.2.1 Stop sources

Let us focus first on the stop sector. When the stops scatter off of the spacetime-dependent Higgs vevs in the bubble wall, the CP-violating phase ϕ_t arising between the tri-scalar coupling A_t and μ results in a non-zero expectation value of the current density $\tilde{t}_R^\mu$ in and in front of the wall, governed by

$$\partial_\mu \tilde{t}_R^\mu(x) = S_{\tilde{t}_R}(x, \{n_i\}). \tag{3.20}$$

Here $S_{\tilde{t}_R}(x, \{n_i\})$ contains both the CP-violating source term as well as the CP-conserving chirality changing rates that also arise from stop scattering off of the Higgs vevs in the plasma, Yukawa interactions and strong sphaleron rates. To obtain the Boltzmann equations for the stop case as in Eqs. (5.35-3.13), one must verify that the supergauge interactions governing the various particle and sparticle densities are in fact in equilibrium for the range of parameters we consider. Since we will vary the soft breaking masses of both stops, one should be concerned that in some regions of the parameter space, the supergauge interactions involving $\tilde{t}_R$ and $\tilde{t}_L$ will be slow (since

these rates are Boltzmann suppressed) or kinematically forbidden, since these rates arise from three-body interactions of the (s)quarks with gauginos. We plot the super-gauge equilibration time scale in Fig. 3.9 along with τ_{diff} for comparison (note that the kinematically forbidden region depends on the precise choice for the gaugino masses). While the supergauge rate $\Gamma_V^{\tilde{t}t}$ is kinematically forbidden for very light RH stops, $\Gamma_V^{\tilde{q}q}$ is nowhere forbidden. This is because the latter is a sum of both $\tilde{W}$ and $\tilde{B}$ contributions which are disallowed for different $M_{\tilde{Q}_3}$, and so when $\tilde{W}$ interactions are disallowed, $\tilde{B}$ interactions can still be active and vice versa (again, this depends on the details of the gaugino masses). Everywhere else both LH and RH rates are quite fast compared to τ_{diff}. The only other exception is the region corresponding to heavy squarks, where the baryon asymmetry is also expected to be suppressed. Since $\tau_{eq} \ll \tau_{\mathrm{diff}}$ for most of the parameter space relevant for EWB we work under the simplifying approximation that stop-top supergauge equilibrium holds in all regions of interest when computing Y_B. Additionally, there are supergauge rates involving the other charge densities occurring in Eqs. (5.35-3.13): we have verified that the corresponding rates for Higgs and higgsino densities are also fast compared to τ_{diff} for our choices of parameters, detailed below. The supergauge rates for the heavy squarks we consider are suppressed, and their equations decouple from the full set in Ref. [22]. As a result, the density Q_1 consists entirely of fermions, $Q_1 = q_1$.

In computing the baryon asymmetry we use the form of the sources computed in Ref. [23] and related work, which exhibit resonant behavior for nearly degenerate RH- and LH- stop masses. We quote the form of the stop CP-violating source $S_{\tilde{t}}^{CPV}$
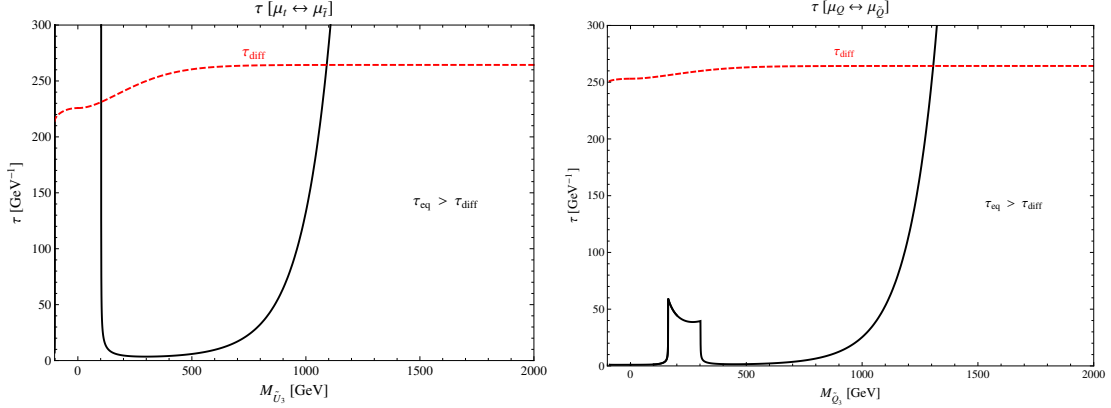
Figure 3.9: Supergauge equilibration time scales for the RH (s)tops (Left) and LH (s)quarks (Right), where $M_{\tilde{Q}_3}$ ($M_{\tilde{U}_3}$) = 1000 GeV in computing the RH (LH) stop rates and M_1 = 100 GeV, M_2 = 200 GeV. Also shown is the diffusion time-scale τ_{diff} in both cases. The superequilibrium timescale is longer than τ_{diff} only in kinematically forbidden regions and for heavy squarks, where the baryon asymmetry is suppressed.

here, to allow straightforward generalizations to the cases of sbottom and stau sources in the following sections:

$$
\begin{aligned}
S_{\tilde{t}}^{CPV}(x) = &\frac{N_C y_t^2}{2\pi^2} \text{Im}(\mu A_t) v^2(x) \dot{\beta}(x) \\
&\times \int_0^\infty \frac{dk k^2}{\omega_R \omega_L} \text{Im} \left[\frac{n_B(\mathcal{E}_R^*) - n_B(\mathcal{E}_L)}{(\mathcal{E}_L - \mathcal{E}_R^*)^2} + \frac{n_B(\mathcal{E}_R) + n_B(\mathcal{E}_L)}{(\mathcal{E}_L + \mathcal{E}_R)^2} \right]
\end{aligned}
\tag{3.21}
$$

The various quantities involved are given by

$$
\mathcal{E}_{L,R} = \omega_{L,R} - i\Gamma_{L,R}
\tag{3.22}
$$

$$
\omega_{L,R} = \sqrt{|\mathbf{k}|^2 + m_{\tilde{t}_{L,R}}^2}
\tag{3.23}
$$

$$
h_B(x) = -\frac{e^{x/T}}{(e^{x/T} - 1)^2}
\tag{3.24}
$$

$$
n_B(x) = \frac{1}{e^{x/T} - 1}
\tag{3.25}
$$

where Γ_i are the thermal widths of the stops which are $\mathcal{O}(10^{-1}T)$, $v_{u,d}$ are the spacetime-dependent Higgs vevs, $v^2 = v_u^2 + v_d^2$, $\tan\beta = v_u/v_d$, y_t is the top Yukawa coupling, T is the EWPT temperature, N_C is the number of colors, and $m_{\tilde{t}_{R,L}}$ are the effective

62

stop masses given in terms of the corresponding soft breaking and thermal masses by $m_{\tilde{t}_{L,R}}^2 \equiv M_{\tilde{Q}_3,\tilde{U}_3}^2 + M_{T;L,R}^2$. The dependence of Eq. (3.21) on the CP-violating phase ϕ_t is apparent. Also, the CP-violating source (and the chirality-changing CP-conserving rates) are manifestly spacetime-dependent, as they are proportional to the Higgs vevs. We use a simplified step-function profile for these rates and sources, deferring a careful treatment of the bubble profile to future study. Note also that we have omitted a temperature-independent contribution to the numerator of the second term in Eq. (3.21) that appears in the corresponding expression in Ref. [23]. The current density from which the CP-violating source is derived must be properly normal-ordered through a subtraction of the zero-temperature matrix element. Implementing this normal ordering effectively removes the temperature-independent contribution to the numerator[6].

In addition to the CP-violating source Eq. (3.21), we use the form of the relaxation, Yukawa, triscalar, and strong sphaleron rates worked out in Ref. [22]; we do not reproduce them here for brevity. Since we are interested in only the stop CP-violating source contribution to the BAU, we take the RH sbottom and RH, LH stau masses to be heavy which allows us to neglect the (s)bottom, (s)tau Yukawa rates - with heavy superpartners, only SM-like Yukawa interactions contribute to these rates, resulting in $\Gamma_{yb,\tau} \ll \Gamma_{yt}$, Γ_{ss} in virtually all of the parameter space we consider. With this choice of spectrum we can also neglect the CP-conserving chirality changing rates Γ_{mb} for the (s)bottoms, which are suppressed by factors of $\left(\frac{y_b}{y_t}\right)^2 \cot^2 \beta$ with respect to Γ_{mt} [21]. With these simplifications, the only source for B charge density are strong

_____

[6]We thank C. Lee for this observation and T. Liu for highlighting this issue in an earlier version of this work.

sphalerons, implying that $B = -(Q+T) = -\frac{1}{2}Q_1$ and consequently simplifying Eq. (3.7)

to

$$n_L = \frac{k_q}{k_Q}Q + 4(Q+T). \tag{3.26}$$

Due to the relation between B and Q_1 and the decoupling of the (s)leptons which occurs when neglecting their Yukawa couplings, the full set of Boltzmann equations reduces to Eqs. (5.35), (5.36), and (3.11) with the replacements $\Gamma_{yb,y\tau}$, $\Gamma_{mb} \to 0$, $Q_1 \to 2(Q+T)$, coinciding with the set described in Ref. [23] and which we use in our numerical computation of the BAU.

There are several uncertainties built into our computation of the baryon asymmetry. In addition to those arising from the vev-insertion approximation, theoretical uncertainties in several other parameters associated with the phase transition such as the bubble wall thickness, velocity, and variation of the Higgs vevs $\Delta\beta$ can introduce $\mathcal{O}(100~\text{GeV})$ uncertainties in the curves of constant baryon density, similarly to the case of higgsino/gaugino sources, as discussed in the preceding Section. For concreteness, here we consider conservative values for the wall velocity, $v_w = 5/100$, and thickness, $L_w = 5/T_c$. Additionally, non-resonant sources such as those computed in Refs. [43] and related work yield results for the BAU that can differ significantly from the values computed using the vev-insertion approximation, especially away from the resonance. To take into account the uncertainties associated with a precise calculation of the BAU, we show on selected plots curves corresponding to $10 \times Y_{Obs}$, as a rough upper bound on the stop source scenario, as well as curves of $0.1 \times Y_{Obs}$ as a more conservative estimate of the BAU. As we will see, our conclusions hold across this wide range of uncertainty.

3.2.1.1 Parameter Space

The baryon asymmetry produced by stop sources depend on the masses $m_{\tilde{t}_{L,R}}$, which are temperature dependent. Since the thermal masses are constant at a given temperature, we can equivalently investigate the potential of stop sources to produce the observed BAU by varying the values of the LH and RH stop SUSY breaking soft masses, $M_{\tilde{Q}_3,\tilde{U}_3}$. We vary $M_{\tilde{U}_3}$ over the range -100^2 GeV^2 $\leq M_{\tilde{U}_3}^2 \leq 2000^2$ GeV^2, which includes the so-called "light stop scenario" for $M_{\tilde{U}_3}^2 < 0$ (and multi-TeV $M_{\tilde{Q}_3}$), a region of the parameter space where the light RH stop provides the strongly first order phase transition needed for successful baryogenesis. We stress that away from negative values of $M_{\tilde{U}_3}^2$, some other mechanism is needed to generate a strongly first order phase transition. Several such mechanisms have been proposed [61, 37, 38] that are decoupled from the spectrum required for EWB and from the physical processes of interest for the present discussion. Thus, in evaluating the potential of stops, sbottoms, and staus for EWB, we consider only the strength of the CP-violation in each case and assume a strongly first-order EWPT generated by one of these other mechanisms. For the LH stops, we vary $M_{\tilde{Q}_3}$ over the range 100 GeV $\leq M_{\tilde{Q}_3} \leq 4000$ GeV. Within these mass ranges there are regions where the choice of soft mass leads to negative or zero mass squared for the lightest stop at $T = 0$ for various values of the triscalar coupling and μ; we indicate these regions (along with more stringent constraints on stop masses from direct searches discussed in Sec. 3.2.1.2) on all of our plots. For the stops, we focus on $\tan\beta = 10$. One should note that larger $\tan\beta$ yields larger SM-like Higgs masses along

with more stringent EDM constraints.

There are several other parameters whose values need to be fixed in order to calculate the BAU. We choose values for these parameters conservatively, bearing in mind the various constraints from Higgs mass measurements, stop searches, and EDM search null results as well as theoretical considerations such as the avoidance of color and charge-breaking vacua. In computing the baryon asymmetry, we take $m_A = 200$ GeV. For larger m_A, the baryon asymmetry is reduced due to the dependence of $\Delta\beta$ on m_A, which scales as $\Delta\beta \sim 1/m_A^2$ [43]. The gaugino soft masses are taken to be real, with $M_1 = 80$ GeV, $M_2 = 250$ GeV to ensure a light neutralino χ_i^0 as the lightest supersymmetric particle (LSP) while other gauginos are rather heavy. For the scenario we consider here the resulting baryon asymmetry and Higgs mass constraints do not depend sensitively on M_1, M_2. The gluino soft mass is largely decoupled from the phenomenology relevant here, and was set to $M_3 = 10$ TeV. For the higgsino mass parameter μ (which we take to be real, so that ϕ_t arises only from the phase in A_t), we choose $\mu = 200$ GeV, 1000 GeV to illustrate the behavior of the baryon asymmetry and the various constraints in these cases. Small values of μ suppress the BAU (c.f. Eq. (3.21)), while large values can make the zero-temperature physical stop masses squared negative by making the off-diagonal components of the mixing matrix large, as well as strengthen the various EDM constraints. Similarly, we vary the magnitude of the trilinear scalar coupling $|A_t| = 100$ GeV, 250 GeV, 1000 GeV; larger values of $|A_t|$ also result in larger exclusions from EDM constraints. We typically consider the case of maximal CP-violating phase $\phi_t = \pi/2$ to show the maximal extent of the

EWB-compatible parameter space. We rely on this phase to produce all of the baryon asymmetry, setting all other CP-violating phases $\phi_i = 0$ to isolate the contribution from the stop sources to the BAU. Otherwise, non-stop sources such as those arising from gaugino-higgsino-vev interactions will further contribute to the baryon asymmetry and there will be additional contributions to the EDM constraints. Finally, all other triscalar couplings are taken to be zero, and all other sfermions in our analysis are taken to be heavy, $m_{sf} = 10$ TeV. As shown in Ref. [22], this effectively decouples them from the network of transport equations, since superequilibrium and Yukawa rates that can transfer charge density between SM particles and their superpartners vanish for any of the masses much larger than the temperature. As a result, the densities $\{I\}$ appearing in the transport equations for these sfermions (e.g. Q_1) correspond entirely to an SM particle charge density, $k_I = k_i$.

Using this spectrum, we calculate the baryon asymmetry generated by stop scattering off of the bubble wall and outline regions of the stop mass parameter space suitable for successful EWB in Figs. 3.10-3.11; regions consistent with the observed value of Y_B are shaded. The contours shown correspond to maximal CP-violating phase $\sin \phi_t$, while for smaller phase the baryon asymmetry is suppressed as are the EDM constraints. Decreasing $|\sin \phi_t|$ does not open up any additional parameter space for EWB. Several important features of the sources are shown in Figs. 3.10-3.11. From Eqs. 3.21, 3.22, the CP-violating source is resonant for $m_{\tilde{t}_R} \sim m_{\tilde{t}_L}$. This manifests itself as a resonance for $M_{\tilde{U}_3}^2 \sim M_{\tilde{Q}_3}^2 + (M_{T;L}^2 - M_{T;R}^2) \approx M_{\tilde{Q}_3}^2$ in the parameter space as shown.

Also, there is an increase in the generated BAU for $M_{\tilde{U}_3}^2 < 0$. This feature arises far from the resonance [7] but is straightforward to understand from the form of the CP-violating stop sources. The quantities $w_{R,L}$, $\mathcal{E}_{R,L}$ entering into $S_{\tilde{t}}^{CPV}$ depend on the physical masses $m_{\tilde{t}_{R,L}}^2 = M_{\tilde{Q}_3,\tilde{U}_3}^2 + M_{T;R,L}^2$ and for $M_{\tilde{U}_3}^2 \to -M_{T;R}^2$, the physical mass $m_{\tilde{t}_R} \to 0$. In this regime, the Boltzmann distributions in the integrand for $S_{\tilde{t}}$ begin to diverge for $k = 0$, $n_B(k) \to 1/\left(e^{|k|-i\Gamma} - 1\right)$ which corresponds physically to the abundance of nearly massless squarks produced in the thermal bath. We emphasize that $M_{\tilde{U}_3}^2 < 0$ does not result in a tachyonic stop in the unbroken phase as long as $M_{\tilde{U}_3}^2 > -M_{T;R}^2$ (the thermal masses are $\mathcal{O}(100 \text{ GeV})$ so this is not an issue in the parameter space we consider). On the other hand, the zero-temperature stop mass eigenstates can turn negative in some of the parameter space; the corresponding regions are of course ruled out by direct searches for stops, corresponding to the black shaded regions in Figs. 3.10-3.11.

Finally, we find that there are regions for which the produced baryon asymmetry switches sign. This effect arises due to the competition between Q and T densities in the expression for n_L, Eq. (3.26); since Q and T densities carry opposite sign, when $M_{\tilde{Q}_3}$ is small, k_q/k_Q decreases and the T contribution can win out and drive $n_L \geq 0$. In Figs. 3.10-3.11, regions with $Y_B > 0$ are shaded green, while regions for which $Y_B < 0$ are shaded blue. Since at present the phase ϕ_t is not experimentally constrained, either region can lead to the appropriate overall sign for the baryon asymmetry through an appropriate choice of ϕ_t.

---

[7]We caution the reader that away from the resonance, there may also be non-resonant contributions to the sources [43] which we do not consider here.
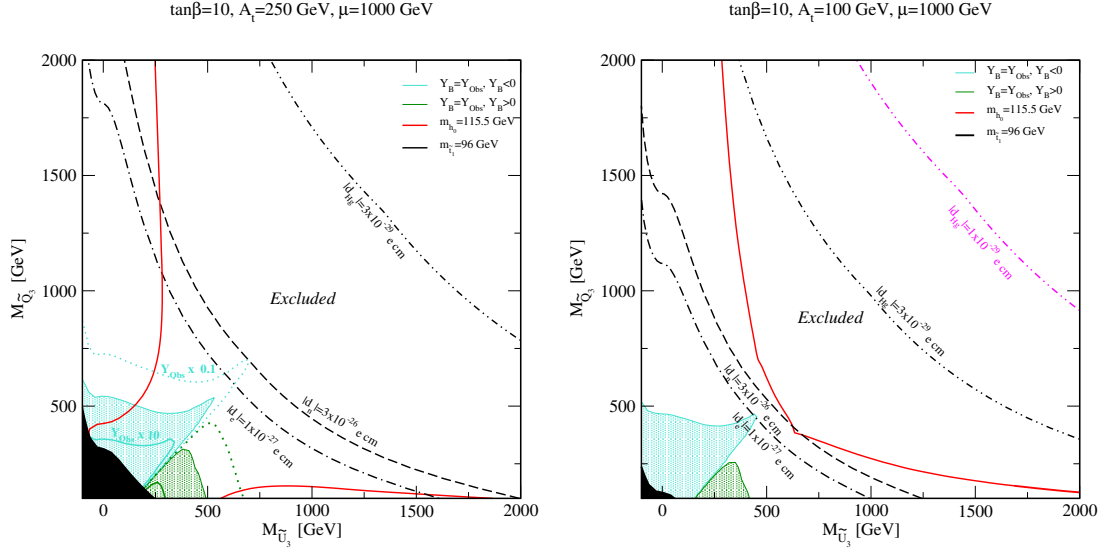
Figure 3.10: Regions of the stop soft supersymmetry breaking mass parameter space consistent with the observed value of the baryon asymmetry resulting from stop sources for $\mu = 1000$ GeV, $|A_t| = 250$ GeV (Left) and $|A_t| = 100$ GeV (Right). Regions shaded blue (green) correspond to $Y_B \geq Y_{Obs}$ with $Y_B < 0$ ($Y_B > 0$) for maximal CP-violating phase. The dotted blue contour on the left marks the region that would be consistent with stop-sourced EWB if the vev-insertion approximation had underestimated Y_B by a factor of 10 (we omit this curve in subsequent plots). On the left we also show, by the darker shaded regions, the parameter space compatible with $10\times$ the observed BAU, i.e. the allowed regions if the vev-insertion approximation overestimated Y_B by a factor of 10. Black shaded regions are excluded by stop mass direct searches; regions to the left of the thick red line are excluded by LEP Higgs mass bounds in both cases. Current constraints on the electron, neutron, and ^{199}Hg EDMs are represented by the black dashed-dot, dashed, and dashed-double-dot lines, respectively, with regions to the left of each line ruled out by null results; the projected future reaches for d_e, d_n, and d_{Hg} measurements are shown in magenta (where applicable). In both cases here, both the d_e and d_n future sensitivities lie above the plane shown. For the $|A_t| = 250$ GeV case, the Mercury EDM future sensitivity also lies above the plane shown.

3.2.1.2   Stop and Higgs Mass Constraints

Having calculated the BAU resulting from stop sources, one should ask how the stop mass parameter space consistent with successful EWB confronts various other phenomenological constraints. We consider three types of constraints on our EWB scenario: stop mass constraints from collider searches, Higgs mass bounds, and electric dipole moment search null results.
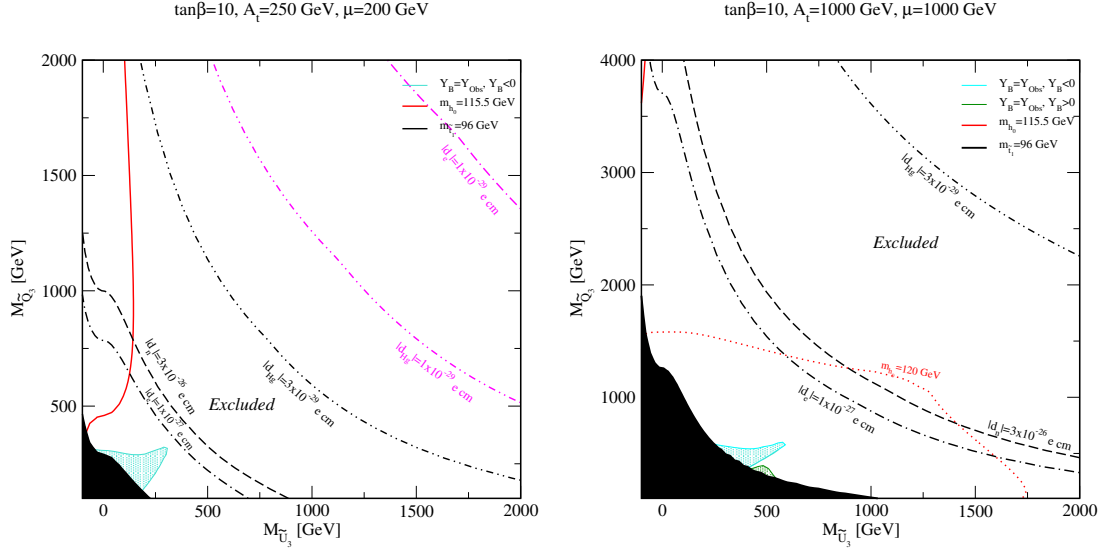
69

Figure 3.11: Same as Fig. 3.10, but for $|A_t| = 250$ GeV, $\mu = 200$ GeV (Left) and $|A_t| = 1000$ GeV, $\mu = 1000$ GeV (Right). For $|A_t| = 250$ GeV, the $Y_B > 0$ curve falls beneath the black shaded region and future measurements of the neuron EDM are expected to probe all parameter space shown. For $|A_t| = 1000$ GeV, the expected reaches of d_e, d_n, and d_{Hg} future measurements lie above the plane shown here.

Zero-temperature stop masses have been constrained by direct searches for superpartners at LEP and the LHC (for particle spectra relevant here) to be $m_{\tilde{t}_1} > 96$ GeV [62]. This lower bound arises from considering stop decays to the LSP, typically assumed to be the lightest neutralino. With our choice of gaugino masses, the lightest stop $\tilde{t}_1$ is heavier than χ_1^0 in all of the parameter space so that this lower bound on $m_{\tilde{t}_1}$ is applicable. There are several specific cases in which the stop masses might be more tightly constrained, however for generality we consider this lower bound for our scenario. We calculate the physical $T = 0$ stop masses using FeynHiggs [63] for the choices of parameters discussed above and indicate $m_{\tilde{t}_1} \leq 96$ GeV on our plots by the black shaded region. Increasing $|A_t|$ leads to larger regions of parameter space for which the lightest stop falls below the lower bound. This is because the triscalar coupling appears in the

off-diagonal entries in the stop mass matrix and large values reduce the value of the smaller eigenvalue.

The mass of the SM Higgs has been constrained by LEP to be $m_{h_0} > 115.5$ GeV [64, 65]. We use `FeynHiggs` to calculate the mass of the SM-like Higgs to two-loop order and indicate the LEP bound by a thick red line on our plots. In addition to the lower bound from LEP, recent preliminary results from both ATLAS and CMS experiments have indicated the possibility of a SM-like Higgs with $m_{h_0} \approx 125$ GeV [66]. However, for light stops and small $|A_t|$, the corrections to m_{h_0} arising from diagrams with stop loops typically needed to increase the mass of the SM-like Higgs in the MSSM are suppressed, and we find no parameter space consistent with $m_{h_0} = 125$ GeV. For larger $|A_t|$, the stop loop corrections can be enhanced and the Higgs mass can be pushed up to $m_{h_0} \approx 120$ GeV (which we indicate on the plot corresponding to $|A_t| = 1000$ GeV, $\mu = 1000$ GeV with a red dotted line), however we find that $m_{h_0} = 125$ GeV is difficult to obtain for our choices of parameters. We note that additional field content, such as the inclusion of a gauge singlet in the superpotential in e.g. the NMSSM, which may be required to provide a strongly first order phase transition in these scenarios, can result in large contributions to m_{h_0}, even at tree level. Thus, our Higgs mass contours should not be taken as strict exclusions, but as illustrating the tension encountered in the MSSM between light third generation scalars and a heavy SM-like Higgs.

3.2.1.3 EDM Constraints

CP-odd couplings in the MSSM will generally give rise to electric dipole moments (EDMs) of elementary fermions, nucleons, and neutral atoms. To date, no EDM has been experimentally observed, with the most stringent limits having been obtained on the EDM of the neutral Mercury atom [60] ($|d_{Hg}| < 3 \times 10^{-29} e$ cm), electron (via the YbF molecule) [67] ($|d_e| < 1.05 \times 10^{-27} e$ cm), and neutron [68] ($|d_n| < 2.9 \times 10^{-26} e$ cm). The non-observation of these EDMs places powerful constraints upon the strength of the CP-odd sources used in EWB (for a discussion of the constraints relevant to Higgsino-Bino-Wino driven MSSM baryogenesis, see, *e.g.*, Refs. [28, 69]) . On-going efforts could improve the sensitivity of EDM searches by up to two orders of magnitude (for a review, see, *e.g.*, Ref. [70]), suggesting the future possibility of even more stringent constraints or the observation of an EDM with a magnitude consistent with the requirements of MSSM EWB.

In order to analyze the impact of the present and prospective constraints, we use the program `CPsuperH` [71] to compute the relevant EDMs under different scenarios. In particular, when CP-violation is generated entirely by the phase ϕ_t, the largest contributions to the relevant EDMs are generated by two-loop graphs that give rise to the Weinberg three-gluon operator (d_G^C) as well as to "Barr–Zee" graph contributions to the elementary fermion EDM (d_f^E) and quark chromo-EDMs (d_q^C). In addition, four-fermion interactions are generated at one-loop order, though the effects of these operators are typically suppressed.

Before proceeding, we note that there exists considerable theoretical uncertainty in the computation of EDMs of strongly-interacting and many-body systems. In the case of diagmagnetic atoms such as ^{199}Hg, the dominant contribution to the EDM arises from the nuclear Schiff moment induced by CP-violating nucleon-nucleon interactions. In general, the most important contribution to the latter is a long-range effect arising from single pion exchange, wherein one of the pion-nucleon vertices (πNN) is CP-odd[8] and the other CP-even. The CP-odd πNN interaction can be induced by the Weinberg three-gluon operator, CP-odd four-quark operator, and/or quark chromo-EDM operator, though in the MSSM the latter contribution typically dominates [72]. The computation of the atomic EDM, thus, encounters several sources of theoretical uncertainty: the calculation of the CP-violating πNN vertices from the underlying CP-violating interaction; the computation of the nuclear Schiff moment that generally requires a scheme for nuclear model-space truncation; and the corresponding atomic physics computation of the induced EDM.

The computation of the neutron EDM is clearly less susceptible to theoretical uncertainties, as only those associated with hadronic effects enter. Nonetheless, these uncertainties can be substantial for both the neutron and atomic EDMs. For example, recent work by the authors of Ref. [73] utilizing the QCD sum rule technique suggests that the sensitivity of the neutron EDM to quark EDM and chomo-EDMs may be a factor of five smaller than given by earlier work [72] that provides the basis for the CPsuperH code. In the case of the nuclear Schiff moment contributions to the ^{199}Hg

---

[8]Technically speaking, the interaction is odd under parity and time-reversal.

EDM, the code has yet to take into account state-of-the-art many body computations [74] that imply substantial differences with the many-body calculations using a simplified, schematic nuclear interaction on which the code is based. Consequently, we caution that the precise numerical results associated with the neutron and ^{199}Hg EDM constraints given below should be taken with a grain of salt (we comment more on the impact of this uncertainty on our results below). To provide an indication of the kind of theoretical uncertainty one might expect, we show in Fig. 3.12(a) computations of the neutron EDM using different approaches as discussed in Ref. [71] (QCD sum rules, the chiral quark model, and parton quark model), though we rely only on the QCD sum-rule technique in our analysis. The QCD sum rule computations tend to give the largest EDM, leading to the strongest constraints.

With these caveats in mind, we observe that the strongest constraint for stop sources comes from the Mercury EDM, for which, in turn, the quark chromo-EDMs provide the most important contribution as shown in Fig. 3.13. We also include the constraint from the electron EDM. For the scenario of interest here, the largest contributions to the d_e EDM come from top and stop loops in Barr–Zee graphs. Note that, like the CP-violating sources, all EDMs are roughly proportional to $|\mu||A_t|$. Therefore, increasing one of these parameters in order to get a model with sufficiently strong baryogenesis also tends to produce a model that is ruled out by EDM searches.
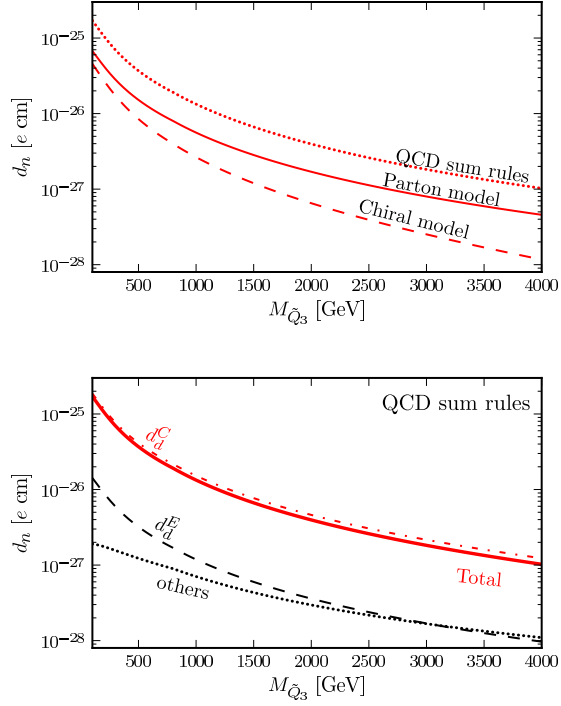
Figure 3.12: Neutron EDMs for $M_{\tilde{U}_3} = 800$ GeV, $\tan\beta = 10$, $\mu = 1000$ GeV and $|A_t| = 250$ GeV. Red denotes negative values. Left: the three independent calculations of the neutron EDM. Right: EDM subcomponents using QCD sum rules. By far the largest contribution comes from the down-quark chromo-EDM d_d^C, followed by the down-quark EDM d_d^E.

3.2.1.4 Results

The various constraints are plotted along with the curves of constant Y_B for different values of μ, $|A_t|$ in Figs. 3.10-3.11. For $|A_t| = 250$ GeV, $\mu = 1000$ GeV, one finds that direct search constraints rule out light, nearly-degenerate stop soft-breaking masses, with the bound from LEP on m_{h_0} excluding portions of the parameter space away from the resonance. Additionally, null results from searches for the electron and neutron EDMs rule out nearly all of the EWB-compatible parameter space except for the
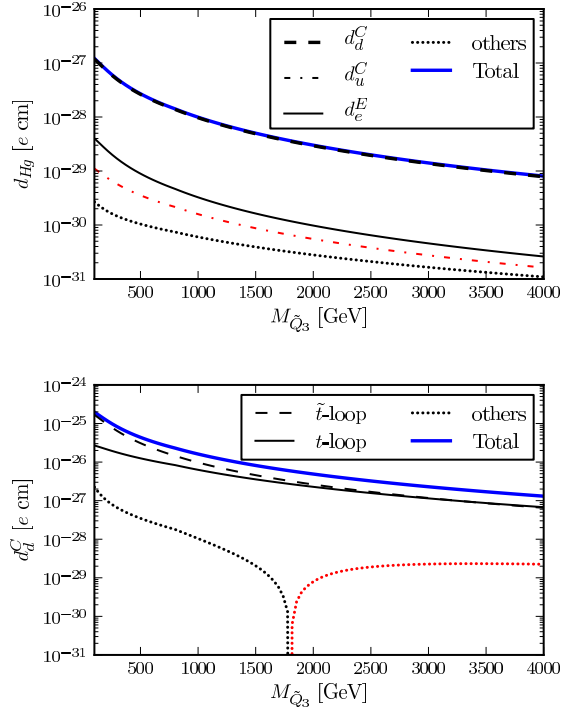
Figure 3.13: Left: a breakdown of the Mercury EDM, using the same parameters as in figure 3.12. Almost the entire contribution comes from the down-quark chromo-EDM (multiplied by a constant factor). Right: a further breakdown of the down-quark chromo-EDM.

tip of the resonance (the expected reach of future EDM experiments are also included in magenta). The strongest constraint is that arising from searches for the ^{199}Hg EDM, which rules out all of the viable parameter space, even excluding regions in which the stops produce 1/10 of the observed BAU. This remarkable result is due to the stringent limit on the Mercury EDM coupled with the relatively large chromo-EDM contributions of diagrams involving stop loops to d_{Hg}. We find a similar landscape for the $|A_t| = 100$ GeV, $\mu = 1000$ GeV case in Fig. 3.10; here the BAU is reduced relative to the $|A_t| = 250$ GeV case and direct searches rule out less of the parameter space because of the reduced

mixing. The Higgs mass constraints are stronger due to the smallness of $|A_t|$ and the LEP bound alone rules out all of the available parameter space for stop-sourced EWB. But once again the ^{199}Hg EDM constraint is the most significant, excluding all parameter space in which the stops produce even 1/10 of the observed BAU. Moving on to the $|A_t| = 250$ GeV, $\mu = 200$ GeV scenario in Fig. 3.11, one might imagine that smaller values of μ, $|A_t|$ may reduce the impact of the EDM constraints enough to open up some of the parameter space for stop-sourced EWB. However, although the EDM constraints are weakened, the baryon asymmetry is also reduced and once again the ^{199}Hg constraints rule out all available parameter space. Finally, increasing both $|A_t|$ and μ to 1000 GeV (see Fig. 3.11) yields larger regions excluded by direct stop searches (due to the large mixing) and weaker Higgs constraints, allowing one to push m_{h_0} up to 120 GeV in parts of the parameter space. The EDM constraints in this case are more stringent, again ruling out all available parameter space for stop-sourced EWB. We note that in addition to the scenarios shown in Figs. 3.10-3.11 we could have also chosen a small value of μ and large $|A_t|$, however in this case the EDM constraints are again very stringent and all the stop-sourced EWB parameter space is excluded; we omit the corresponding figures for brevity (note that in this case one can obtain larger Higgs masses). We have also verified that decreasing $\sin \phi_t$ does not open up any more parameter space for stop sources.

Additionally, varying $\tan \beta$ and/or m_A does not affect our results. Since the stop-sourced baryon asymmetry and EDM predictions for light stop contributions scale with $y_t \sim 1/\sin \beta$, they are both rather insensitive to changes in $\tan \beta$ (we return to the

large-tan β regime in the following section). Increasing m_A suppresses both the overall baryon asymmetry and the expected EDMs, but the BAU varies as $1/m_A^2$ whereas the EDMs only vary as $1/m_A$, so a heavier CP-odd Higgs provides stronger exclusions. Smaller values of m_A can enhance the BAU up to about a factor of 4 (for $m_A = 100$ GeV), but we have checked that this does not overcome the strong EDM exclusions in any of the cases considered.

As discussed above, the computation of d_{Hg} involves significant theoretical uncertainty, which could impact the strength of the above conclusions. However, even if the theoretical prediction for d_{Hg} were in fact an order of magnitude smaller than the values used in Figs. 3.10, 3.11, it would still be just as constraining as the electron-EDM, which by itself rules out virtually all of the parameter space with $|Y_B| \geq Y_{Obs}$. We expect the vev-insertion approximation to *over*-estimate the produced baryon asymmetry, and so it is unlikely that even this large correction would in fact open up any additional space for stop sources in a more careful treatment beyond the approximations used here. Similar considerations hold for the sbottom sources in Sec. 3.2.2 as well.

Summarizing, in considering the various scenarios depicted in Figs. 3.10-3.11, *we find no viable parameter space for MSSM stop-driven resonant EWB consistent with Higgs mass, stop mass, and EDM constraints.* Even conservatively estimating the result of the various uncertainties of the calculations as increasing Y_B by an order of magnitude does not open up any viable parameter space for stop-sourced EWB. The large experimentally excluded regions are primarily a result of the stringent EDM constraints, and particularly that of [199]Hg. We have also verified that even e.g. a factor of ten decrease

in the Mercury EDM limits does not open up any additional parameter space for the stops. It is difficult to see how one might circumvent these constraints to produce the correct baryon asymmetry through a scenario relying primarily on stop sources.

3.2.2 The Large $\tan\beta$ Regime: Sbottom and Stau Sources

We now turn our attention to the other third-generation scalars as a possible source for the observed baryon asymmetry. Since the CP-violating sources arising from triscalar interactions for the sbottoms and staus are proportional to their Yukawa couplings, for these sources to contribute significantly to the BAU, one must consider larger values of $\tan\beta$. For large $\tan\beta$, the sbottom and stau Yukawa couplings, y_b, y_τ, are enhanced as

$$y_b = \frac{m_b}{v\cos\beta}, \qquad y_\tau = \frac{m_\tau}{v\cos\beta}, \tag{3.27}$$

where $v \approx 175$ GeV is the Higgs vev at $T = 0$. In what follows, we take $\tan\beta = 40$ so that the strength of the sbottom and stau CP-violating sources are effectively comparable to that of the stops.

3.2.2.1 Sbottoms

To compute the CP-violating source for resonant sbottom scattering off of the EWPT bubble wall, we make use of the Lagrangian in Eq. (3.2). The sbottom interaction Lagrangian differs from that of the stops by the replacements $\{\tilde{t}, A_t, y_t, v_u, v_d\} \rightarrow \{\tilde{b}, A_b, y_b, v_d, v_u\}$ and the relevant CP-violating phase is $\phi_b = \mathrm{Arg}(\mu A_b b^*)$. One can use these replacements in the non-equilibrium field theory derivation for $S_{\tilde{t}}^{CPV}$ in Ref. [23]

to obtain $S_{\tilde{b}}^{CPV}$. The resulting CP-violating sbottom source is given by

$$
\begin{aligned}
S_{\tilde{b}}^{CPV}(x) = & -\frac{N_C y_b^2}{2\pi^2} \operatorname{Im}(\mu A_b) v^2(x) \dot{\beta}(x) \\
& \times \int_0^\infty \frac{dk k^2}{\omega_R \omega_L} \operatorname{Im}\left[\frac{n_B(\mathcal{E}_R^*) - n_B(\mathcal{E}_L)}{(\mathcal{E}_L - \mathcal{E}_R^*)^2} + \frac{n_B(\mathcal{E}_R) + n_B(\mathcal{E}_L)}{(\mathcal{E}_L + \mathcal{E}_R)^2} \right]
\end{aligned}
\tag{3.28}
$$

where the $\mathcal{E}_{L,R}$, $\omega_{L,R}$ terms are as in Eq. (3.22) with $M_{\tilde{t}} \to M_{\tilde{b}}$ and Γ_i corresponding to the thermal widths of the LH- and RH-sbottoms. Notice that the coupling of the sbottom to the down-type Higgs vev manifests itself as an overall relative sign between $S_{\tilde{b}}^{CPV}$ and $S_{\tilde{t}}^{CPV}$. The source enters into the same set of QBEs, Eqs. (5.35)-(3.13), and since there is now a source for $\tilde{b}_R$, one must include the density Q_1 in the network of equations. Since we take the sleptons to be heavy and the SM leptonic Yukawa interaction rates are small compared to the corresponding rates for the quarks, we neglect $\Gamma_{y\tau}$ in our calculation of the sbottom-sourced baryon asymmetry. As a result, the equations for the densities L and R decouple from the full set of QBEs; the relevant set of Boltzmann equations to solve is then given by Eqs. (5.35), (5.36), (5.37) and (3.11) with the replacement $\Gamma_{y\tau} \to 0$. In terms of the relevant charge densities, the left-handed fermionic charge density in Eq. (3.7) simplifies to

$$
n_L = \frac{k_q}{k_Q} Q + 2Q_1.
\tag{3.29}
$$

We note that since $\tilde{t}_R$ is heavy, the right-handed stops and tops are no longer in superequilibrium. This manifests itself in the contributions to the Yukawa and relaxation rates involving the RH stops vanishing, while the density T in Eq. (5.35) corresponds entirely to a SM charge density. In the parameter space we consider the (s)bottoms are in superequillibrium everywhere except the kinematically disallowed region for the
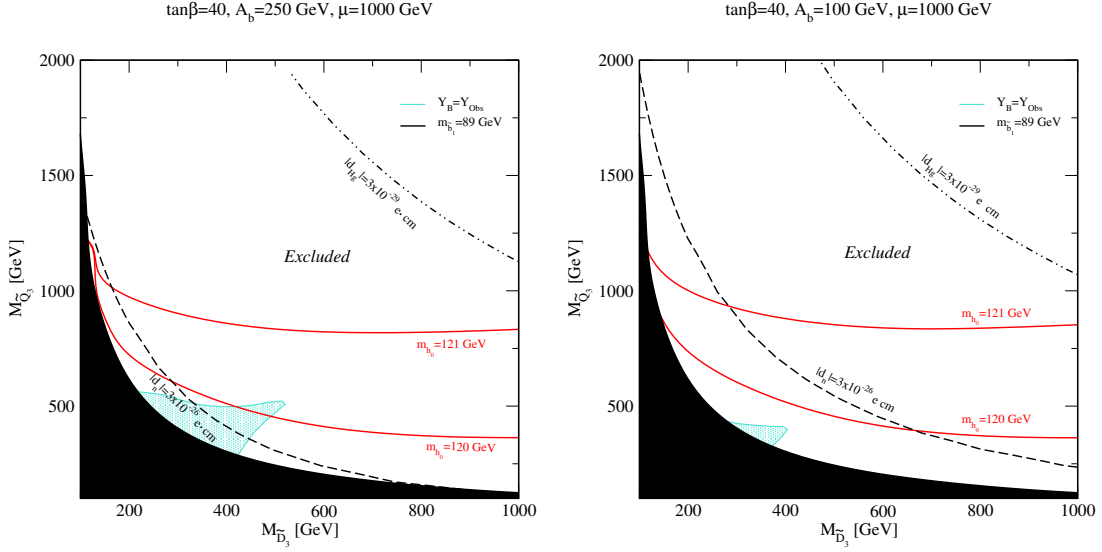
80

Figure 3.14: Regions of the sbottom soft supersymmetry breaking mass parameter space consistent with the observed value of the baryon asymmetry resulting from sbottom sources for $\mu = 1000$ GeV, $|A_b| = 250$ GeV (Left) and $|A_b| = 100$ GeV (Right). Regions shaded blue correspond to $Y_B \geq Y_{Obs}$ for maximal CP-violating phase. The curve corresponding to an overestimate of Y_B by a factor of 10 falls within the black shaded regions, which are excluded by sbottom mass direct searches. Red lines are iso-contours of the SM-like Higgs mass m_{h_0}; the LEP bound is satisfied in all of the parameter space shown. The current constraint on the neutron and Mercury EDMs are represented by the black dashed and dashed-double dot lines, respectively, with regions to the left of each line ruled out by null results. For the $|A_b| = 250$ GeV case, the current d_e bound falls beneath the shaded region while the current constraint on the Mercury EDM rules out all of the parameter space shown. Future EDM measurements of d_e, d_n, and d_{Hg} are expected to definitively probe well beyond the shown parameter space. For the $|A_b| = 100$ GeV case, the electron EDM current bound falls beneath the black shaded region, while future EDM measurements of d_e, d_n, and d_{Hg} will again probe all of the parameter space shown.

RH rate, and we proceed analogously to the (s)top case by assuming $\mu_{\tilde{b}_{L,R}} = \mu_{b_{L,R}}$ superequilibrium in all the parameter space when computing the baryon asymmetry.

We calculate Y_B following the spectrum outlined in Sec. 3.2.1.1, only now with 100 GeV$\leq M_{\tilde{D}_3} \leq 2000$, $M_{\tilde{U}_3} = 10$ TeV, $A_t = 0$, and varying $|A_b| = 100, 250,$ 1000 GeV. As for the stops, we assume that a strongly first order phase transition is generated from some mechanism other than the light stop scenario. The resulting
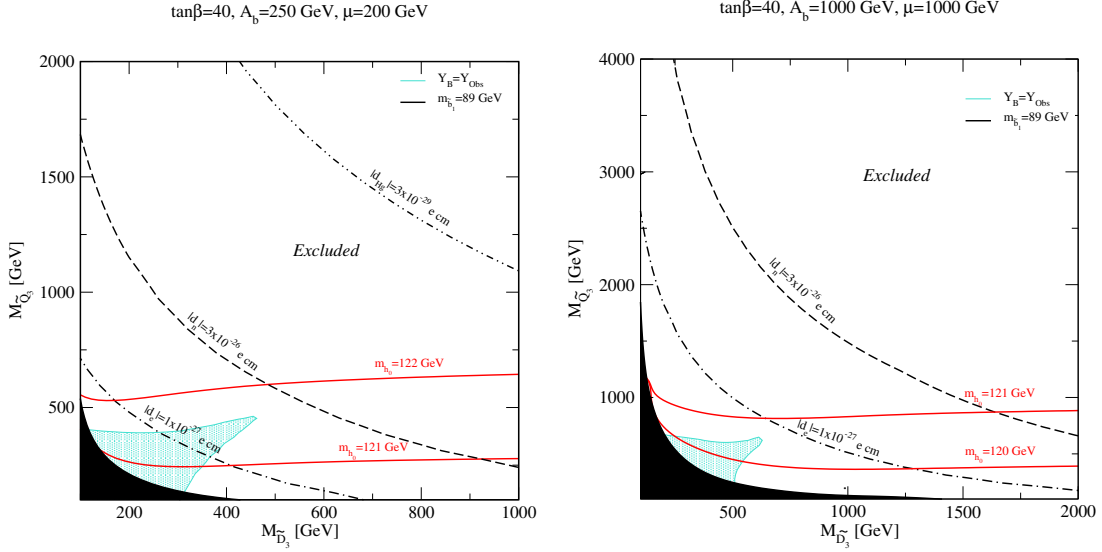
Figure 3.15: Same as Fig. 3.14 but for $|A_b| = 250$ GeV, $\mu = 200$ GeV (Left) and $|A_b| = 1000$ GeV, $\mu = 1000$ GeV (Right). For both the $|A_b| = 250$ and $|A_b| = 1000$ GeV cases, the future reach of electron, neutron, and Mercury EDM measurements is expected to probe the entire parameter space shown. For the $|A_b| = 1000$ GeV case, the current Mercury EDM constraint already rules out all of the parameter space shown.

sbottom-sourced BAU is plotted in Figs. 3.14-3.15, where regions compatible with the observed asymmetry are shaded blue (we find no sign change in Y_B for the sbottoms with our choices of parameters). The resonance in the CP-violating source is again apparent.

In Figs. 3.14-3.15 we also show the lower bound on the sbottom mass from direct searches, $m_{\tilde{b}_1} \gtrsim 89$ GeV [62] and contours of constant SM-like Higgs mass. The LEP bound on m_{h_0} is satisfied in all regions of parameter space considered. Since the mass of the RH stop is heavy, m_{h_0} receives larger contributions from stop loops compared to the stop-source case and one can easily push the Higgs mass up to $m_{h_0} \approx 120$ GeV, however larger values are more difficult to obtain with our choices of parameters (as with the stops, these should not be taken as strict exclusions). The EDM constraints

82

for the sbottom sources are similar to those for the stop sources, but they receive a $\tan\beta$ enhancement, and thus the constraints tend to be more stringent.

The behavior of the produced baryon asymmetry and the various constraints in Figs. 3.14-3.15 is qualitatively similar to that for the stop-source case: increasing $|A_b|$ or μ leads to larger regions compatible with the observed baryon asymmetry but strengthens the various EDM constraints. We note that since the sbottoms have down-type couplings to the Higgs, the roles of A_b and μ in the mass matrix for the $T = 0$ sbottoms are reversed relative to the roles of A_t and μ for the stops, and as a result, the exclusions from direct searches are primarily sensitive to μ for the large value of $\tan\beta$ chosen here. In addition to the cases shown in Figs. 3.14-3.15, we have verified that scenarios for sbottom-sourced EWB with large $|A_b|$ and small μ are also solidly ruled out by the current ^{199}Hg EDM constraint. We have also checked that decreasing the strength of the CP-violating phase opens up no additional parameter space for the sbottom sources (it potentially could have, as the slope of EDM constraints on the shown parameter space is different from that of BAU isolevel curves). Consequently, *taking sbottom mass, Higgs mass, and EDM constraints into account, we find no regions of the sbottom mass parameter space consistent with the observed value of Y_B: as for stop sources, current EDM constraints imply that sbottom sources alone cannot explain the BAU in the context of SUSY EWB.*

3.2.2.2   Staus

Finally, we consider the case where the observed baryon asymmetry may have arisen primarily from CP-violation in the stau sector of the MSSM. For large values of $\tan\beta$, y_τ can become enhanced as per Eq. (3.27). From the Lagrangian, Eq. (3.2), and following Ref. [23], we can proceed in parallel to the calculation of Eq. (3.28) for the CP-violating stau source $S_{\tilde\tau}^{CPV}$ with the replacements $\{\tilde b, A_b, y_b\} \rightarrow \{\tilde\tau, A_\tau, y_\tau\}$, yielding

$$
\begin{aligned}
S_{\tilde\tau}^{CPV}(x) = & -\frac{y_\tau^2}{2\pi^2}\,\mathrm{Im}(\mu A_\tau)v^2(x)\dot\beta(x) \\
& \times \int_0^\infty \frac{dk k^2}{\omega_R \omega_L}\,\mathrm{Im}\left[\frac{n_B(\mathcal{E}_R^*)-n_B(\mathcal{E}_L)}{(\mathcal{E}_L-\mathcal{E}_R^*)^2}+\frac{n_B(\mathcal{E}_R)+n_B(\mathcal{E}_L)}{(\mathcal{E}_L+\mathcal{E}_R)^2}\right]
\end{aligned}
\tag{3.30}
$$

and with the appropriate replacements in the definitions of Eq. (3.22) for the LH and RH staus. The relevant CP-violating phase is now $\phi_\tau = \mathrm{Arg}(\mu A_\tau b^*)$. The source Eq. (3.30) enters the full set of QBEs, since for large $\tan\beta$ all third-generation Yukawa rates should be taken into account. The left-handed fermionic charge density is given by

$$
n_L = Q + 2Q_1 + \frac{k_l}{k_L}L
\tag{3.31}
$$

where k_l is the fermionic contribution to k_L. Note that unlike for quarks, only the third generation LH density L contributes to n_L since there is no generational mixing for leptons and we have neglected the first- and second- generation leptonic Yukawa couplings. We have verified that the staus and taus are in superequilibrium everywhere except in kinematically disallowed regions, so we proceeded as before, assuming $\mu_{\tilde\tau_{L,R}} = \mu_{\tau_{L,R}}$ in computing Y_B.

For the spectrum we again proceed in parallel to the analysis outlined in Sec. 3.2.1.1 with the appropriate replacements for the staus, again assuming a strongly first-order phase transition, either from the light stop scenario or some other mechanism (in calculating the BAU and constraints we assume a heavy RH stop). The resulting slepton-sourced baryon asymmetry is shown in Figs. 3.16-3.17 for various values of $|A_\tau|$, μ and maximal CP-violating phase ϕ_τ; regions of the stau mass parameter space compatible with successful EWB are shaded blue. The resulting baryon asymmetry is strongly peaked near the resonance. This is because the thermal widths of the staus in the plasma, which enter into $\mathcal{E}_{L,R}$ in the denominator of $S_{\tilde{\tau}}^{CPV}$, are much smaller than those for the squarks, $\Gamma_{Q,T} \simeq 0.5T$, $\Gamma_{L,R} \simeq 0.003T$ [22]. As a result, successful stau-sourced EWB requires nearly degenerate $\tilde{\tau}_L$, $\tilde{\tau}_R$; from Figs. 3.16-3.17 we find $\left| M_{\tilde{L}_3} - M_{\tilde{E}_3} \right| \lesssim 100$ GeV to produce the observed value of Y_B for $\sin \phi_\tau = 1$.

The results shown in Figs. 3.16-3.17 demonstrate that the resonance supplied by the small thermal widths of the staus present in the denominator of Eq. 3.30 can overcome the suppression effect of the resonant relaxation rate $\Gamma_{m\tau}$. This can be understood by noting that the overall baryon asymmetry scales with [23] $\sim S_{\tilde{\tau}}^{CPV}/\sqrt{\Gamma_{m\tau}}$ so although both the source and relaxation rates are resonantly enhanced by the small widths, the asymmetry will tend to increase with decreasing widths. Also, the strong resonance in the denominator of $S_{\tilde{\tau}}^{CPV}$ can overcome the Boltzmann suppression in the numerator for stau soft masses up to ~ 1 TeV in most cases. Physically, this corresponds to the very efficient production of chiral charge by a relatively small abundance of staus in the plasma. These results hinge on the small values of $\Gamma_{L,R} = 0.003$, which
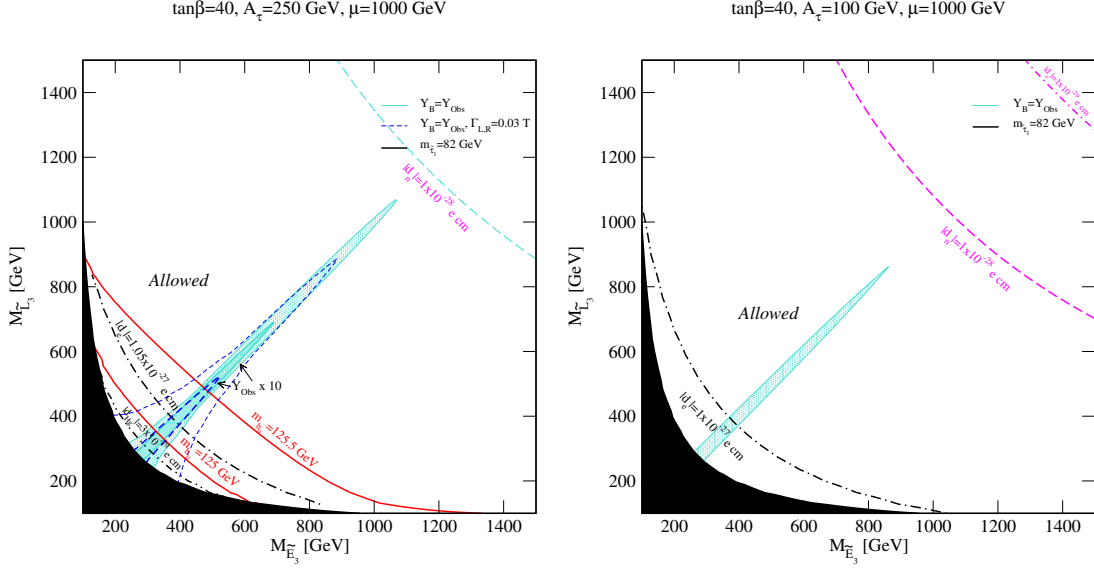
Figure 3.16: As in Figs. 3.10-3.11, but for stau sources. For the $|A_\tau| = 250$ GeV case, the dashed blue lines correspond to constant-Y_B curves computed for a factor of ten larger thermal stau widths. In this case, the expected reach of future d_e measurements will probe all of the parameter space shown. For the $|A_\tau| = 100$ GeV case, neutron and Mercury EDM bounds fall beneath the black shaded region. In both cases the expected reach of future d_{Hg} measurements is nearly degenerate with the current bound from measurements of d_e and is not shown.

we take from Ref. [22] and which were computed for $\tan\beta = 15$. One might expect the widths to be enhanced for the larger values of $\tan\beta$ we consider here, since e.g. the otherwise negligible Yukawa decay $\tilde{\tau} \to \tilde{H}\tau$ can become important in this regime, yielding an enhancement of $\Gamma_{L,R}$ from this extra decay channel of a factor of order 2 at most. Also, $\Gamma_{L,R}$ are not necessarily equal, due to the differing hypercharges in the decays $\tilde{\tau} \to \tau\tilde{B}$, as well as the $SU(2)$ decay to $\tau\tilde{W}$ which can be open for our choices of gaugino masses. To demonstrate the sensitivity of our results to the precise values of the thermal widths, we include on the LHS of Fig. 3.16 the curves of Y_{Obs}, $10 \times Y_{\text{Obs}}$ calculated for an order-of-magnitude larger widths, $\Gamma_{L,R} = 0.03T$, which we expect to over-estimate the uncertainty in $\Gamma_{L,R}$ associated with these considerations. Even this
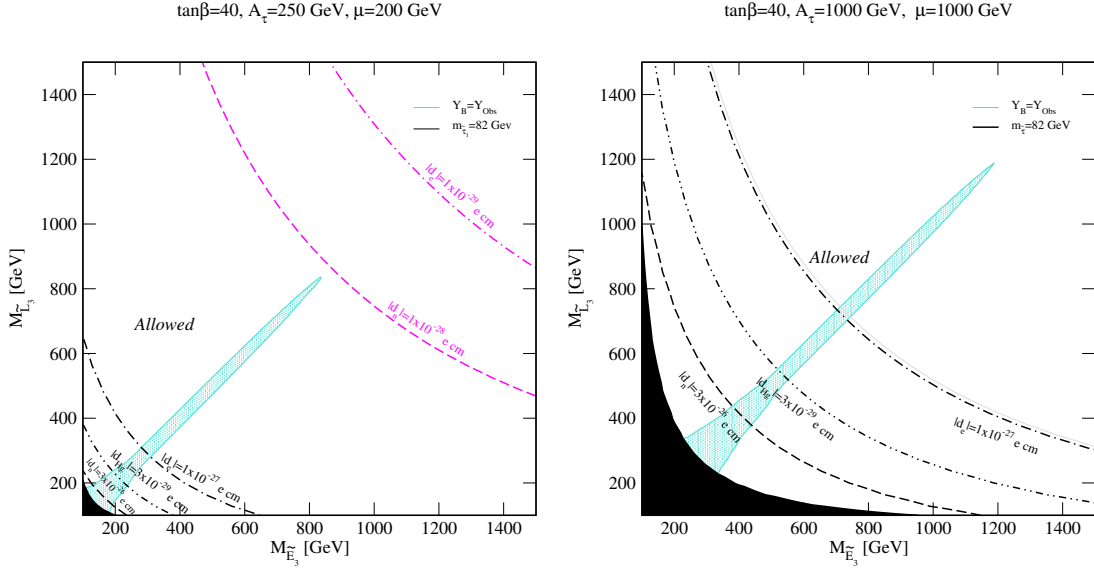
Figure 3.17: As in Fig. 3.16 for different values of A_τ, μ. For the $|A_\tau| = 1000$ GeV case, future electron and neutron EDM experiments will probe all parameter space shown. In both cases the expected reach of future d_{Hg} measurements is nearly degenerate with the current bound from measurements of d_e and is not shown here

factor of 10 increase in $\Gamma_{L,R}$ admits a significant amount of parameter space compatible with stau-sourced EWB. We thus expect that our overall conclusions are rather insensitive to the details entering into a more precise determination of the stau thermal widths, however we encourage the Reader to keep the above caveats in mind when interpreting our results.

In Figs. 3.16-3.17 we also plot constraints from direct searches for staus, $m_{\tilde{\tau}_1} \gtrsim$ 82 GeV [62], which display the down-type dependence on $|A_\tau|$ and μ similar to that of the sbottoms. We also show iso-level contours of constant Higgs mass for the $|A_\tau| = 250$ GeV, $\mu = 1000$ GeV case. We omit these curves for the other plots since the exact values of the SM-like Higgs mass in each case are sensitive to the details of e.g. squark and gluino masses which do not impact the determination of Y_B in slepton-sourced EWB.

Two significant features emerge:

(1) From Fig. 3.16 we see that one can achieve a Higgs mass in this scenario consistent with the hints from ATLAS and CMS, $m_{h_0} \sim 125$ GeV. In contrast to our analysis of the stop and sbottom sources wherein we found no viable regions of parameter space for $m_{h_0} \gtrsim 120$ GeV, we are able to easily obtain a heavier Higgs mass for the stau source case since we are free to consider heavy squarks which contribute large loop corrections to m_{h_0}. Also note that the excess events observed in the $H \to \gamma\gamma$ channel with respect to general MSSM expectations [66] could favor a scenario with light staus [59].

(2) Alternatively, one may also obtain the correct baryon asymmetry from stau sources along with a light right-handed stop; since there is no CP-violating phase in A_t, the EDM constraints will not be affected, however the large loop contributions to m_{h_0} will be lost.

We also consider EDM constraints on the stau-source scenario in Figs. 3.16-3.17. In order to generate chromo-EDMs, one needs a CP-violating phase that couples to (s)quarks. When the only phase is ϕ_τ, the chromo-EDMs disappear. Consequently, both the neutron and Mercury EDM constraints are much weaker in this scenario, while the electron EDM is the relevant one. The electron EDM in the case of CP violation in the stau sector entirely stems from a single Barr–Zee graph with a stau loop. From Figs. 3.16-3.17, we see that the lack of chromo-EDMs opens up large sections of parameter space, allowing for viable baryogenesis while satisfying the experimental

88

constraints. Future EDM experiments are expected to probe all of the parameter space available for stau-mediated EWB. Note that since the primary constraint on stau sources is the electron EDM, the available parameter space is rather insensitive to the theoretical uncertainty in the calculation of d_{Hg}: an order of magnitude *under*-estimate of the mercury EDM would make its constraints comparable to that of the electron EDM. This picture holds even for smaller values of the CP-violating phase; we find that one can produce the correct BAU and still satisfy the various constraints for $\sin \phi_\tau \gtrsim 10^{-2}$ in most cases considered.

Summarizing the results of Figs. 3.16-3.17, *we conclude that it is possible to produce the observed baryon asymmetry with CP violation in the stau sector only, for nearly degenerate staus and $300\ GeV \lesssim M_{\tilde{L}_3, \tilde{E}_3} \lesssim 1.2\ TeV$, depending on the magnitudes of the stau triscalar coupling and μ, while satisfying EDM and direct search constraints. This scenario can also naturally accommodate an SM-like Higgs mass $m_{h_0} \sim 125\ GeV$ for heavy squarks, or possibly a strongly first order phase transition via the light stop scenario for light $m_{\tilde{t}_1}$.* Should future searches for electron, neutron, and Mercury EDMs yield null results, all scalar sources in the MSSM will be ruled out for resonant EWB.

3.3   Discussion and Summary

Let us summarize what we have found for each class of sources in the MSSM.

Recent results from both direct and indirect dark matter detection experiments significantly constrain the regions of the MSSM otherwise viable for electroweak baryo-

genesis with Higgsino-gaugino CPV sources. We have illustrated this for two particular classes of supersymmetry-breaking models, however since our results follow primarily from the relative hierarchy of the neutralinos and charginos and not the precise values of the individual gaugino masses, we consider our conclusions to be quite general for a given gaugino mass hierarchy satisfying either $M_1 < M_2$ or $M_1 > M_2$. In particular, we have found that:

- EWB scenarios with a wino- (or higgsino-, higgsino-wino-) like LSP, occurring when $M_2 < M_1$, are essentially ruled out by recent dark matter search null results, unless R-parity is violated or the LSP is not the primary DM constituent. This is due to the sensitivity of direct detection experiments and neutrino telescopes to light neutralinos with significant wino-higgsino mixing combined with the sensitivity of dwarf spheroidal galaxy gamma ray observations to the complementary wino- and higgsino-like LSP parameter space.

- Although EWB models with a bino-type LSP ($M_1 < M_2$) are not entirely ruled out, only a small portion of the neutralino-driven EWB parameter space is still viable for small values of m_A and large $\sin \phi_\mu$; for large m_A and/or small CP-violating phase, chargino-driven EWB with a large wino mass becomes the only possibility. Additionally, with moderate improvements in sensitivity, direct and indirect DM detection results will probe larger portions, and in some cases all, of the $M_1 \sim \mu$ funnel and the lower portion of the $M_2 \sim \mu$ funnel. Further, if the LSP is the primary DM candidate, enforcing the correct relic density rules out the

whole $M_1 \sim \mu$ funnel for maximal CP-violating phase.

- The LHC will probe only the low-mass portions of the EWB-compatible parameter space for both the $M_2 > M_1$ and $M_2 < M_1$ scenarios with 100 fb^{-1} through events with neutralino and chargino pairs in the final state via the clean trilepton signature. Thus, we expect DM searches to typically provide more stringent constraints on the EWB-compatible regions of the MSSM than the LHC through this channel.

We emphasize that the conclusions above follow simply from requiring EWB to account for the observed baryon asymmetry and the LSP to be stable and to compose the dark matter density; relaxing these two requirements will weaken our conclusions by potentially extending EWB-compatible regions beyond those considered here and by mitigating the impact of the various dark matter searches on the gaugino-higgsino mass planes. However, it is clear that dark matter searches alone significantly constrain EWB scenarios with Higgsino-gaugino sources.

Regarding CP-violating sources in the sfermion sector, we have found that:

- Neither the stop nor the sbottom sector are viable options to account for the bulk of the observed baryon asymmetry of the universe: two-loop Barr-Zee diagrams contribute to the chromo-EDM of the down quark to a level that is ruled out by current constraints of the Mercury EDM across the entirety of the parameter space where stop or sbottom sources could source a large enough amount of baryon asymmetry. Moreover, stop- and/or sbottom-mediated EWBG is disfavored by

indications of $m_{h_0} \approx 125$ GeV, though present Higgs search constraints on the CP-violating sources are not nearly as decisive as those arising from EDMs.

- The stau sector (where no chromo-EDMs are produced) has milder constraints from EDMs, and hence can be responsible for producing the net left-handed chiral charge density needed to produce, via weak sphaleron transitions, the observed baryon asymmetry in the universe. It is also possible in this case to achieve $m_{h_0} \approx 125$ GeV or a light RH stop as needed for a strong first order phase transition, but not both. Due to the relatively small stau thermal widths, however, this scenario of "slepton-mediated" electroweak baryogenesis requires almost degenerate staus, with masses between 300 GeV and 1.2 TeV, depending on the size of the stau triscalar coupling and μ. This scenario also requires large values of $\tan\beta$.

While, from the standpoint of requiring a strongly first order phase transition, electroweak baryogenesis in the MSSM is being conclusively tested by ongoing searches for a light stop and the Higgs [75], these results provide important, complementary information on the nature of the new sources of CP violation, the second key ingredient for successful supersymmetric electroweak baryogenesis. Future results from Dark Matter experiments, the LHC, and the next generation of EDM searches are therefore expected to yield an increasingly sharper, if not definitively clear, picture of whether or not the electroweak scale in the MSSM is related to the generation of the observed baryon asymmetry.

We have seen that the window in the MSSM for successful electroweak baryo-

genesis is closing quickly. As a result, it is important and timely to consider models of baryogenesis beyond the MSSM. We turn our attention to two such scenarios in the subsequent Chapters.

4

Accidental Supersymmetric

Baryogenesis and Dark Matter

The Standard Model (SM) of particle physics is missing several key ingredients needed for a satisfactory phenomenological description of nature. First, it does not provide an explanation for the observed baryon asymmetry of the universe (BAU). Second, the SM does not contain any viable particle candidates for dark matter (DM), which is needed to explain a large array of astrophysical and cosmological observations. From a more theoretical perspective, the SM additionally falls short of explaining the large hierarchies between fundamental physical scales. In particular, it provides no satisfactory explanation for why the Planck scale, $M_{\mathrm{Pl}} \sim 10^{19}$ GeV, is so much higher than the electroweak (EW) scale, $m_{\mathrm{EW}} \sim 100$ GeV. This is known as the hierarchy problem.

In recent years, several models have been suggested that address the hierarchy

problem. In particular, models with warped extra dimensions, such as Randall-Sundrum (RS) scenarios, have been proposed which naturally generate the hierarchy between the Planck and EW scales [76]. In RS models, the universe is described by a five-dimensional (5D) geometry with two four-dimensional (4D) branes located at the UV (Planck) and IR (TeV) points. The Higgs fields are localized on (or near) the IR brane, and the warped fifth dimension "redshifts" the Planck scale to the TeV scale, providing a rather elegant solution to the hierarchy problem. Additionally, by placing the SM fermions in the bulk, hierarchies between the Yukawa couplings can be accounted for by the wave-function overlap with the Higgs boson in the fifth dimension [77].

While explaining the hierarchy problem, simply embedding the SM in a RS scenario is not fully satisfactory. To prevent sizable CP-violating effects from Kaluza-Klein (KK) modes in the absence of additional flavor structure, the IR scale must be at or above $\mathcal{O}(10 \text{ TeV})$[78]. Precision electroweak experiments also dictate that the IR scale must be larger than the EW scale, hence some additional tuning is required between these scales. This is an incarnation of the so-called *little* hierarchy problem. To resolve this issue, models of "emergent" or "accidental" supersymmetry have been proposed (see e.g. Refs. [79, 80, 81]), in which supersymmetry (SUSY) emerges as an accidental symmetry in the IR, with SUSY broken on the UV brane. As a result, the Higgs mass can be protected from radiative corrections up to the IR scale, while the warped extra dimension generates the hierarchy between the TeV and Planck scales. Within this framework, which we describe in more detail in Sec. 4.1, both hierarchy problems can potentially be resolved. The specific particle content of the theory depends on the

model of SUSY embedded in the Randall-Sundrum spacetime. Since we are interested in the general features of accidental supersymmetric models, we will consider the particle content of the minimal supersymmetric extension of the standard model (MSSM) as a conservative case from the standpoint of the field content of the theory.

Randall-Sundrum scenarios can do more than just solve the big and little hierarchy problems. In fact, we show here that models with warped extra dimensions may also provide an explanation for the origin of the baryon asymmetry via the mechanism of electroweak baryogenesis (EWB). Crucial to this mechanism are a number of conditions, ultimately related to those generically needed for any dynamical mechanism for the production of a baryon asymmetry [7]: first, one needs departure from thermal equilibrium at the electroweak scale; second, one needs large enough charge (C) and charge-parity (CP) violation; third, one needs violation of baryon number. The second and third conditions are easily satisfied in the context of supersymmetric EWB models: any minimal supersymmetric extension to the SM, in fact, contains numerous (albeit constrained) new sources of CP violation, while baryon number (B) violation, is provided by SM weak sphalerons — we will comment on this more below. More critical is how to have a large deviation from thermal equilibrium — a condition in practice realized, in the context of EWB, via a strongly first-order electroweak phase transition. As pointed out in Ref. [82], here the RS setup may be of crucial importance, as we also explain below.

While the universe is described by the Randall-Sundrum spacetime at zero temperature, at finite temperature, RS models possess an additional high-temperature

phase, described by an Anti-de Sitter-Schwarzschild (AdS-S) spacetime with a black hole horizon replacing the TeV brane [83]. Alternatively, a holographic description facilitated by the AdS-CFT correspondence also exists in which the two phases correspond to a deconfined and to a confined phase of a strongly coupled gauge theory, respectively. Provided that the free energy of the RS phase is less than the free energy of the AdS-S phase, $F_{RS} < F_{AdS-S}$, a phase transition can occur between the two: as the universe cools below a temperature T_c, bubbles of the TeV brane can begin to nucleate out of the black hole horizon [83] (see also Refs. [84, 85, 82] for further discussion of the confining phase transition).

Because, from the CFT perspective, conformal invariance is only spontaneously broken in the RS phase, $F_{RS} > F_{AdS-S}$ implies that the RS phase is metastable. For the confining phase transition to occur, one must introduce some mechanism to explicitly break conformal invariance. From the AdS perspective, this can be accomplished by stabilizing the radion (the field governing the separation between the UV and IR branes) with a potential generated e.g. by additional 5D fields. Once the radion is stabilized, the free energy of the two phases will be equal at some temperature $T = T_c$ producing a phase transition via bubble nucleation with nucleation temperature $T_n \leq T_c$. In many cases, T_n can be significantly lower than the temperature of the electroweak phase transition (EWPT) predicted by the 4D Minkowski theory [82]. Since the Higgs sector is typically confined to the IR brane, this low nucleation temperature results in a "*supercooled*" EWPT (i.e. taking place at lower temperatures than otherwise possible), thereby potentially strengthening the phase transition. While this supercooling was

97

studied specifically in the case of the SM embedded in RS with a Goldberger-Wise potential [86] for the radion in Ref. [82], this possibility is a consequence of the geometry and localization of the Higgs sector in the IR and is largely independent of the particle content of the theory and can therefore potentially arise in accidental SUSY as well. As a result, models of accidental SUSY may provide a strongly first order EWPT even *without* e.g. a light right-handed scalar top (stop) quark [19, 36], or additional singlets contributing to the Higgs potential [38], as is typically required for successful EWB in the MSSM. Alternatively, as we explain in the next section, certain incarnations of the accidental SUSY framework also posit, as a solution to the μ-problem, an additional extension to the Higgs sector via a singlet scalar field. This potentially provides an additional route to a strongly first order electroweak phase transition.

Since a strongly first order phase transition appears to be a natural possibility in accidental SUSY, the remaining issue pertinent to EWB is the requirement of large enough CP-violation to seed weak sphalerons, which will be the primary focus for the rest of this study. In fact, accidental SUSY naturally satisfies this requirement as well. Even in its MSSM incarnation, there are several new CP-violating phases which can source the baryon asymmetry. In particular, there are new phases arising in the higgsino-gaugino and third-generation scalar sectors. It has recently been shown that of the third-generation scalars, only CP-violating stau sources can account for the observed baryon asymmetry while still conforming to various phenomenological and experimental constraints from electric dipole moment searches [87]. Here we concern ourselves with moderate values of the ratio of Higgs vevs, $\tan \beta = 10$, in which case the stau sources

98

are suppressed. We will therefore be interested in EWB with higgsino-gaugino sources in accidental SUSY. Electroweak baryogenesis utilizing these sources in the MSSM has been extensively analyzed in recent studies (e.g. [27, 18, 23, 24, 21, 22, 25, 88, 89, 32, 43, 19, 28, 33, 30, 90, 91, 92]), and we build on these analyses in our study of the accidental SUSY scenario. Note that extending the particle content beyond that of the MSSM would provide more potential sources of CP-violation.

Supersymmetric RS models also have the added benefit of generically containing a viable dark matter candidate, if the lightest supersymmetric particle (LSP) corresponds to the lightest neutralino, over some regions of parameter space. This is a result of R-parity conservation, whereby the LSP is stable. Thus it may be possible for accidental SUSY to simultaneously explain the origin of the BAU and the nature of dark matter, while also solving both the big and little hierarchy problems. In fact, the production of both the relic DM density and the baryon asymmetry via higgsino-gaugino sources are closely connected [30, 90], since both depend predominantly on the higgsino mass term μ and on the gaugino soft-supersymmetry breaking masses M_1 and M_2. Consequently, enforcing both the correct DM properties and baryon asymmetry in conformity with various observational constraints may result in sharp predictions for the regions of interest within the accidental SUSY parameter space. This is an attractive possibility and one which we explore in the present study.

In what follows we compute the baryon asymmetry across the parameter space of a minimal (MSSM-like) incarnation of accidental SUSY. We do so independently of the specifics of SUSY breaking, choosing higgsino and gaugino masses which yield the

correct DM relic density (this is the so-called "well-tempered neutralino" setup [93]) and assuming a strongly first-order electroweak phase transition arising either from the supercooling provided by the AdS-S transition or from the contribution of a gauge singlet super-field to the effective potential. We then impose constraints from electric dipole moment (EDM) measurements and from dark matter searches to outline potentially viable regions of the parameter space. We also consider the impact of the projected sensitivities of these various experiments. In doing so, we find that accidental SUSY models, even in their most minimal incarnations, may allow for successful EWB and a viable DM candidate provided that the resulting soft breaking wino mass, M_2, and the higgsino mass parameter μ are roughly degenerate, with the LSP a bino-higgsino admixture; we also require the MSSM heavy Higgs sector to lie relatively close to twice the LSP mass. These findings can be used to hone in on specific models of accidental SUSY giving rise to the observed properties of our universe.

4.1 Accidental Supersymmetry

The framework of accidental SUSY can be used to both generate a hierarchy between the Planck and IR scales and a little hierarchy between the electroweak and IR scales by embedding supersymmetry in an RS spacetime [81]. The Higgs mass is protected from higher order corrections up to the IR scale m_{IR} by requiring the superpartners of the third-generation quarks[1], as well as those of the gauge and Higgs

---

[1]Typically, the RH sbottom is taken to be heavy, as sbottom loop contributions to the Higgs mass are subdominant

bosons, to be light in order to cancel the loop corrections from their SM counterparts to the Higgs mass. The warped extra dimension then takes over in protecting the hierarchy between the IR and Planck scales for scales above m_{IR}. On the other hand, superpartners of the quarks and leptons of the first two generations should be heavy to avoid excessive flavor and CP-violation which would occur if the mediation of SUSY breaking is not flavor blind. This spectrum is reminiscent of so-called "Split SUSY" models [94].

Much previous work has been devoted to the study of supersymmetric Randall-Sundrum models [77, 95, 79, 96, 80, 81]; the specifics of the resulting particle spectrum inherently rely on the underlying assumptions about particle content, SUSY breaking, localization of the particles in the 5D spacetime, etc. However, here we are concerned with the generic features of accidental supersymmetry relevant to EWB and to dark matter phenomenology, and so we limit our assumptions to a few key points representing the main features of this setup. For the sake of generality, we take the particle content embedded in the RS spacetime to be the minimal supersymmetric spectrum of the MSSM. Our assumptions about the resulting spectrum, typical of accidental SUSY models, are listed in the bullet points below. For the sake of illustration, we focus in this section on the model set forth in Ref. [81] as a concrete example demonstrating how these features arise in accidental SUSY scenarios, briefly and qualitatively summarizing some of the aspects of the setup relevant for our investigation below. We stress, however, that the remainder of this study will not necessarily depend on this particular model. We work in the 5D gravity language of the gauge-gravity duality except where noted.

Readers comfortable with the general setup of accidental SUSY may skip down to our bullet points below.

We consider a minimal supersymmetric theory embedded in a RS spacetime with metric

$$ds^2 = e^{-2k|y|}\eta_{\mu\nu}dx^\mu dx^\nu + dy^2 \tag{4.1}$$

where $\eta_{\mu\nu}$ is the Minkowski metric and k denotes the scale of AdS curvature. The 5th dimension is an S^1/Z_2 orbifold with coordinate y. The points $y = 0, \ell$ are the positions of the UV and IR branes, respectively, corresponding to the orbifold fixed points. Denoting the 4- and 5-dimensional Planck masses as M_4, M_5, respectively, the warped-down IR scale on the $y = \ell$ brane is assumed to be $m_{\mathrm{IR}} = e^{-k\ell}k$ (we assume $k\ell \sim 30$ throughout), and we assume the UV cutoff on the IR brane is given by $\Lambda_{\mathrm{IR}} = e^{-k\ell}M_5$. In Ref. [81], to naturally implement the split SUSY spectrum, supersymmetry is broken on the UV brane at an intermediate scale $M_{\mathrm{SUSY}} \ll M_5$, with light standard model fermions localized near the UV brane so that their superpartners feel SUSY-breaking maximally. This results in heavy first- and second-generation sfermions. Meanwhile, the higgsinos and stops are localized near the IR brane so that they remain light. The gauginos are protected by an accidental R-symmetry (they have sizable wavefunction overlap with the UV brane, and so would typically be heavy without this symmetry). One can introduce both (i) a bulk hypermultiplet, which obtains an F-term when SUSY breaking occurs from its coupling to a SUSY-breaking spurion on the UV brane, and (ii) a constant superpotential on the IR brane[2] with mass scale C. Combined, both (i)

_____

[2]A constant superpotential must also be added to the UV brane to tune the cosmological constant

and (ii) generate a potential for the radion (whose chiral superfield is denoted by ω), stabilizing the radion at a scale m_{IR} which we take to be around 10 TeV (see Ref. [81] for details concerning the radion potential in this scenario).

We are ultimately interested in the low energy phenomenology of accidental SUSY models, below the cutoff Λ_{IR}. To extract the low energy effective theory, one must integrate over the extra dimension and account for the effects of the radion superfield by canonically normalizing the radion and chiral superfields localized on the IR brane. This yields masses for the scalar (and pseudoscalar) degrees of freedom (associated with the real and imaginary parts of the complex radion field, respectively) near the soft scale at the minimum of the potential [81]. Denoting this canonically normalized radion superfield as φ, one can show [95], given certain ansätze, that the effective low energy superpotential on the IR brane, $W_{\text{eff}}^{\text{IR}}$, reads, after canonical normalization,

$$W_{\text{eff}}^{\text{IR}} = e^{-3\varphi/\Lambda_{\text{IR}}} W^{\text{IR}}(Q_i, H_i), \tag{4.2}$$

where W^{IR} is the superpotential for the IR-localized chiral superfields (the Higgs and third-generation quarks in our case). As a result, any dimensionful coupling in the superpotential of the embedded supersymmetric theory, which is naturally near the 4D Planck scale, will be warped down to the IR scale. In the case of an MSSM-like superpotential $W_{\text{MSSM}}^{\text{IR}}$, employed here, this results in $\mu \sim m_{\text{IR}}$ and thus a supersymmetric little hierarchy must be reintroduced so that μ is near the soft scale, as required to obtain the correct dark matter relic abundance (discussed in Sec. 4.2). We comment more on this below, but for the moment we shall simply assume some tuning so that

to zero.

$\mu \sim 100 - 1000$ GeV.

The effective superpotential $W_{\mathrm{eff}}^{\mathrm{IR}}$ in Eq. 4.2 shows that there can be considerable differences between the low energy phenomenology of a supersymmetric RS theory and its 4D flat-space counterpart due to the presence of the radion superfield. The Kähler potential is also typically non-minimal in such theories [95]. The effective superpotential and Kähler potential can result in mixing between the radion and Higgs, between the radion superpartner (the "radino") and higgsinos, as well as couplings of the radion fields to the other IR-localized degrees of freedom. While these effects are interesting from the standpoint of low-energy phenomenology, they are largely model-dependent and so we neglect them for the remainder of our study. In particular, we assume that: (1) the radino mass (which depends on the details of SUSY breaking) is large enough so that it decouples from the phenomenology, and (2) that the IR-localized fields couple minimally to gravity so that there is no mixing between the Higgs and radion. While these assumptions still allow for couplings of the radion to the IR-localized fields (and thus potentially impacting the calculation of the baryon asymmetry), we estimate that the relevant rates are small compared to other processes of interest (see Eq. 4.9 and the surrounding discussion). In addition to the radion, RS models are accompanied by the usual Kaluza-Klein excitations, which can also play a role in the phenomenology. However, as discussed above, we assume that these modes are heavy, in order to avoid constraints from e.g. CP- and flavor-violation; this assumption effectively decouples them from the processes of interest here. Summarizing, as a result of these assumptions, *the particle content we consider is simply that of the MSSM, with the*

mass hierarchy typical of accidental SUSY models, discussed below. One should bear in mind that effects associated with the radion which we neglect here can significantly impact other aspects of low-energy phenomenology, such as those associated with collider searches [97].

The main virtue of accidental SUSY models for our purposes, then, is that they can provide an attractive supersymmetric spectrum for the sectors relevant for dark matter and electroweak baryogenesis, in addition to facilitating the requirement of a strongly first-order EWPT. With SUSY breaking occurring on the UV brane, the various parts of the visible sector feel SUSY breaking in different ways. In Ref. [81], SUSY breaking for the UV-localized supermultiplets is felt primarily from the effects of heavy UV-localized messengers. Integrating out the messengers (with mass scale M_X), yields the 5D effective Lagrangian [81]

$$\mathcal{L}_5 \supset \delta(y) \int d^4\theta \frac{\Phi^\dagger \Phi}{k^2 M_X^2} Q^\dagger Q, \tag{4.3}$$

where Φ is the SUSY-breaking spurion. Upon inserting the wavefunction of the zero-mode for the multiplet Q, one obtains

$$m_{\text{soft}}^{\text{UV}} \sim \frac{M_{\text{SUSY}}^2}{M_X} \tag{4.4}$$

for the soft masses of UV-localized sfermions. For reasonable choices of the messenger scale, these large masses effectively decouple them from the processes of interest for electroweak baryogenesis, which occur below the TeV scale.

In order to protect the Higgs mass from gauge boson loops, the gauginos must also be light, implying that the generically leading contribution to the gaugino masses

105

$\Phi W_\alpha W^\alpha$ must be suppressed; otherwise, the gauginos would acquire soft masses m_{gaugino} of the same order as Eq. 4.4. This can be done, as in Ref. [81], by charging the spurion Φ under a $U(1)'$ gauge symmetry, in which case the leading contribution to m_{gaugino} typically arises from

$$\mathcal{L}_5 \supset \delta(y) \int d^4\theta \frac{\Phi^\dagger \Phi}{k^2 M_X^3} W^\alpha W_\alpha + \text{h.c.}. \tag{4.5}$$

Inserting the zero-mode gaugino wavefunction yields gaugino soft masses

$$m_{\text{gaugino}} \sim \left(\frac{M_{\text{SUSY}}^2}{M_X^2 k\ell} \right) m_{\text{soft}}^{\text{UV}} \tag{4.6}$$

which can be of order the soft IR scale $m_{\text{soft}}^{\text{IR}}$ provided that $M_X \sim M_{\text{SUSY}}^{4/3}/m_{\text{IR}}^{1/3}$. The SUSY-breaking scale is confined to be in the range 10^7 GeV $\lesssim M_{\text{SUSY}} \lesssim 10^{11}$ GeV to obtain a sufficiently large $m_{\text{soft}}^{\text{UV}}$ while preventing excessive contributions from radion mediation to the gaugino masses [81].

Finally, the IR-localized supermultiplets must also be light to stabilize the electroweak scale. If these particles are sufficiently localized on the IR brane, the largest contributions to the corresponding soft masses arise from gravity mediation. These contributions arise from the part of the 4D effective Lagrangian given by [81]

$$\mathcal{L}_4 \supset \int d^4\theta \omega^\dagger \omega \frac{[\Phi^\dagger \Phi]_{\text{IR}}}{M_5^3} \left(Q^\dagger Q + H_u^\dagger H_u + H_d^\dagger H_d \right) \tag{4.7}$$

where we have considered the Higgs sector of the MSSM (this differs from Ref. [81] as already mentioned). The above Lagrangian leads to IR soft masses

$$m_{\text{soft}}^{\text{IR}} \sim \sqrt{6} \left(\frac{C}{M_5} \right)^3 m_{\text{IR}} \tag{4.8}$$

106

which can provide the little hierarchy between soft and IR scales for only a modest hierarchy between the scale of the constant IR superpotential and the 5D Planck scale.

As is well known, in the MSSM, some tension exists between having light stops and obtaining a Higgs mass consistent with the (tentative) 125 GeV Higgs reported by CMS and ATLAS [66]. A way out is having significant mixing in the stop sector, which can allow for a heavy enough Higgs without decoupling the stops (see e.g. Ref. [98]). This possibility would not change the phenomenology relevant for calculating the baryon asymmetry or dark matter density (although it would require some additional tuning). On a related note, in considering the particle content of the MSSM embedded in the RS spacetime, we have not ameliorated the so-called "μ-problem", which reintroduces a supersymmetric little hierarchy as mentioned above, since μ will typically be of the order of the warped-down Planck scale, $m_{\rm IR}$ which is necessarily higher than the EW scale. This could be addressed by considering e.g. the NMSSM Higgs sector (as in Ref. [81]), which dynamically gives rise to μ near the soft IR scale, while at the same time raising the tree-level Higgs mass so that tuning of the stop mixing is not required. In fact, the additional gauge singlet superfield is not crucial to the phenomenology we are interested in here and so we could very well frame our discussion in the NMSSM (provided that the LSP is not singlino-like). However, we content ourselves with considering the particle content of the MSSM despite these issues, specifically to emphasize that one does not necessarily require the singlet introduced in the NMSSM for successful baryogenesis in accidental supersymmetric models, as discussed in the introduction. This fact, along with the minimal set of additional CP-violating phases in the MSSM, suggests that

107

MSSM-like accidental SUSY scenarios provide a conservative look at the prospects for accidental supersymmetric dark matter and baryogenesis.

We note that in addition to the soft-breaking masses in Eqs. 4.4, 4.6, 4.8, there are also hard-SUSY breaking terms in the effective 4D Lagrangian which affect the couplings of the gauginos (such as those governing CP-violating higgsino-gaugino source and the so-called "supergauge interactions" discussed in Sec. 4.3) and (scalar)^4 interactions [80]. These enhanced couplings will affect the light scalar masses through loop corrections, and a mild tuning must generally be invoked to keep these effects small, implying corrections $\lesssim \mathcal{O}(10\%)$ to the couplings [81]. While we neglect these (model-dependent) corrections in our calculations, the reader should bear in mind that larger gaugino couplings will enhance the baryon asymmetry, strengthen the EDM constraints, and increase the various dark matter cross-sections, thereby potentially strengthening the exclusions discussed in Sec. 4.7 for models with large hard-breaking effects.

The above considerations are only one specific realization of the accidental supersymmetric framework. However, some general features emerge for the spectrum typical of such theories. Specifically, accidental SUSY naturally accommodates:

- Light third generation squarks, gauginos, and higgsinos, $m_{\text{soft}}^{\text{IR}}$, $m_{\text{gaugino}} \lesssim 1$ TeV;

- Heavy sleptons and first- and second-generation squarks ($m_{\text{soft}}^{\text{UV}} \gtrsim 1000$ TeV);

- Heavy Kaluza-Klein modes, possibly starting at around 40 TeV;

- A radion at the soft scale

- A neutralino LSP

- Model-dependent masses for the heavy Higgs sector, gravitino, and radino.

The effective 4D theory at low energies we will consider is described by the MSSM with the above spectral features (we assume that the effects of the gravitino, radion fields and KK modes on processes of interest are negligible). Rather than considering one detailed model of SUSY breaking and the resulting mass patterns, we proceed model-independently in choosing values for the various relevant parameters in our calculations as described in the following sections. As we will see, the above features of the typical accidental SUSY spectrum are attractive from both the standpoint of dark matter and electroweak baryogenesis.

4.2   A Well-Tempered Neutralino

In the context of minimal supersymmetric extensions to the Standard Model with heavy sfermion masses and a neutralino LSP, as in the low-energy effective theories of accidental SUSY of interest here, the thermal relic density of the LSP is fixed by (i) the relevant entries in the neutralino mass matrix: the higgsino mass term μ, the bino soft supersymmetry breaking mass term M_1, and the wino soft supersymmetry breaking mass term M_2; and (ii) the presence or absence of a resonant annihilation channel via the light (h) or heavy (H, A) Higgses, or with the Z boson. The accidental SUSY scenario does not imply either a rigid hierarchy among μ, M_1 and M_2, or a specific mass range for the lightest neutralino or for the heavy Higgs sector. We therefore take here the model-independent view of treating all the relevant parameters as free, while

at the same time enforcing the requirement of a thermal relic density matching the cold dark matter density, $\Omega_\chi h^2 \simeq \Omega_{\rm DM} \simeq 0.11$.

Numerous studies have addressed the set of $(\mu,\ M_1,\ M_2)$ producing a "well-tempered" thermal relic neutralino [93]: early analyses of bino-higgsino mixing generating the right thermal relic density include e.g. Refs. [99, 100, 101, 102, 103], while wino-bino mixing was originally studied, to our knowledge, in Refs. [103, 104, 105]. With heavy sfermion masses, bino-like neutralinos have very suppressed pair-annihilation cross section, making it indispensable to have either some degree of higgsino- or wino-mixing, a resonant annihilation channel, or one (or more) co-annihilation partner(s). Generically, mixed higgsino-wino neutralinos have masses well above one TeV, with lighter, sub-TeV higgsino-wino neutralino LSPs being systematically under-abundant as thermal relic dark matter candidates. Such heavy LSPs push the mass of the particles relevant to the CP violating sources responsible for EWB to exceedingly large values, making them too heavy to produce the observed baryon asymmetry.

In this study, we explore the $(\mu,\ M_1,\ M_2)$ parameter space by focusing on the $(M_1,\ M_2)$ plane, where we calculate (using the DarkSUSY code [106] for the computation of the neutralino thermal relic density) the value of μ that leads to the correct thermal relic density. Since, as we will show, low (meaning at or below a TeV) values for the mass-scale of the heavy Higgs sector will be generically needed to produce a large enough BAU, we choose for the sake of illustration the two values $m_A = 500$ GeV and $m_A = 1000$ TeV. This choice will lead to resonances for neutralino masses $m_\chi \simeq m_A/2 \simeq 250,\ 500$ GeV. We choose $m_A = 500$ GeV as the lower limit to the range

in the mass scale of the heavy Higgs sector based on two considerations. First, it is difficult to reconcile values of m_A smaller than 500 GeV with limits on the inclusive branching ratio $b \to s\gamma$ for the values of $\tan\beta$ we consider here. While in general supersymmetric settings the chargino-stop diagram can potentially control and cancel out the contribution from the charged Higgs-top loop, here we do not assume a light stop, and therefore we can only rely on a heavy enough $m_{H^\pm} \simeq m_A$ to suppress $b \to s\gamma$. We find that $m_A \gtrsim 500$ GeV is consistent with experimental bounds. Additionally, we find that $m_A \ll 500$ GeV produces excessively large electric dipole moments via two-loop contributions, which further pushes the viable range for m_A to the range we utilize in the present study.

Fig. 4.1 presents the results of the procedure outlined above. The yellow region with $M_2 < M_1$ features wino-like neutralinos, with $\Omega_\chi h^2 \ll \Omega_{\rm DM} h^2$ for any value of μ. The red region at the bottom of the plot has charginos lighter than the LEP limit of about 103 GeV, and is thus ruled out (note that at present LHC searches do not significantly constrain this parameter space in a generic way, i.e. not assuming any relation between gaugino masses, and thus for generic gluino masses). The resonances appear for $M_1 \simeq m_\chi \simeq m_A/2$. Additionally, large values of μ correspond to the $M_1 \simeq M_2$ region, where bino-wino mixing efficiently suppresses the abundance of relic neutralinos. The generic feature of the plots is that for each value of M_1 a value of $\mu \gtrsim M_1$ is selected, with larger μ for smaller M_2, where bino-wino mixing starts being important.

In the remainder of this study, we employ the values of μ shown in Fig. 4.1, thus enforcing the correct thermal relic density, and vary quantities (such as the CP
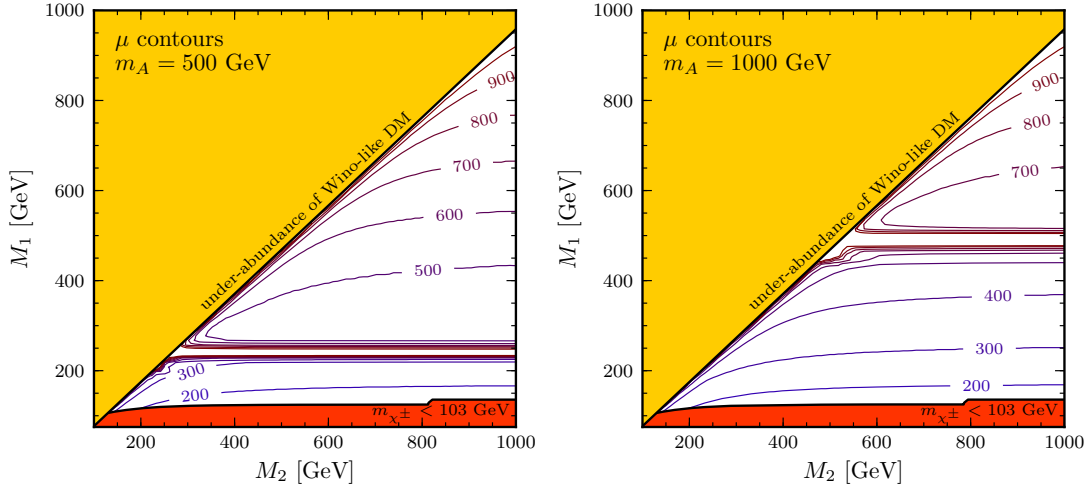
Figure 4.1: Curves of constant μ (in GeV) on the (M_1, M_2) plane corresponding to "well-tempered" neutralinos producing a thermal relic density matching the observed cold dark matter density. The red regions are ruled out by LEP searches for charginos, while the yellow region has wino-like neutralinos with a largely under-abundant density for any value of μ. In the left panel we set $m_A = 500$ GeV, while in the right panel to 1000 GeV.

violating phases) that affect very marginally the thermal relic density (see e.g. the discussion in Ref. [30]) while being crucial to the BAU calculation. We then compute the BAU produced by EWB (Sec. 4.3), electric dipole moments (Sec. 4.4), and dark matter detection rates (Sec. 4.5), comparing model predictions with existing experimental data and with the performance of future experiments.

4.3   The Baryon Asymmetry

In supersymmetric models of electroweak baryogenesis, the baryon asymmetry is produced by baryon number-violating weak sphalerons, acting on a net left-handed (LH) fermionic charge density n_L. The LH density arises from CP-violating interactions of the particles with the EWPT bubble wall. For a detailed and recent review of EWB

in supersymmetry, see Ref. [10].

At the practical level, the calculation of the baryon asymmetry in supersymmetric EWB requires two steps: first, a set of coupled quantum Boltzmann equations (QBEs) must be solved for the production and transport of the chiral charge; second, since weak sphalerons are essentially decoupled from the system of QBEs, to obtain the baryon asymmetry Y_B one simply integrates over the LH charge density in the unbroken phase, where weak sphalerons are active[3]. While a detailed study of the electroweak phase transition in accidental SUSY would be interesting and necessary to establish the details surrounding e.g. the nucleation temperature in these models, it is beyond the scope of this paper and so we simply assume the necessary strongly first order electroweak phase transition in our calculations as a result of either the supercooling by the AdS phase transition or of some additional particle content not related to the mechanism of EWB (e.g. an additional singlet superfield in the superpotential).

To solve the set of QBEs for n_L, one must keep track of all relevant particle number-changing interactions active near the EWPT. These consist of:

1. CP-violating sources. The relevant CP-violating phases for the low-energy accidental SUSY effective theory near the EWPT are those of the MSSM in our setup. As discussed in the Introduction, the sources we consider are those associated with higgsino-gaugino-vev interactions.

2. Tri-scalar and Yukawa interactions between the quark and Higgs superfields. These

---

[3]Weak sphalerons are inactive in the broken phase precisely because of the required strongly first order phase transition

113

rates arise from the interactions in the MSSM superpotential, as well as through the soft breaking effects discussed in Sec. 4.1.

3. Chiral relaxation rates for the (s)quark and higgsino densities. These rates are CP-conserving, arising from the interaction of the various fields with the Higgs vevs at the EWPT bubble wall. They tend to dilute the overall baryon asymmetry.

4. Supergauge rates, responsible for converting between the SM particles and their corresponding superpartners. If these rates are fast, then chemical equilibrium is established between SM densities and their superpartner counterparts. Throughout our calculations, we follow previous studies [90, 23, 24, 21] and assume superequilibrium for all relevant particle species in the transport equations, so that we can consider common densities for the interacting particles and their superpartners.

5. Strong sphalerons, which convert third generation quarks to the first- and second generation, and vice versa. Strong sphalerons can efficiently erase the net chiral charge generated by the CP-violating sources if the stop masses are heavy [40, 107]. As a result, we assume that the stops are light enough so that this suppression does not occur, but also heavy enough not to be the LSP. This is in fact a natural feature of accidental SUSY scenarios, and one of its virtues from the standpoint of EWB. For our numerical calculations of the baryon asymmetry, as in previous studies [90], we assume a RH stop soft mass $m_{U_3} = 0$ GeV and LH soft mass $m_{Q_3} = 1000$ GeV to show the maximal extent of the parameter space compatible

with the observed baryon asymmetry in this setup.

6. Interactions involving the radion. As discussed in Sec. 4.1, these interactions should be generically small relative to the usual MSSM-like rates, since for particles of mass m they are typically suppressed by powers of m/m_{IR} (or T/m_{IR} at high temperatures). For example, the radion couples to the trace of the energy momentum tensor of the IR-localized fields [108, 109], which results in Higgs-like interactions proportional to the masses of the various particles but suppressed by m_{IR}. A simple estimate comparing the rates for radion-top and top Yukawa interactions at finite temperature T, yields

$$\frac{\Gamma_{\varphi t}}{\Gamma_{yt}} \simeq \left(\frac{T}{y_t m_{\mathrm{IR}}}\right)^2 \lesssim 10^{-4} \tag{4.9}$$

where y_t is the top Yukawa coupling and we have assumed T is much larger than the top thermal mass. Eq. 4.9 implies that the radion interaction rates are typically small, and so we neglect them in our calculation of the baryon asymmetry. One should bear in mind that any particle-changing relaxation rate, such as those involving the radion, will tend to suppress the overall baryon asymmetry as $1/\sqrt{\Gamma}$.

With the above considerations, *the calculation of the baryon asymmetry in our effective accidental SUSY theory is analogous to the calculation in the MSSM with light third generation squarks, higgsinos, and gauginos*, and the relevant interaction rates then are simply those of the MSSM. A more detailed account of the rates in 1-5 above is provided in Ref. [22], to which we refer the interested reader.

With the above considerations, we calculate the baryon asymmetry following

115

the techniques and assumptions detailed in Refs. [23, 25, 24, 21, 22]. The evaluation

of the CP-violating sources, as well as the CP-conserving chiral relaxation rates, is

carried out using the so-called Higgs "vev-insertion approximation", in which interac-

tions between the particles and the spacetime-varying Higgs vevs in the bubble wall are

treated perturbatively [110]. This prescription leads to a resonance in both the CP-

violating and conserving rates for roughly degenerate particle masses for the relevant

species involved. Schematically, the higgsino gaugino source is given by terms of the

form

$$
\begin{aligned}
S_{\tilde{H}i}^{\mathrm{CPV}} &= \frac{g_i^2}{\pi^2} v(x)^2 \dot{\beta}(x) \, \mathrm{Arg}(M_i \mu) \\
&\times \int_0^\infty \frac{dk k^2}{\omega_{\tilde{H}} \omega_i} \, \mathrm{Im} \left\{ \frac{n_F(\mathcal{E}_i) - n_F(\mathcal{E}_{\tilde{H}}^*)}{(\mathcal{E}_i - \mathcal{E}_{\tilde{H}}^*)^2} - \frac{n_F(\mathcal{E}_i) + n_F(\mathcal{E}_{\tilde{H}})}{(\mathcal{E}_i + \mathcal{E}_{\tilde{H}})^2} \right\}
\end{aligned}
\tag{4.10}
$$

where $\omega_{\tilde{H},i}^2 \equiv |\mathbf{k}|^2 + M_{\tilde{H},i}^2$, $\mathcal{E}_{\tilde{H},i} \equiv \omega_{\tilde{H},i} - i\Gamma_{\tilde{H},i}$ (here the $\Gamma_{\tilde{H},i}$ are the thermal widths of

the corresponding particles in the plasma), n_F is the Fermi distribution function, and

the index i denotes the various quantities for the wino or bino contributions to either

the neutral or charged sources. From the structure of Eq. 4.10, we see that in our setup

the CP-violating sources are strongest in parameter space regions where either the bino

or wino soft mass (M_1 or M_2) is nearly degenerate with the higgsino mass parameter

μ so that the corresponding denominator $\mathcal{E}_i - \mathcal{E}_{\tilde{H}}^*$ in Eq. 4.10 is small, and where the

relevant particles are light (c.f. the Boltzmann suppression factors in Eq. 4.10).

A few comments on these calculational techniques are in order. First, the

vev-insertion approximation tends to overestimate the production of the overall baryon

asymmetry: in considering an approximate all-orders re-summation of the Higgs vev-

insertions in perturbation theory, Refs. [44, 43] showed that the resonance exhibited in

Eq. 4.10 is smoothed out (hence suppressed) by the resummation. Second, the resummation techniques of Refs. [44, 43] show that there are other, non-resonant contributions to S^{CPV} not appearing to lowest order in the vev-insertion approximation. These contributions are the dominant ones away from the resonance and for large values of the pseudoscalar Higgs mass, m_A, which we discuss below. The drawback of these approximately resummed sources is that it is not clear whether or not they are consistent with the power-counting done to calculate the relevant relaxation rates in the closed-time-path formalism [23] (for more details concerning the different existing techniques for evaluating the baryon asymmetry in the literature, see Ref. [10]). Since these non-resonant sources may open up more parameter space for EWB, we consider their impact separately in Sec. 4.6: we show there that our conclusions obtained in the vev-insertion approximation are qualitatively largely unchanged.

From the above form for the higgsino-gaugino source, Eq. 4.10, we see that accidental SUSY, with its prediction of light higgsinos and gauginos, can result in a sizable baryon asymmetry through the source terms described above, provided the relevant mass terms are nearly degenerate. Additionally, as mentioned above, the prediction of a rather light RH stop in accidental SUSY (c.f. Eq. 4.8), also fares well for EWB, since a light stop is required to prevent the efficient erasure of chiral charges by strong sphaleron processes[4]. These considerations, in conjunction with the generic strongly first-order phase transition potentially provided by the RS geometry, suggest that successful electroweak baryogenesis may be naturally and successfully accomplished in ac-

---

[4]Note that the suppression of the BAU with heavy stops can be ameliorated by considering so-called "lepton-mediated" scenarios of EWB [21]

cidental SUSY models. The question remains: what regions of the accidental SUSY parameter space are most likely to produce the observed baryon asymmetry while satisfying available experimental and observational constraints?

To address this question, we calculate the baryon asymmetry produced by higgsino-gaugino CP-violating interactions with the EWPT bubble wall. We vary the masses of the gauginos, $M_{1,2}$, while fixing μ by requiring the correct DM relic density, as discussed in Sec. 4.2. We show the resulting regions compatible with the observed baryon asymmetry (Y_{Obs}) for $m_A = 500, 1000$ GeV, maximal CP-violating phases, and with the choices for the other parameters discussed above in Fig. 4.2 on the left and right, respectively. Comparing Figs. 4.1 and 4.2, we see that the asymmetry is largest near the wino-higgsino resonance as expected, with a bino-like LSP. We discuss the resulting implications for viable accidental SUSY EWB and DM in light of the other relevant DM and EDM constraints in Sec. 4.7.

There are several theoretical uncertainties associated with the production of the baryon asymmetry at the electroweak phase transition. Dependence on the bubble wall parameters (the velocity, thickness, and variation of the ratio of Higgs vevs, $\Delta\beta$, across the wall) can introduce $\mathcal{O}(10 - 100$ GeV) uncertainties in the constant-BAU contours in the gaugino mass planes. For some of these parameters, the effect on Y_B is simple - for example, Y_B is linear in $\Delta\beta$ for the resonant sources used here. For the values of m_A we consider, $\Delta\beta$ ranges from $(0.2 - 2) \times 10^{-3}$ (using the two-loop results of Ref. [47]). The dependence on the wall width and velocity is not as straightforward, since these quantities enter into other terms of the transport equations
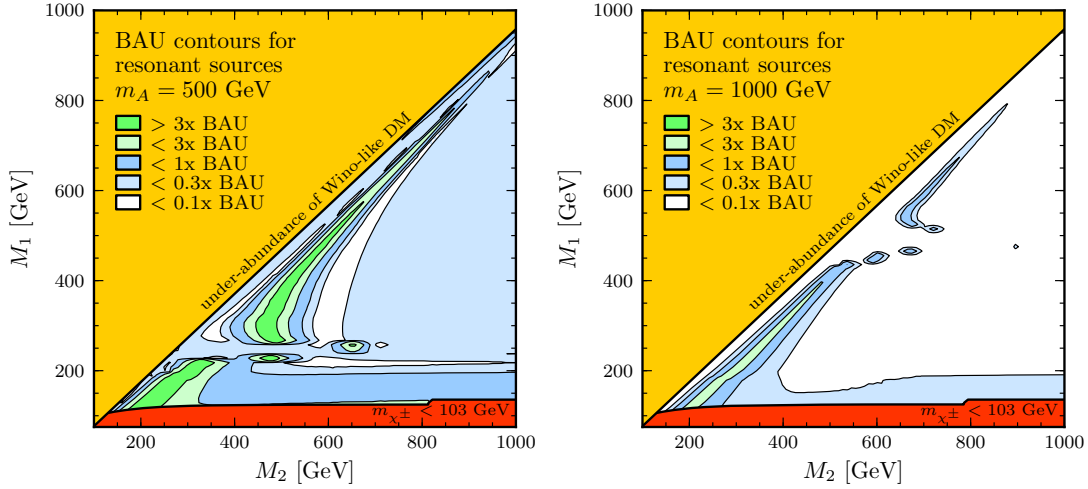
Figure 4.2: Curves of constant BAU (in units of the observed BAU) for the "well-tempered" neutralinos of Fig. 4.1 for $m_A = 500$ GeV (left) and 1000 GeV (right), assuming maximal CP-violating phases and the values of the various other parameters discussed in the text.

besides the CP-violating source, as well as in the integral over n_L. The BAU generally

decreases with increasing L_w and is maximized for values of v_w around a few $\times 10^{-2}$

(large velocities render the transport of chiral current inefficient, while smaller velocities

lead to a quasi-equilibrium situation, also suppressing the asymmetry) [41, 90]. In our

numerical calculation of the BAU we choose the optimistic values $v_w = 0.05$, $L_w = 5/T$

to estimate the maximal extent of the EWB-compatible parameter space.

An additional, significant, but to our knowledge less appreciated, uncertainty

on Y_B in the present calculational framework is that associated with the nucleation

temperature, T_n, around which the processes relevant for EWB occur. In Fig. 4.2, we

assumed $T_n = 100$ GeV; however, the nucleation temperature can in principle be lower

or higher than this value, and without a more detailed and model-dependent study

of the EWPT in accidental SUSY models, its value is at best known to an order of

magnitude.

It is however possible to quantitatively assess the impact of this uncertainty: we compute the baryon asymmetry for different values of T_n in Fig. 4.3. Lower temperatures reduce the baryon asymmetry, as the sphaleron rates are "slower" and the Boltzmann suppression stronger in this regime. Conversely, larger temperatures enhance the BAU. From considering constraints from EDMs (see below), we find that if the EWPT is made strongly first order by the mechanism of supercooling described above, the resulting nucleation temperature must not be too low ($\gtrsim 80$ GeV), otherwise much of the potentially viable parameter space for EWB and DM discussed in Sec. 4.7 will be ruled out[5]. We encourage the reader to bear this caveat in mind in interpreting our results in the following sections.

4.4 Electric Dipole Moments

The general MSSM contains 40 CP-violating phases in addition to the single CP-violating phase in the standard model CKM matrix. These generally give rise to EDMs and chromo-EDMs in elementary fermions, nucleons, and neutral atoms. The current non-observation of any such EDMs puts stringent constraints on beyond-the-standard-model physics (for a recent study of constraints on CP-violating phases from EDM searches see e.g. Ref. [111]).

In our model, all relevant one-loop single-particle EDMs are suppressed by the

_____

[5]This can be viewed as an upper limit on the number of inflationary e-folds surrounding the phase transition as discussed e.g. in Ref. [82]
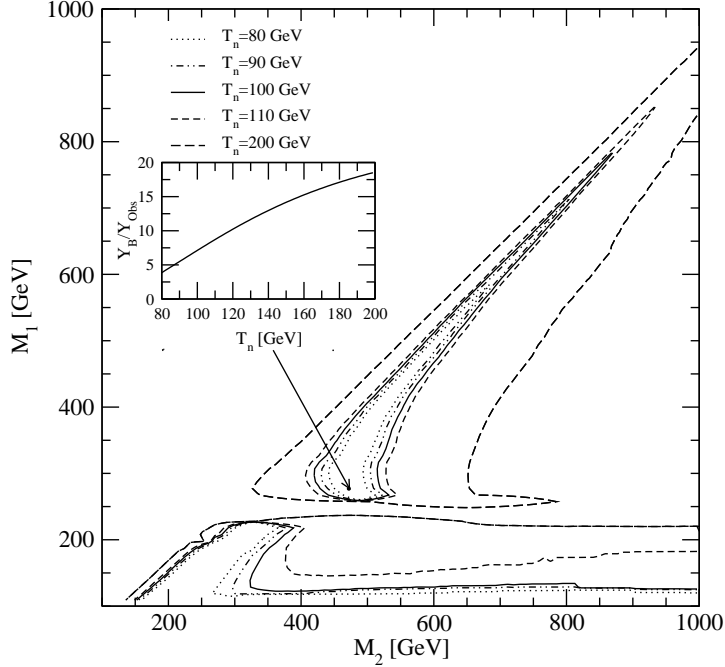
Figure 4.3: Curves of $Y_B = Y_{\text{Obs}}$ for different nucleation temperatures and for $m_A = 500$ GeV with maximal CP-violating phase. The points inside the contours can thus produce the observed baryon asymmetry for non-maximal CP-violating phases. The inset shows the temperature dependence of the resulting baryon asymmetry for a point near the resonance. Smaller nucleation temperatures reduce the weak sphaleron rate and result in larger Boltzmann suppression while larger temperatures can enhance the BAU.

large masses of the first and second-generation sfermions. Since we consider only CP-violation in the phases of M_1 and M_2 (or, equivalently, in μ)[6], there are no contributions to chromo-EDMs. Instead, the dominant contributions come from two-loop Barr–Zee-like diagrams [112] involving chargino-neutralino loops. The electron-EDM provides the most stringent constraint on our model, with an experimental bound of $|d_e| <$

---

[6]Technically, the physical CP-violating phases correspond here to $\phi_{M_{1,2}} \equiv \text{Arg}(\mu M_{1,2} b^*)$, with b the soft SUSY-breaking Higgs mass parameter.

$1.05 \times 10^{-27} e$-cm (coming from experiments on the YbF molecule) [67]. The current constraint from the neutron-EDM is also quite strong ($|d_n| < 2.9 \times 10^{-26} e$-cm) [68], but tends to be about 30% weaker than the electron constraint relative to our model's predictions. On-going experiments may improve the sensitivity to the electron EDM by up to two orders of magnitude (see, e.g., Ref. [70]), which has the potential to constrain almost the entire parameter space for baryogenesis in an accidental SUSY model. A non-null observation at that sensitivity level could also point to new physics consistent with this model.

We use the expressions in Ref. [69] to calculate the electron and neutron EDMs in our model, along with the FeynHiggs package [63] to calculate the Higgs mass and mixing angles including the full effects of CP violating phases. Fig. 4.4 shows curves of constant electron-EDM along the M_1–M_2 plane with maximal CP-violating phases, $\phi_{M_1} = \phi_{M_2} = \pi/2$. At each point, the value of μ is taken from Fig. 4.1 to provide the correct dark matter relic abundance. The experimental bounds on both electron and neutron-EDMs rule out the entire plotted parameter space *for maximally CP-violating phases*. Of course, smaller CP-phases are viable: the appropriate size of the CP violating phase depends on the requirement of matching the observed BAU, as calculated, for $\phi_{M_1} = \phi_{M_2} = \pi/2$, in Fig. 4.2. We postpone the calculation of the resulting EDM constraints to our summary section on the accidental SUSY parameter space in Sec. 4.7.
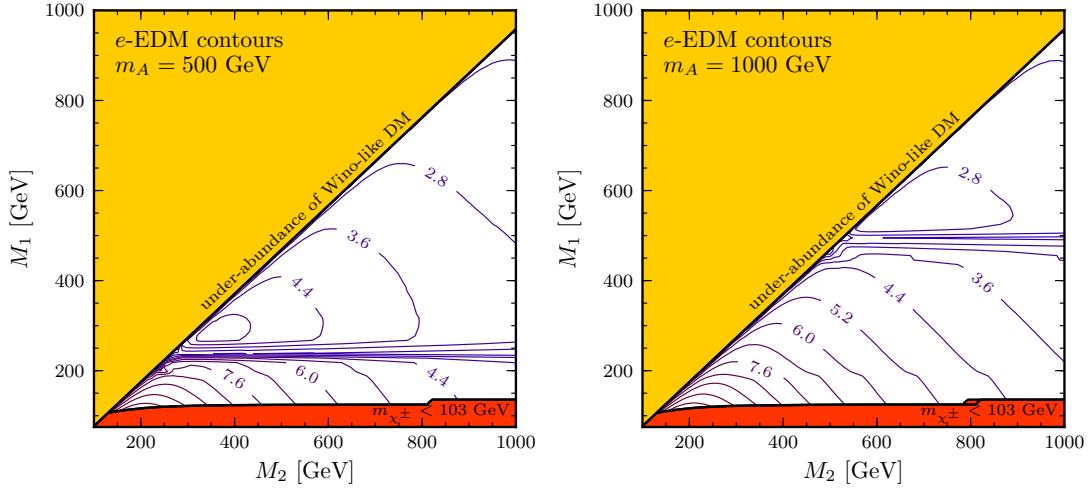
Figure 4.4: Curves of constant electron-EDM for $m_A = 500$ GeV (left) and 1000 GeV (right) and maximal CP-violating phase, $\phi_{M_1} = \phi_{M_2} = \pi/2$. The labels are in terms of the current experimental bounds: $d_e/d_{e-bound}$, where $d_{e-bound} = 1.05 \times 10^{-27} e$-cm. Curves of constant neutron-EDM (not shown) are qualitatively similar, but provide less stringent constraints.

4.5 Direct and Indirect Dark Matter Searches

The phenomenology of neutralino dark matter in the incarnation of the MSSM corresponding to the accidental SUSY framework described above depends, generically, on a relatively small set of parameters. These include the relevant mass scales entering the neutralino mass matrix (μ, M_1, M_2) and the mass scale of the heavy Higgs sector (e.g. fixed by the physical mass m_A). Other light particles, including the radion, radino, and stops, are largely non-influential, as long as none of those particles is the LSP. Our analysis of the (M_1, M_2) plane therefore satisfactorily exhausts the relevant dark matter phenomenology for the model under study.

We calculate in this section rates for the direct and indirect detection of dark matter. We start with the exploration, in Fig.4.5, of the spin-independent neutralino-
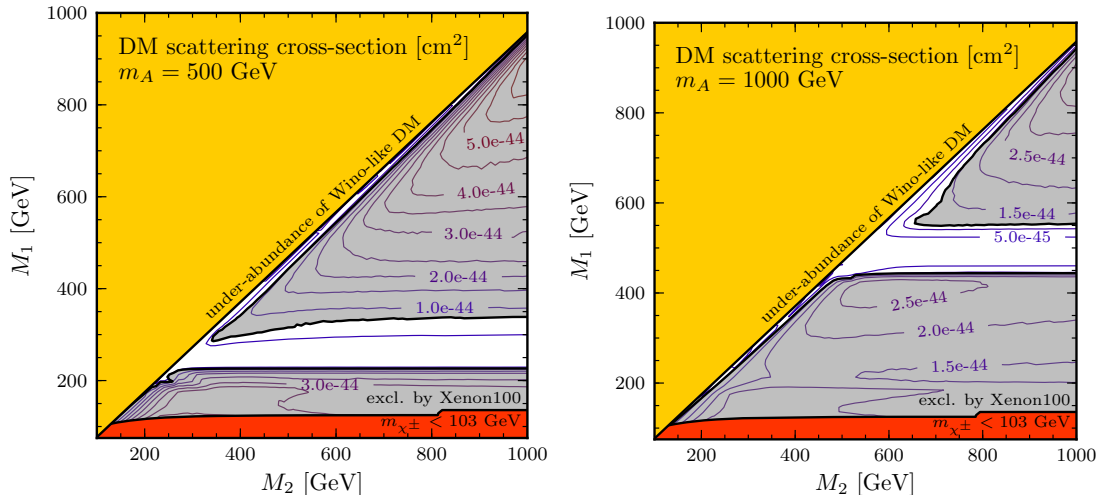
Figure 4.5: Curves of constant neutralino-proton elastic spin-independent scattering cross section, for the "well-tempered" neutralinos of Fig. 4.1, for $m_A = 500$ GeV (left) and 1000 GeV (right). Gray shaded regions are excluded by Xenon100.

proton scattering cross section, for which we show several iso-level curves[7]. In the present framework, this quantity depends on the coupling of the lightest neutralino to the CP-even Higgses h and H and thus, in turn, on the lightest neutralino's higgsino fraction. Small higgsino fraction, as encountered near the $M_1 \simeq M_2$ border and in the $m_\chi \simeq m_A/2$ resonance region, suppresses the scattering off of nucleons. The larger the higgsino mixing, the larger the cross section (which at large $\tan\beta$ is proportional to $(N_{11}(N_{12} - N_{13}))^2$, where N is the matrix that diagonalizes the neutralino mass matrix), as can be appreciated by noticing the increase in the cross section with M_1, which corresponds to values of μ that are increasingly more degenerate with M_1 in order to satisfy the relic density constraint.

We shade in grey the region that is already excluded by current, recent results

---

[7]For these and all other dark matter detection cross sections and rates, we employ the DarkSUSY code [106] with default parameters for the Galactic dark matter halo, quark content of the proton, etc.

from the Xenon100 experiment [113]. The recent results from 225 live days represent a very significant improvement over the previous years' results [114], with an important impact on the regions ruled out by direct dark matter searches. The region ruled out corresponds to $M_1 \lesssim 220$ GeV and $M_1 \gtrsim 300 - 350$ GeV for $m_A = 500$ GeV, and to $M_1 \lesssim 450$ GeV or $M_1 \gtrsim 550$ GeV for $m_A = 1000$ GeV (with the exception of the narrow regions at $M_1 \simeq M_2$). The pattern observed for the two values of m_A under consideration here continues for other values of m_A, leaving strips 60-100 GeV wide around $M_1 = m_A/2$.

In our calculations we have used the default nucleon matrix elements as in Ref. [115], although we note that there are significant uncertainties, stemming from both recent theoretical and experimental work, that affect the calculation of the proton-neutralino cross section via the relevant nucleon matrix elements (especially the strange quark content of the proton). We find that this uncertainty ranges from suppressing our results by a factor 0.6 to enhancing them by a factor 2.3. Correspondingly, the direct detection constraints become tighter or looser: the Reader can appreciate from the iso-level cruves we show in Fig. 4.5 how this impacts the parameter space ruled out by the Xenon100 limits. Additional uncertainties in where the constraints lie stem from astrophysical quantities such as the velocity distribution of dark matter in the vicinity of the Sun and the local dark matter density. Since there is at present no agreement on the determination of the relevant matrix elements, and in view of additional uncertainties from astrophysics, we take our default choice as a reasonable middle-ground estimate for the current experimental constraints from direct dark matter detection.
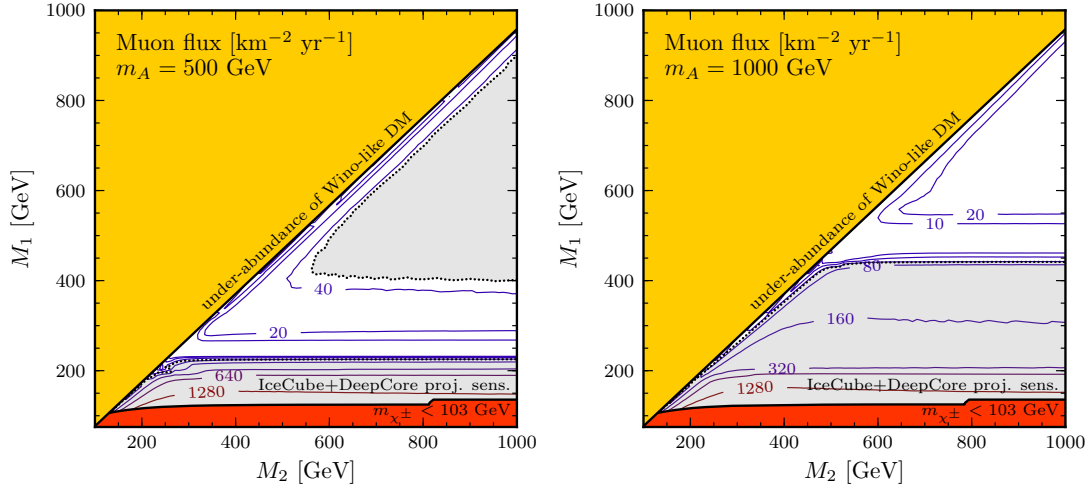
Figure 4.6: Curves of constant flux of muons from neutrinos produced by neutralino pair-annihilation in the Sun, for the "well-tempered" neutralinos of Fig. 4.1. Points in the gray shaded regions are expected to be probed by IceCube + DeepCore.

We now turn to indirect detection, and specifically to the search for high-energy neutrinos from the Sun produced by dark matter annihilation. In the very near future, the now-completed km^3 high-energy neutrino detector IceCube and the compact Cherenkov detector DeepCore operating at IceCube's center (and featuring a comparatively much lower energy threshold), will deliver data of great relevance in the search for particle dark matter. For the parameter space of interest here, the key search will be targeting high-energy neutrinos originating from neutralino pair-annihilation at the core of the Sun, where the neutralinos had been trapped by successive scattering with the Sun's nuclei.

Fig. 4.6 shows the predicted integrated muon flux for muons resulting from muon neutrino charged-current interactions, integrated above a conventional 1 GeV

threshold[8] for 180 live-days (roughly one year of operations), from neutrinos produced by neutralino pair-annihilation in the Sun. Current constraints from operating neutrino telescopes [52] do not exclude any of the shown parameter space. We shade in grey the region that will be probed with 180 days of IceCube80 plus Deep-Core data [52]. The neutrino flux from the Sun depends primarily on the capture rate in the Sun which, in turn, is highly sensitive to the spin-dependent neutralino-nucleon cross section. Again, this cross section depends on the higgsino fraction, and is suppressed in the regions of wino-bino mixing as well as in those where the mechanism that sets the correct neutralino thermal relic density is resonant annihilation, and where the higgsino fraction is much lower (see Fig. 4.1). Future prospects for neutrino telescopes are, overall, rather promising, covering most of the parameter space where resonant pair-annihilation does not occur. Current direct detection results (Fig. 4.5), however, exclude the possibility to have a signal from neutrino telescopes in this model at the sensitivity level under consideration here.

Finally, in Fig. 4.7 we concentrate on other indirect detection methods, such as the search for gamma-rays or of antimatter resulting from the pair-annihilation of dark matter in the Galactic halo. All of the associated rates depend linearly upon the (zero temperature, thermally averaged) pair-annihilation cross section $\langle \sigma v \rangle$, and, generically, on the inverse of the dark matter particle mass. We thus plot curves of constant $\langle \sigma v \rangle / m_\chi^2$. We find that the neutralino pair annihilation cross section is uniformly close

---

[8]We note that IceCube has a much higher energy threshold, but the combined reach of IceCube-DeepCore is customarily expressed in terms of the integrated flux above 1 GeV, for a given final state (in this case pair-annihilation into W^+W^- and ZZ).
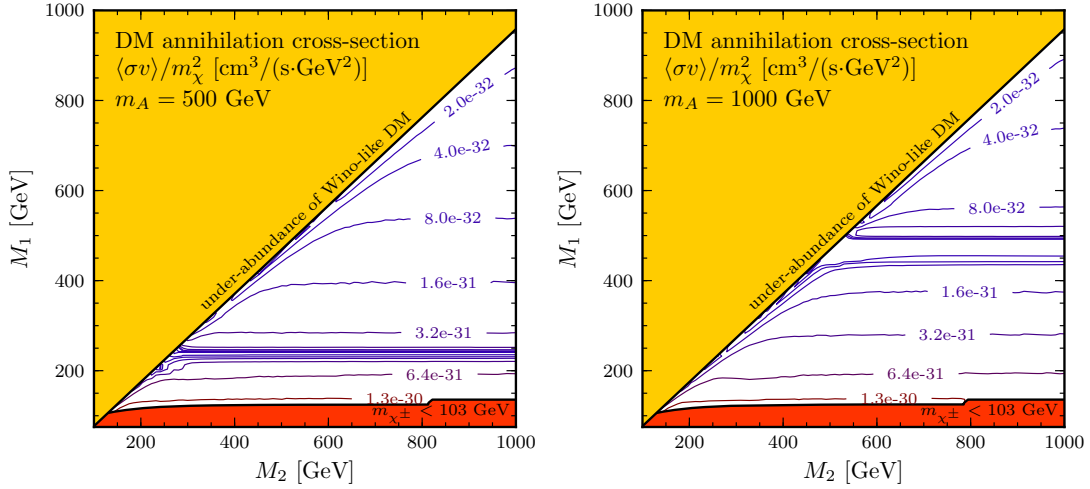
Figure 4.7: Curves of constant neutralino zero-temperature thermally averaged pair-annihilation cross section $\langle \sigma v \rangle$ divided by the neutralino mass squared, for the "well-tempered" neutralinos of Fig. 4.1.

to $\langle \sigma v \rangle \simeq (1 - 2.5) \times 10^{-26} \mathrm{cm^3/s}$; we note that this value differs from the canonical $\langle \sigma v \rangle \simeq 3 \times 10^{-26} \mathrm{cm^3/s}$ because of neutralino co-annihilation with the chargino and next-to-lightest neutralino that contribute significantly to the freeze-out process when $M_1 \simeq \mu$. The ratio $\langle \sigma v \rangle / m_\chi^2$ illustrates that all parameter space is beyond current constraints from gamma-rays [116], from which $\langle \sigma v \rangle / m_\chi^2$ is constrained to be smaller than approximately 3×10^{-29} $\mathrm{cm^2 s^{-1} GeV^{-2}}$. This is primarily due to the relatively large values of the neutralino masses in the regions of interest, $m_\chi \gtrsim 100$ GeV. We note, incidentally, that constraints from antimatter are highly dependent on assumptions on cosmic ray propagation, and are not tighter than those from gamma-rays for conservative choices of the parameters describing cosmic-ray Galactic diffusion. The low-M_1 region has values of $\langle \sigma v \rangle / m_\chi^2$ only a factor of about 4 beyond current limits, and they might thus be testable with increased statistics from the Fermi Large Area Telescope

[117]. Going beyond the projected reach of neutrino telescopes would, however, need an improvement of more than one order of magnitude over existing limits, which appears unrealistic in the immediate future.

4.6   Non-resonant sources

Before discussing the accidental SUSY DM and EWB parameter space, we briefly address the potential effects of non-resonant CP-violating sources on EWB. The source we consider in Eq. 4.10 was computed in the Higgs vev-insertion approximation, in which interactions of the higgsinos, gauginos, and Higgs vevs at the EWPT bubble wall are treated perturbatively. This framework is also used to compute the chiral relaxation rates, whose resulting resonant structure must be taken into account to obtain more realistic estimates for the BAU. Alternatively, one can implement a resummation of the vev-insertions for the CP-violating sources by considering the interactions with the Higgs vevs as resulting in spacetime-dependent mass matrices for the supersymmetric particles. This was carried out in Refs. [44, 43], which showed that the resummation effectively "smooths out" the resonance predicted by the vev-insertion approximation, and results in new sources that are not obtained in the vev-insertion method. These new CP-violating sources are not resonant and are not proportional to $\Delta\beta$, hence escaping the suppression for increasing m_A. While the resonant sources will dominate for regions with $M_{1,2} \sim \mu$, the non-resonant contributions may become important away from these regions.

To investigate the impact of non-resonant sources on the accidental SUSY EWB parameter space, we calculate the baryon asymmetry[9] following the methods of Refs. [44, 43] with the well-tempered neutralino values in the gaugino mass planes and the same assumptions for the particle spectrum as in Sec. 4.3. The results are shown in Fig. 4.8 for $m_A = 500, 1000$ GeV on the left and right, respectively, for maximal CP-violating phase. As expected, the non-resonant contributions dominate away from the resonance, as can be seen by comparing Figs. 4.2 and 4.8. However, for our choices of parameters, these sources do not open up any additional viable parameter space for EWB, other than potentially the green region on the right of Fig. 4.8, which is solidly ruled out by direct dark matter searches. We discuss the effects of including non-resonant contributions on the EWB-compatible accidental SUSY parameter space below. Note that these sources enter with *opposite sign* relative to the resonant sources we consider in Sec. 4.3.

4.7   The Accidental SUSY baryogenesis parameter space

In this section we summarize our findings, and search for the portions of the parameter space of accidental supersymmetry that produce both a good thermal relic neutralino abundance and successful baryogenesis at the electroweak phase transition. To do so, we consider both resonant sources only (Fig. 4.9) and resonant plus non-resonant sources (Fig. 4.10). We calculate the maximal BAU that can be produced at

---

[9]As in Refs. [44, 43], we consider only the chargino contribution to the CP-violating source in this Section.
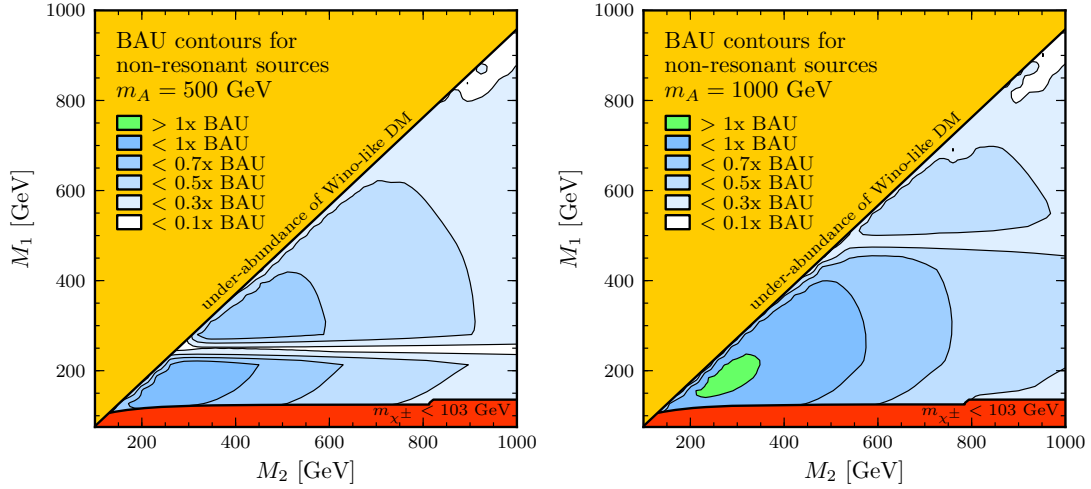
Figure 4.8: Curves of constant BAU from non-resonant sources, in units of the observed BAU, for the "well-tempered" neutralinos of Fig. 4.1, for $m_A = 500$ GeV (left) and 1000 GeV (right)

each parameter space point such that constraints from EDM searches are not violated, and we superimpose limits deriving from dark matter direct searches with Xenon100. As noted above, results for intermediate values of m_A interpolate between what we find for the two specific values chosen here.

The key findings of this section are that:

- the lightest neutralino mass must have a mass between 200 and 500 GeV

- the masses of all charginos and neutralinos lie within a factor 2 of the lightest neutralino mass

- the heavy Higgs sector must be below 1 TeV (no viable parameter space is open for $m_A \gtrsim 1$ TeV, see the right panel of Fig. 4.9 and 4.10) and lies within approximately 20-25% of twice the lightest neutralino mass (to comply with direct detection constraints)
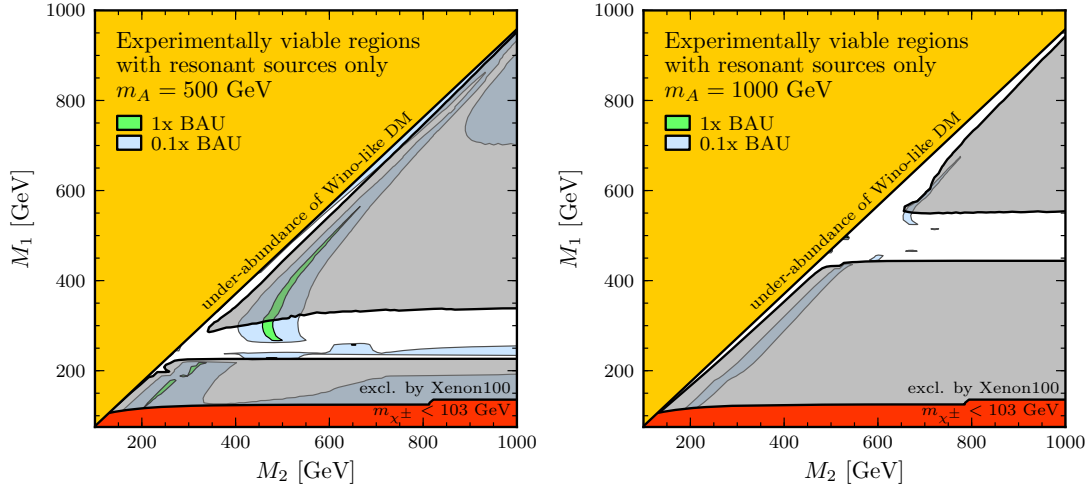
Figure 4.9: A summary plot for the parameter space of accidental supersymmetry compatible with successful electroweak baryogenesis, constraints from EDMs and dark matter searches. The green regions correspond to regions that produce 100% of the BAU and that are compatible with EDM searches; within the light blue regions, CP-violating phases compatible with EDM constraints yield a BAU greater or equal to 10% of the observed value. We shade in gray the portion of parameter space ruled out by direct dark matter searches with Xenon100 [113], and as in all other plots we set $m_A = 500$ GeV in the left panel and 1000 GeV in the right panel.
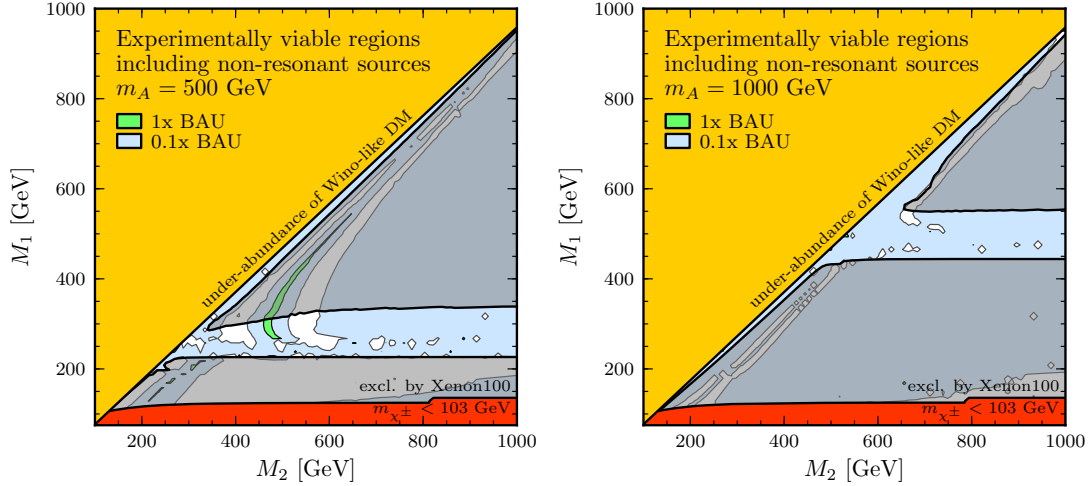
Figure 4.10: Same as in Fig. 4.9, but now including non-resonant sources, for $m_A = 500$ GeV (left) and 1000 GeV (right).

Fig. 4.9 shows the allowed parameter space that is consistent with the observed dark matter relic abundance, electroweak baryogenesis, EDM constraints, and dark matter direct detection constraints, ignoring the contribution of non-resonant sources. As in all other plots, at each point on the M_1–M_2 plane, μ is set to give the correct dark matter abundance. The phases $\phi_{M_1} = \phi_{M_2}$ are set to the maximal value compatible with EDM searches. The green central region is consistent with all of the baryon asymmetry coming from the electroweak phase transition, whereas in the larger blue regions electroweak baryogenesis would only account for a fraction of the asymmetry, at least 10%, unless a correction of order unity is applied to the calculation of the BAU.

Across the parameter space we consider here, the only viable regions are those for which the baryon asymmetry (as calculated, for a maximal CP-violating phase, in Fig. 4.2) is large enough such that the regions still satisfy the BAU requirement when the CP-phase is reduced to avoid the EDM constraints. For $m_A = 1000$ GeV, we find no viable region of parameter space satisfying all requirements we impose; in fact, the allowed region (shaded green in Figs. 4.9-4.10) vanishes for $m_A \gtrsim 700$ GeV. We note that M_1 (and thus the lightest neutralino mass, in the parameter space of interest here) ranges between 200 (for smaller values of m_A, consistent with particle physics constraints such as e.g. those arising from $b \rightarrow s\gamma$) and 500 GeV; μ and M_2 are both within a factor 2 of M_1, with a degree of degeneracy that increases with increasing mass. As a result, all four neutralinos and two charginos in the electroweak "-ino" sector are compressed to within a factor 2 of the lightest neutralino mass, whose value is, in turn, constrained to $200 \lesssim m_\chi/\text{GeV} \lesssim 500$. Also, Fig. 4.9 and 4.10 illustrate that direct

133

detection constraints imply that the heavy Higgs sector lie within 20-25% of twice the LSP mass.

Fig. 4.10 adds to the calculation of the BAU the non-resonant sources contribution discussed in sec. 4.6. Non-resonant sources play an important role in opening up most of the accidental SUSY parameter space outside the regions where resonant terms (with which they negatively interfere) are important. Still, non-resonant contributions fall short of producing 100% of the observed BAU, which is again limited to an even narrower region of parameter space with $M_1 \sim M_2 \sim \mu$. Also, we find again that no parameter space is open at $m_A = 1$ TeV if one insists on successful EWB. Qualitatively, the addition of non-resonant sources does not change our conclusions.

4.8 Discussion and Summary

Accidental supersymmetry is a particle physics framework that naturally addresses both the large and the little hierarchy problems as well as the potential CP and flavor problems of supersymmetry, while in principle providing a successful thermal dark matter candidate. We argued here that this framework naturally accommodates successful electroweak baryogenesis, for the following reasons:

(i) a strongly first order electroweak phase transition may be a generic feature of this framework, either as a consequence of supercooling produced by the phase transition between the high and low-temperature RS spacetimes, or from the contribution of a singlet to the superpotential as may be required to solve the μ-problem;

(ii) light third-generation stops and gauginos allow for resonant CP-violating sources to produce potentially large net chiral currents fueling a large enough net baryon number via sphaleron transitions;

(iii) heavy first- and second-generation sfermions prevent excessive one-loop contributions to observable electric dipole moments in the presence of the needed large CP-violating phases.

Here, we carried out a model-independent study (from the standpoint of supersymmetry breaking), although for definiteness we picked a specific accidental SUSY spectrum realization. Specifically, we let the relevant $U(1)_Y$ and $SU(2)$ gaugino soft supersymmetry breaking masses M_1 and M_2, as well as the higgsino mass parameter μ vary freely. We constrained this triplet of mass parameters enforcing that the lightest supersymmetric particle be a neutralino with a thermal relic density matching the observed density of dark matter. In practice, this amounted to selecting values of μ across the $(M_1,\ M_2)$ parameter space so that the higgsino fraction drove the thermal relic density of the lightest neutralino to the desired value.

After enforcing the relic density constraint, we proceeded to calculate the baryon asymmetry resulting from electroweak baryogenesis across the $(M_1,\ M_2)$ parameter space. We included both resonant and non-resonant sources, and we picked two representative values for the heavy Higgs sector mass scale, which is relevant for resonant sources. The requirement of successful baryogenesis generically restricted the viable parameter space to a relatively narrow funnel at $M_1 \lesssim M_2$, with $\mu \sim M_1,\ M_2$;

recent direct detection constraints also enforce $M_1 \simeq m_A/2$ to within 20-25%.

The strongest constraints on this framework derive from the non-observation of electric dipole moments and of signals from dark matter direct detection, most notably with the Xenon100 experiment [113]. We calculated in detail how these constraints restrict the parameter space relevant for baryogenesis, concluding that dark matter direct searches eliminate neutralinos with a large higgsino fraction (requiring to some degree resonant annihilation through the heavy Higgs sector, and hence $M_1 \simeq m_A/2$), while electric dipole moments greatly restrict regions of viable electroweak baryogenesis to those parameter space points producing, for maximal CP violating phases, a BAU much larger than observed (those parameter space regions are then compatible with successful baryogenesis as the CP phases are lowered to comply with EDM searches).

We calculated the predicted EDM and dark matter search rates in the framework of accidental supersymmetric baryogenesis and we concluded that:

- the most sensitive EDM search to constrain this model is provided by searches for the electron EDM; an improvement of one order of magnitude on the current experimental sensitivity would conclusively test the framework, even allowing for some theoretical uncertainties in the calculation of the BAU;

- the entire parameter is highly constrained by current direct, spin-independent dark matter-nucleon cross section limits, and will soon be fully tested even for resonant neutralino annihilation

- the predicted signal at neutrino telescopes from neutralino annihilation in the

core of the Sun is potentially large enough for detection, although direct detection results imply that no signal is expected within approximately one year of data taking

The parameter space compatible with successful baryogenesis and thermal dark matter is highly constrained, and is characterized by a lightest neutralino with a mass between 200 and 500 GeV, with all other neutralino and chargino masses within a factor 2 of the lightest neutralino mass, with $m_A \simeq 2M_1 < 1$ TeV. This compressed electroweak "inos" spectrum might be challenging for LHC searches, but would be ideally targeted with an e^+e^- linear collider with a TeV center of mass energy.

Concluding, we demonstrated here that accidental supersymmetry is an explicit realization of a framework for successful thermal relic dark matter and electroweak baryogenesis, which is motivated by an entirely different set of theoretical arguments based upon addressing the hierarchy, CP and flavor problems. We showed that accidental supersymmetric baryogenesis is a highly constrained setup, but one with very sharp experimental predictions for electric dipole moment, dark matter, and collider searches. We therefore anticipate that this scenario be falsified or produce signals in the very near future in a variety of experiments.

5

NMSSM Electroweak Baryogenesis with a 130 GeV Fermi Line

In the search for signatures from the annihilation (or the decay) of dark matter particles, a gamma-ray line in the multi-GeV energy range has long been considered a Holy Grail. Given that, in the weakly interacting massive particle (WIMP) paradigm, Galactic dark matter is virtually at rest, the pair annihilation of two particles into a final state consisting of two photons would produce a monochromatic line with an energy exactly corresponding to the particle dark matter mass (or to half its mass in the case of decay). The advent of the Fermi gamma-ray Large Area Telescope (LAT) heralded promise of potentially delivering this smoking gun signal, which would then serve as a beacon for further searches to close in on a well-defined particle dark matter mass.

Despite a null result presented by the LAT collaboration in Ref. [118], independent scholars analyzed the Fermi data employing optimized signal-to-noise regions,

unveiling a tantalizing excess localized around 130 GeV[1] and originating from regions

including the Galactic center [120, 121]. Subsequent independent analyses confirmed the

original claim, typically attributing an even larger level of confidence to the discovery

of a monochromatic line in the Fermi-LAT data from the center of the Galaxy [122].

Understandably, the discovery of the line spurred a great deal of interest in

the community: a feature in the Earth limb photon events at the same energy was

found, albeit with a much lower statistical significance [122]; despite significant efforts

in pinpointing possible instrumental or environmental effects that could explain the

excess (see e.g. Ref. [123]), at present the line feature appears statistically significant

enough to deserve serious consideration.

From a model-building and phenomenological standpoint, the 130 GeV line

poses interesting challenges: with default choices for the dark matter density profile in

the Galaxy, the required pair-annihilation cross section for dark matter (at rest, i.e.

at "zero temperature") into two photons is about $\langle \sigma v \rangle_{\gamma\gamma} \sim 10^{-27} cm^3/s$, much larger

than would be expected by suppressing by a factor α^2 the pair annihilation cross section

expected for WIMP thermal production in the early universe. Even more problematic is

the absence of a continuum gamma-ray signal accompanying the line in the region where

the line is detected. This poses the question of how to suppress final states that would

generously produce e.g. neutral pions from hadronization showers of strongly interacting

particles, or inverse Compton or bremsstrahlung photons from charged leptons.

Simple paradigms for WIMP dark matter fail at explaining the needed features

---

[1]Recent re-analyses with reprocessed data using "Pass 7 Clean" events put the line at 135 GeV [119], but nothing qualitative changes in the present discussion, where we will assume the line is at 130 GeV.
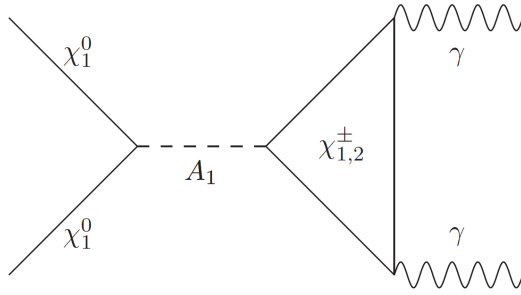
Figure 5.1: *The dominant diagram leading to the two-photon pair-annihilation of neutralinos in the NMSSM scenario under consideration in this study.*

of the 130 GeV line. For example, neutralinos within the minimal supersymmetric extension of the Standard Model (MSSM) feature large suppressions in the pair annihilation into two photons with respect to any other final state, and the required large rate for neutralino pair-annihilation into two photons cannot be accommodated with the right thermal relic abundance [124].

A simple extension to the field content of the MSSM, however, allows for an interesting caveat to both shortcomings mentioned above, as first realized in Ref. [125]: within the next-to-MSSM (or NMSSM, hereafter), an s-channel resonant contribution exists to the annihilation cross section arising from the diagram shown in Fig. 5.1, where two approximately 130 GeV bino-like neutralinos annihilate into a singlet-like pseudoscalar A_1, which then decays into photons via a chargino loop. For $m_{A_1} \sim 260$ GeV, the process is resonant and the resulting cross-section can easily satisfy $\langle \sigma v \rangle_{\gamma\gamma} \sim 10^{-27} cm^3/s$ as required to produce the observed line [120].

The NMSSM possesses the interesting additional possibility of naturally realizing a mechanism known as *electroweak baryogenesis* to produce the observed baryon

asymmetry of the universe (BAU) at the electroweak phase transition (EWPT) (for a recent review, see Ref. [10]). The NMSSM framework, in fact, accommodates tree-level cubic couplings entering the relevant scalar effective potential driving the EWPT needed to produce a sufficiently strongly first-order phase transition (this is in turn needed to prevent wash-out of the generated baryon asymmetry in regions of broken electroweak phase), as realized a long time ago [61, 126] and reinforced in recent analyses [127] (see Refs. [91, 92] for similar arguments in related models). Additionally, the NMSSM, like the MSSM, possesses enough room to host the level of CP violation needed for baryogenesis while being consistent with constraints from the non-observation of electric dipole moments (EDMs).

In the present study, we argue that the NMSSM can simultaneously accommodate:

1. a thermal dark matter candidate that can produce the 130 GeV line while being consistent with constraints from other gamma-ray observations and direct detection searches;

2. a Higgs sector consistent with the recent LHC findings [14, 15];

3. a strongly first-order phase transition as needed by electroweak baryogenesis (for which we calculate in detail the effective finite temperature potential);

4. the generation of the observed baryon asymmetry of the universe at the EWPT, while being consistent with constraints from EDMs.

Requiring all four conditions above forces us to very special corners of the

theory's parameter space: the goal of our study is not to explore exhaustively the NMSSM parameter space but, rather, to outline the general implications for the theory parameter space of the four requirements above, and to draw predictions from the regions of parameter space that do satisfy these requirements. As a result, we do not concern ourselves with issues of fine-tuning but, rather, we produce a detailed set of predictions that put this framework for the origin of baryonic and dark matter on very testable grounds. At the same time, we provide benchmarks for corners of the NMSSM theory parameter space where all conditions listed above may be fulfilled.

This paper is organized as follows: in Sec. 5.1 we outline the NMSSM parameter space, detail the neutralino and Higgs sectors, and discuss the phenomenological constraints we implement; Sec. 5.2 discusses the nature of the electroweak phase transition and the constraints that a strongly first-order transition places upon the parameter space; in Sec. 5.3 we discuss the computation of the baryon asymmetry; we conclude in Sec. 5.4

5.1 A 130 GeV Line in the NMSSM

To begin, we review the NMSSM setup, and show how it is possible to hone in on parameters consistent with the 130 GeV gamma-ray signal and with a broad set of additional phenomenological constraints. We follow closely the strategy outlined in Refs. [125, 128] and consider the simplest incarnation of the NMSSM with a scale-

invariant, $\mathbb{Z}_3$-symmetric superpotential:

$$W = W_{\mathrm{MSSM}}|_{\mu=0} + \lambda \widehat{S} \widehat{H}_u \widehat{H}_d + \frac{\kappa}{3} \widehat{S}^3, \qquad (5.1)$$

where hatted quantities denote the corresponding superfields, and where S is a gauge singlet. The soft supersymmetry-breaking Lagrangian is given by

$$-\mathcal{L}^{soft} = -\mathcal{L}^{soft}_{\mathrm{MSSM}} + m_S^2 |S|^2 + \left(\lambda A_\lambda S H_u H_d + \frac{1}{3} \kappa A_\kappa S^3 \right) + \mathrm{h.c.} \qquad (5.2)$$

After electroweak symmetry breaking (EWSB), the Higgs and singlet fields obtain vacuum expectation values (vevs) of $\langle H_u \rangle \equiv v_u$, $\langle H_d \rangle \equiv v_d$, and $\langle S \rangle \equiv v_s$. As in the MSSM, we denote the ratio of the $SU(2)$ Higgs vevs as $\tan\beta \equiv v_u/v_d$. The singlet vev generates an effective μ-term in the superpotential given by $\mu \equiv \lambda v_s$. We assume that $\lambda, v_s \in \mathbb{R}$ so that μ is real and there is no CP-violation at tree level in the Higgs sector. While CP-violating effects can enter at one-loop from gaugino interactions if we allow $M_{1,2}$ to carry a complex phase, we neglect these contributions when considering radiative corrections to the Higgs sector, since these effects are typically sub-dominant. The six parameters λ, κ, A_λ, A_κ, μ and $\tan\beta$ then determine the tree-level Higgs spectrum after minimizing the scalar potential and solving for the SUSY-breaking Higgs masses.

At this level, deviations from the spectrum of the MSSM originate from the singlet superfield in the superpotential, and are crucial in order to obtain a neutralino consistent with the 130 GeV gamma-ray signal (without an associated continuum gamma-ray background), with a 125 GeV Higgs, and with successful electroweak baryogenesis. Specifically, the present set-up contains one each of additional neutral CP-even and CP-odd states which enter into the respective Higgs mixing matrices. Complete expressions

for the various relevant mass matrices in the NMSSM which match our conventions can be found in, e.g., Ref. [129].

The pseudoscalar mass matrix will be of particular importance; its elements are given, to one-loop order, by [129]

$$
\begin{aligned}
\mathcal{M}^2_{P,11} &= \lambda v_s \left(A_\lambda + \kappa v_s \right) \left(\frac{\tan \beta(Q)}{Z_{H_d}} + \frac{\cot \beta(Q)}{Z_{H_u}} \right) \\
\mathcal{M}^2_{P,22} &= 4\lambda \kappa v_u(Q) v_d(Q) + \lambda A_\lambda \frac{v_u(Q) v_d(Q)}{v_s} - 3\kappa A_\kappa v_s \\
\mathcal{M}^2_{P,12} &= \lambda \left(\frac{v_u(Q)^2}{Z_{H_d}} + \frac{v_d(Q)^2}{Z_{H_u}} \right)^{1/2} \left(A_\lambda - 2\kappa v_s \right),
\end{aligned}
\tag{5.3}
$$

where Q is the relevant SUSY energy scale; $v_{u,d}(Q)$ and $\tan \beta(Q)$ are the Higgs vevs and $\tan \beta$ at the scale Q; and $Z_{H_{u,d}}(Q)$ are wave-function renormalization factors. The matrix $\mathcal{M}_P$ can be diagonalized to obtain the pseudoscalar mass eigenstates A_1 and A_2. As we discuss below, in the present setup A_1 must be singlet-like; the state A_2 will therefore correspond to an MSSM-like pseudoscalar Higgs boson.

In addition to the new degrees of freedom in the Higgs sector, there is an additional Weyl fermion (the "singlino", $\widetilde{S}$), corresponding to the fermionic component of the singlet superfield $\widehat{S}$. This fermionic degree of freedom enters into the neutralino mixing matrix, whose components are given at tree level by [129]

$$
\mathcal{M}_{\chi^0} =
\begin{pmatrix}
M_1 & 0 & \frac{g_1 v_u}{\sqrt{2}} & -\frac{g_1 v_d}{\sqrt{2}} & 0 \\
\cdot & M_2 & \frac{g_2 v_u}{\sqrt{2}} & \frac{g_2 v_d}{\sqrt{2}} & 0 \\
\cdot & \cdot & 0 & -\mu & -\lambda v_d \\
\cdot & \cdot & \cdot & 0 & -\lambda v_u \\
\cdot & \cdot & \cdot & \cdot & 2\kappa v_s
\end{pmatrix}.
\tag{5.4}
$$

144

Here, we shall consider the case in which the baryon asymmetry is sourced by CP-violation in the higgsino-gaugino sector [10]. The masses in Eq. (5.4) are therefore generically complex-valued. We will further restrict ourselves to the case of a single complex physical phase, in the wino mass M_2, with all other parameters real[2]. This results in CP-conservation at tree-level in the Higgs sector. Since in our construction the LSP is bino-like throughout all of the parameter space we consider, a CP-violating phase in M_1 would produce large effects on the calculation of the various dark matter properties; we therefore impose $M_1 \in \mathbb{R}$. Eq. (5.4) is diagonalized by the unitary complex matrix $\mathcal{N}$:

$$\mathcal{M}'_{\chi^0} = \mathcal{N}^* \mathcal{M}_{\chi^0} \mathcal{N}^\dagger \tag{5.5}$$

and the neutralino masses are given by

$$\text{diag}\left(m^2_{\chi_1^0},\ m^2_{\chi_2^0},\ m^2_{\chi_3^0},\ m^2_{\chi_4^0},\ m^2_{\chi_5^0}\right) = \mathcal{M}'^\dagger_{\chi^0} \mathcal{M}'_{\chi^0}. \tag{5.6}$$

The five neutralinos are admixtures of $\widetilde{B}$, $\widetilde{W}$, $\widetilde{H}_{u,d}$, and $\widetilde{S}$, the lightest of which will be the lightest supersymmetric particle (LSP) in our setup. The chargino mass matrix is simply that of the MSSM, again with a possible complex phase in the wino mass entry, yielding the mass eigenstates $\chi^\pm_{1,2}$.

Motivated by the lack of a SUSY particle discovery at the LHC, we will typically assume that all sfermions are heavy[3], with $m_{sf} \gtrsim 1.5$ TeV. This effectively decou-

---

[2]Note that the physical phase we consider here effectively corresponds we to the phase $\phi \equiv \arg(\mu M_2 b^*)$, see e.g. Ref. [48]

[3]Note that the authors of Ref. [125] considered rather light sleptons to account for the possible discrepancy of the muon $g - 2$ with the value predicted by the SM. However, in the present case, such light sleptons can result in large one-loop contributions to the electric dipole moments inconsistent with the constraints discussed in Sec. 5.3.3, barring cancellations.

ples them from any process of interest here. As a result, to determine the properties of neutralino dark matter, the electroweak phase transition, and the CP-violating sources for electroweak baryogenesis in the present set-up, one must specify the following nine NMSSM parameters:

$$\lambda, \quad \kappa, \quad A_\lambda, \quad A_\kappa, \quad \mu, \quad \tan\beta, \quad M_1, \quad |M_2| \quad \phi \equiv \arg(M_2). \tag{5.7}$$

As we argue below, many of these parameters are tightly constrained by the phenomenological and observational constraints we impose, in particular by requiring a 130 GeV gamma ray line from resonant neutralino annihilation consistent with other particle and dark matter searches.

Throughout this study, we will assume that the large required pair-annihilation cross-section into two photons, $\langle\sigma v\rangle_{\gamma\gamma} \geq 10^{-27}$ cm^3/s, arises from the on-resonance s-channel annihilation of neutralinos into A_1, which in turn couples to two photons through a chargino loop (see Fig. 5.1). The dominant contribution to the thermally averaged cross-section for this process at zero temperature is given by [124]

$$\langle\sigma v\rangle_{\gamma\gamma} = \frac{\alpha^2 m_{\chi_1^0}^2}{16\pi^3} \left| \sum_{i=1,2} \frac{M_{\chi_i^\pm} m_{\chi_1^0}}{4 m_{\chi_1^0}^2 \left(4 m_{\chi_1^0}^2 - m_{A_1}^2\right)} \; g_{A_1\chi_1^0} \; g_{A_1\chi_i^\pm} \; F\left(\frac{m_{\chi_1^0}}{m_{A_1}}, \frac{M_{\chi_i^\pm}}{m_{A_1}}\right) \right|^2 \tag{5.8}$$

where the function $F(a,b)$ is defined by

$$F(a,b) \equiv \int_0^1 \frac{dx}{x} \log\left(\left|\frac{4ax^2 - 4ax + b}{b}\right|\right) \tag{5.9}$$

and the couplings $g_{A_1\chi_1^0}$, $g_{A_1\chi_i^\pm}$ depend on the neutralino, chargino, and CP-odd Higgs diagonalizing matrices. To compute these couplings, we use the Feynman rules found in Ref. [129], appropriately modified to match our conventions for the neutralino and

146
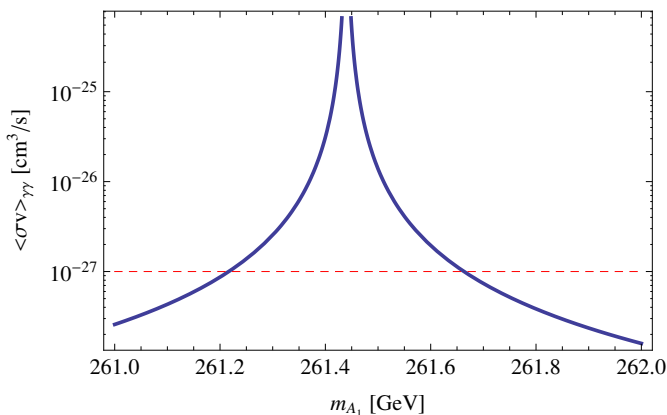
Figure 5.2: The zero-temperature thermally-averaged cross-section times velocity for neutralino annihilation into two photons as a function of the singlet-like pseudoscalar mass m_{A_1} for the EWPT benchmark point discussed in Sec. 5.2: $\lambda = 0.75$, $\kappa = 0.45$, $\tan \beta = 1.7$, $A_\lambda = 545$ GeV, $A_\kappa = -88$ GeV, $\mu = 275.8$ GeV, $M_1 = 143.5$ GeV, and $M_2 = 635.5$ GeV. The red dashed line indicates the lower bound on $\langle \sigma v \rangle_{\gamma\gamma}$ required to produce the 130 GeV Fermi line. Note that decreasing M_1 (thereby increasing μ) will narrow down the resonance.

chargino matrices, which contain complex mass entries. This cross-section is plotted as a function of m_{A_1} for a particular choice of parameters, in Fig. 5.2, which clearly shows the narrow resonant structure.

5.1.1   Suitable Higgs and Neutralino Sectors

Given our set-up, we can elucidate the parameter space regions capable of producing the gamma-ray line while satisfying all other dark matter and particle physics constraints. As we show below, requiring a 130 GeV line from resonant neutralino annihilation restricts the NMSSM parameter space to a narrow region in which we can study electroweak baryogenesis and the electroweak phase transition, in addition to producing unambiguous predictions for several experimentally observable quantities, such as electric dipole moments and dark matter detection rates.

In general, the properties associated with the neutralino LSP depend sensitively on the details of the various parameters involved; this can be appreciated by considering the different benchmark points discussed in Refs. [125, 128]. For example, the annihilation cross-section into photons, Eq. (5.8), is strongly affected by the mass splitting $\left| m_{A_1} - 2m_{\chi_1^0} \right|$, as shown in Fig. 5.2. Correspondingly, other resonant processes, such as the s-channel neutralino pair annihilation into $b\bar{b}$ through A_1, also depend on the mass difference. The details of the various resonant channels significantly affect both the zero-temperature and the finite-temperature annihilation cross sections (the latter being relevant for the calculation of the thermal relic density of dark matter). The amplitudes associated with these processes can however be tuned so that the neutralinos produce a 130 GeV gamma-ray line while satisfying all other indirect detection and relic density constraints, as we show here.

Since we will be concerned with properties of the electroweak phase transition and baryogenesis which do not depend sensitively on the details of the resonance, it is sufficient, for our purposes, to consider the simple parameter choice $A_1 = 2m_{\chi_1^0} = 260$ GeV and proceed to consider the implications for electroweak baryogenesis (a slightly off-resonance value would not at all affect the electroweak phase transition or the resulting baryon asymmetry). From this starting point, we shall dial in the various parameters point-by-point to satisfy all of the phenomenological and observational constraints we describe below.

First and foremost, besides requiring the desired neutralino annihilation structure, demanding a 130 GeV LSP neutralino and the associated 260 GeV singlet-like A_1,

we require a 125 GeV SM-like Higgs, in accordance with recent experimental findings from the LHC collaborations [14, 15]. Given our parameter space, the requirements on the bino-like LSP and on A_1 lead us to vary M_1 and A_λ in the range

$$
\begin{aligned}
135\text{GeV} &\leq M_1 \leq 145\text{GeV} \\
150\text{GeV} &\leq A_\lambda \leq 600\text{GeV}.
\end{aligned}
\tag{5.10}
$$

For each point in the M_1, A_λ parameter space, we use the following strategy to choose values for the seven remaining parameters:

1. To obtain a Higgs mass of 125 GeV in the NMSSM without excessive tuning in the stop sector requires relatively large λ and small $\tan\beta$, as seen from the tree-level inequality:

$$
m_{h_1}^2 \leq \left(\cos^2 2\beta + \frac{2\lambda^2 \sin^2 2\beta}{g_1^2 + g_2^2} \right) m_Z^2.
\tag{5.11}
$$

We take $\tan\beta$ in the range $1.7 \leq \tan\beta \leq 1.8$. In principle λ can be either positive or negative. We focus on positive λ and consider $0.6 \leq \lambda \leq 0.8$ (see, e.g. Ref. [128] for a discussion of the case of $\lambda < 0$). For $|\lambda|$ much smaller than this value, one must rely heavily on stop loops to raise the Higgs mass. Also, λ determines the coupling of neutralinos to A_1, as well as the coupling of A_1 to photons, and so for much smaller $|\lambda|$ the neutralino annihilation cross-section into photons is suppressed. For values $\lambda \gtrsim 0.7$, λ becomes non-perturbative below the GUT scale; this can be remedied by including higher-dimension operators resulting from integrating out new physics which enters below the GUT scale[4]

---

[4]We will in fact assume that this is the case for our benchmark EWPT point which features $\lambda = 0.75$.

(see e.g. Refs. [130, 131] for explicit implementations of this strategy in similar contexts).

2. The pseudoscalar A_1 must be predominantly singlet-like to be compatible with indirect detection results. The amount of mixing between A_1 and the MSSM-like CP-odd Higgs A_2 is governed by $\mathcal{M}_{P,12}$ in Eq. (5.3) and is minimized for

$$\kappa \approx \frac{\lambda A_\lambda}{2\mu}. \tag{5.12}$$

Given the relatively large values of λ we consider, we take $\kappa \geq 0.3$. For a given choice of κ, the $A_1 - A_2$ mixing will vary point-by-point in the parameter space under consideration. Therefore in some regions of parameter space the lightest pseudoscalar can obtain a large branching ratio into fermions and be incompatible with indirect detection constraints for a given mass difference $\left| m_{A_1} - 2m_{\chi_1^0} \right|$. As mentioned above (and discussed in more detail in Sec. 5.1.2), one can typically dial in the details of the resonance to satisfy these constraints for a given point, however the BAU does not depend sensitively on this tuning.

3. To obtain a lightest neutralino mass of 130 GeV, we must fix μ and M_2 or, equivalently, μ and Δ appropriately, where we define the quantity Δ via

$$M_2 \equiv (|\mu| + \Delta)e^{i\phi}. \tag{5.13}$$

When considering CP-violation in Sec. 5.3, we will typically set the CP-violating phase ϕ to its maximal value, $\sin\phi = 1$, in our calculations to show the maximum extent of the EWB parameter space, although viable regions will typically

have phases of $\mathcal{O}(10^{-1})$. In calculating the baryon asymmetry, Δ will govern the strength of the resonant CP-violating source. In considering the higgsino-gaugino CP-violating sources we will typically take $\Delta = 0$ as an optimistic EWB scenario. Given a particular choice of Δ and ϕ, we fix μ by diagonalizing Eq. (5.4) and solving for μ such that $m_{\chi_1^0} = 130$ GeV (note that we can rewrite $v_s = \mu/\lambda$). This procedure fixes all the relevant parameters in the neutralino and chargino sectors.

4. Finally, to obtain a large photon annihilation cross-section, we need the annihilation channel $\chi_1^0 \chi_1^0 \to A_1$ to be near resonance at $T = 0$, which implies $m_{A_1} \approx 260$ GeV. As discussed above and shown in Fig. 5.2, there is a narrow ($\lesssim 1$ GeV) window for which $\langle \sigma v \rangle_{\gamma\gamma}$ is large enough to be compatible with the line. Since the properties of the electroweak phase transition and baryogenesis are not sensitive to the precise value of m_{A_1}, we choose to sit exactly on top of the resonance, i.e. enforce $m_{A_1} = 260$ GeV, by diagonalizing Eq. (5.3) and solving for the appropriate value of A_κ. Therefore, at each point in the parameter space, $\langle \sigma_{\gamma\gamma} v \rangle > 10^{-27} \text{cm}^3/\text{s}$. Once again, the precise mass splitting between A_1 and the LSP can typically be tuned point-by-point to produce the line while providing the correct relic density and satisfying the other indirect detection constraints as described below.

The strategy outlined above is useful to automatically select the regions in the NMSSM producing the tentatively observed 130 GeV gamma-ray line, and provides an efficient way to study the properties of electroweak baryogenesis in these regions by exploring

the remainder of the parameter space. Note that we are not concerned with tuning or naturalness in this scenario, since we have narrowed in on this region by demanding consistency with the (tentative!) observation of a gamma-ray line which we postulate to be associated with dark matter pair annihilation.

We shall now use our suitably selected Higgs and neutralino sectors to close in onto electroweak baryogenesis in regions of the NMSSM producing a 130 GeV line. However, we first comment further on the impact of various other dark matter and particle physics constraints on the parameter space under consideration.

5.1.2   Phenomenological Constraints

The NMSSM parameter space of interest features relatively light neutralino, chargino, and Higgs sectors and is thus quite constrained on multiple fronts. Here we highlight the most important constraints on the parameter space and consider their impact on our current set-up. We use `NMSSMTools 3.2.1`[132] and `MicrOmegas 2.4.5`[133] to calculate the various cross-sections and quantities of interest. We summarize in Fig. 5.3 the impact of the constraints we consider here (and that we discuss in detail below) on the relevant parameter space, for the particular choice $\lambda = 0.6$, $\kappa = 0.32$, and $\tan\beta = 1.8$ as an illustrative example. In these calculations, we take M_2 to be real; since the LSP has only a very small wino component across the parameter space, and since the other neutralinos and charginos are significantly heavier than the lightest neutralino, the DM constraints will be largely unaffected by allowing M_2 to be complex. The Higgs couplings are also insensitive to ϕ.

$$\Delta=0$$

$m_{h_1} < 124\ \text{GeV}$

$|d_e| > 1.05 \times 10^{-27}\ e\ \text{cm}$

$m_{A_1} < 127\ \text{GeV}$

$\sin\phi = 1/3$

$\sin\phi = 1/4$

Excluded by
XENON 100

$\sin\phi = 1/5$

$\sin\phi = 1/6$

$m_{h_1} < 124\ \text{GeV}$
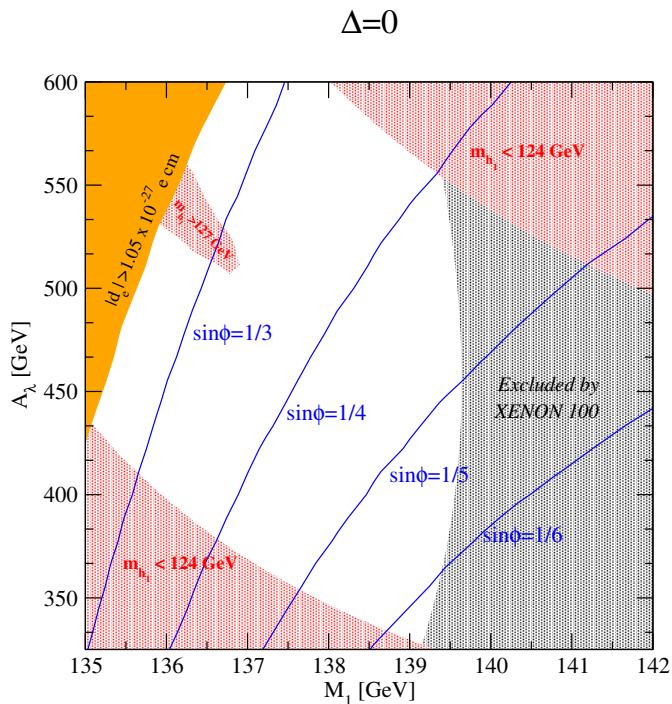
A_λ [GeV]

M_1 [GeV]

Figure 5.3: An example of the NMSSM parameter space for successful electroweak baryogenesis and a 130 GeV gamma-ray line. Here we take $\lambda = 0.6$, $\kappa = 0.32$, $\tan\beta = 1.8$ and $\Delta = 0$ (so that the CP-violating sources are on resonance), while the rest of the parameters are chosen as described in Sec. 5.1.1 to be consistent with the Fermi line. The gray shaded region is excluded by the XENON100 225 live day results, calculated with the default settings in `MicrOmegas`. Red shaded regions are excluded by measurements of the Higgs mass (although these regions can be shifted around by changing e.g. the squark masses). The orange shaded region is excluded by the non-observation of an electric dipole moment of the electron. The blue contours correspond to points consistent with the observed baryon-to-entropy ratio of the universe for different values of the CP-violating phase ϕ.

5.1.2.1 Indirect Dark Matter Detection and Thermal Relic Density

Indirect detection places important constraints on the parameter space in question. In considering $m_{A_1} \approx 2m_{\chi_1^0}$, there will also be a resonant tree-level neutralino annihilation channel into quark-antiquark, and especially $b\bar{b}$, final states, eventually leading to gamma rays via hadronization producing neutral ions. The lack of an excess of gamma-rays associated with this emission puts constraints on the branching ratio for

neutralino pair-annihilation into, e.g., $b\bar{b}$ [134]. As mentioned above, however, one can generally dial in the mass splitting $\left| m_{A_1} - 2m_{\chi_1^0} \right|$ to obtain both $\langle \sigma_{\gamma\gamma} v \rangle \gtrsim 10^{-27}$ cm^3/s and $\langle \sigma_{b\bar{b}} v \rangle \lesssim 10^{-24}$ cm^3/s as required by Fermi observations [134] of the diffuse gamma ray background (see e.g. the benchmark point in Table 5.1). Additionally, neutralino annihilation into W^+W^- will receive a contribution at tree-level from the pseudoscalar channel; however, this contribution also typically falls well beneath the 10^{-24} cm^3/s bound from Fermi by adjusting m_{A_1}. Consequently, this tuning allows one to satisfy all continuum gamma-ray constraints [135] while reproducing the observed intensity of the 130 GeV line, something that cannot be done in the MSSM. The parameter space we consider for electroweak baryogenesis can thus be dialed in to agree with indirect detection results without drastically affecting the details of the electroweak phase transition or the generation of the baryon asymmetry.

Similar reasoning applies to the DM thermal relic abundance. For χ_1^0 to be a suitable thermally-produced dark matter candidate, it must be compatible with the bounds on the relic density from WMAP7 [4]: $\Omega_{DM} h^2 = 0.112 \pm .011$. While at zero-temperature the neutralino sits very close to the pseudoscalar resonance, at the freeze-out temperature $T_{\text{f.o.}} \sim m_{\chi_1^0}/20 \approx 6.5$ GeV, the resonance is shifted higher by about 10 GeV for the case of $m_{A_1} = 260$ GeV. This can be seen by evaluating the thermally-averaged center-of-mass (C.O.M.) energy, $\langle s \rangle$, at $T = T_{\text{f.o.}}$, given by

$$\langle s \rangle \simeq 4m_{\chi_1^0}^2 + 6m_{\chi_1^0} T_{\text{f.o.}} \simeq 270 \ \text{GeV}. \tag{5.14}$$

However, in evaluating $\langle \sigma v \rangle$ at $T_{\text{f.o.}}$, one integrates over center-of-mass energies, and

154

hence effectively picks up contributions from the resonances, which decrease as one moves $\langle s \rangle$ further away from $4m^2_{\chi^0_1}$. Therefore, as is the case for the zero-temperature cross-sections, by dialing in the detailed neutralino and pseudoscalar masses, as well as the $A_1 - A_2$ mixing, one can typically achieve a total annihilation thermally averaged cross-section of $\langle \sigma v \rangle \sim 3 \times 10^{-26}$ cm^3/s required to obtain the correct relic density.

Previous studies [125, 128] have relied on a sizable higgsino component in the LSP to drive the relic density down. However, this requires small values of μ which are difficult to reconcile with the most recent direct detection constraints, except in the case of cancellations which can occur for negative μ as exploited in Ref. [128] (we have found it difficult to achieve a strongly first-order EWPT consistent with the 130 GeV line for the $\mu < 0$ case, but it may still be possible). Another possibility is to open a co-annihilation channel by e.g. allowing a light stau [5] with mass near 130 GeV to drive the relic density down. Light staus are not yet significantly constrained by LHC searches and, interestingly, they could provide an explanation of the enhanced Higgs diphoton rate as observed by ATLAS, albeit for large $\tan \beta$ (see e.g. Ref. [136]). We do not pursue these avenues further, but emphasize that we find that the relic density (and the zero-temperature neutralino annihilation cross-sections) can be made to agree with observations in this scenario by tuning or other mechanisms that do not significantly affect the properties of the EWPT nor the calculation of the baryon asymmetry. Consequently, we do not focus on the detailed bounds from indirect detection or the thermal relic abundance point-by-point in our present study of EWB in this scenario,

---

[5]Of course with CP-violation in the gaugino sector one must verify that such a light slepton satisfies constraints from EDMs.

but we do emphasize that these constraints can all be met in principle, as illustrated by a worked-out example in the EWPT benchmark point we show explicitly in Table 5.1.

5.1.2.2 Direct Detection

Unlike the case of indirect detection and relic density constraints, the bounds from DM direct detection (i.e. the scattering of the lightest neutralino off of nucleons) do not depend sensitively on the details of the resonance, but rather on the composition of the lightest neutralino. This in turn depends on M_1: larger values of M_1 require smaller values of μ to obtain $m_{\chi_1^0} = 130$ GeV and consequently enhance the spin-independent neutralino-proton cross section.

We require that the LSP satisfy the current upper bound from XENON100 for a 130 GeV WIMP for the spin-independent cross-section[6], $\sigma_{SI} \lesssim 3 \times 10^{-9}$ pb [113]. We show the impact of this constraint on our parameter space in Fig. 5.3: points excluded by XENON100 are shown in the gray shaded region. These bounds are computed assuming default values for the various underlying parameters, such as the quark content of the nucleon, local distribution of dark matter, etc. We employ the `MicrOmegas 2.4.5`[133] package for the calculation of the relevant scattering cross section, and employ the default parameters thereof. As expected, points with smaller μ values, and hence a larger higgsino component in χ_1^0, are ruled out.

We note here that the exclusions are somewhat stronger than those reported in Ref. [125] due to the release of the 2012 XENON results (and consequently the window

---

[6]We also consider the bound on the spin-dependent cross-section, but the corresponding constraints are much weaker than those on σ_{SI} in our scenario

for m_{A_1} is somewhat more constrained than that in Ref. [125]). Since these limits depend on parameters affected by significant uncertainty, they should also be taken with a grain of salt. For example, by considering the strange quark content of the nucleons near the end of the error bars from Ref. [137] ($\sigma_{\pi N} = 39$ MeV, $\sigma_0 = 43$ MeV), one can push the XENON limits out to allow M_1 up to ~ 145 GeV consistent with the 2012 XENON100 results (see e.g. the EWPT benchmark point in Table 5.1).

5.1.2.3 Higgs Constraints

The lightest CP-even Higgs in our scenario is SM-like. We require that 124 GeV $< m_{h_1} <$ 127 GeV, in agreement with results from ATLAS [15] and CMS [14]. The region of parameter space incompatible with these results is shown in Fig. 5.3 by points within the red shaded regions. We have also checked against constraints from $h_1 \rightarrow b\bar{b}$, $\tau\tau$, etc. as implemented in `NMSSMTools 3.2.1`[132]. The couplings of h_1 to the various SM fermions and gauge bosons all fall within $\sim 3\%$ of the corresponding SM predictions, hence well within experimental limits.

The lightest CP-odd Higgs must also be compatible with collider searches. In particular, we verified that the couplings of A_1 to $b\bar{b}$, $\tau\tau$ are small compared to that of the SM-like Higgs for compatibility with LHC results. In the parameter space under consideration, we find that the couplings of A_1 are at most of order 1% of the SM Higgs couplings.

157

5.1.2.4   Other Considerations

There are several other constraints which are in fact satisfied over nearly all of the parameter space we consider. Constraints from LEP on light charginos are everywhere satisfied, since charginos are always heavier than the 130 GeV LSP. Also, constraints from B-physics, as implemented in `NMSSMTools 3.2.1`, do not constrain the parameter space since we consider small values of $\tan\beta$. Finally, we have also verified the absence of unphysical global minima of the effective potential for all points we consider, as well as the absence of Landau poles below the GUT scale, with the exception of the EWPT benchmark point, for which we take $\lambda = 0.75$. As discussed above, this issue can be remedied with the modest assumption of new physics entering below the GUT scale.

In summary, Fig. 5.3 shows that there exist regions of NMSSM parameter space consistent with a 130 GeV gamma-ray line, a 125 GeV SM-like Higgs, and which can satisfy all relevant dark matter and experimental particle physics constraints. We can now proceed to investigate the phenomenology and properties of electroweak baryogenesis in these regions.

5.2   The Electroweak Phase Transition

Successful electroweak baryogenesis requires a strongly first-order electroweak phase transition. In the absence of a strongly first-order transition, $SU(2)$ sphaleron processes, which provide the necessary baryon number violation, are unsuppressed in

the broken electroweak phase and tend to wash out any existing generated baryon asymmetry. The strength of the phase transition can be parametrized by the order parameter $\varphi(T_c)/T_c$, where T_c is the critical temperature, defined as the temperature for which the symmetric and broken phases are degenerate[7]. To prevent sphaleron washout requires $\varphi(T_c)/T_c \gtrsim 1$, which we take as the definition of a "strongly first-order" transition[8]. As we will show in this section, this requirement can be readily satisfied in the region of the NMSSM compatible with the 130 GeV gamma-ray line and without relying on a light stop squark, as is instead typically required in the MSSM [140, 19].

The strength of the electroweak phase transition is governed by the finite-temperature effective potential, which comprises several parts: the tree-level scalar potential, zero-temperature quantum corrections, finite-temperature quantum corrections, and thermal mass terms. The tree-level potential comes directly from the superpotential (Eq. (5.1)) and the soft supersymmetry-breaking terms (Eq. (5.2)):

$$V_0(h_u, h_d, s) = \frac{1}{32}(g_1^2 + g_2^2)\left(h_u^2 - h_d^2\right)^2 + \frac{1}{4}\kappa^2 s^4 - \frac{1}{2}\lambda\kappa s^2 h_u h_d + \frac{1}{4}\lambda^2\left(h_d^2 h_u^2 + s^2\left(h_d^2 + h_u^2\right)\right)$$
$$+ \frac{\sqrt{2}}{6}\kappa A_\kappa s^3 - \frac{\sqrt{2}}{2}\lambda A_\lambda s h_u h_d + \frac{1}{2}m_d^2 h_d^2 + \frac{1}{2}m_u^2 h_u^2 + \frac{1}{2}m_s^2 s^2. \quad (5.15)$$

The fields h_u, h_d, and s are defined by

$$H_u = \frac{1}{\sqrt{2}}\begin{pmatrix} 0 \\ h_u \end{pmatrix} \; ; \; H_d = \frac{1}{\sqrt{2}}\begin{pmatrix} h_d \\ 0 \end{pmatrix} \; ; \; S = \frac{1}{\sqrt{2}}s. \quad (5.16)$$

---

[7]Note that this quantity is not gauge invariant, see e.g. the discussion in Ref. [138, 139].

[8]More precisely, one should actually consider the system at the nucleation temperature, T_n. However, the amount of supercooling in this model is small, and for simplicity we assume that $T_n \approx T_c$ as in previous work.

We assume that the scalar fields are real at all temperatures, and we do not consider charged vacua (although we do ensure that the potential is stable in the charged and imaginary directions).

Using $\overline{MS}$ renormalization, the one-loop zero-temperature quantum corrections are

$$V_1(T\!=\!0) = \sum_i \frac{\pm n_i}{64\pi^2} m_i^4 \left[\log\left(\frac{m_i^2}{\Lambda^2}\right) - c\right], \tag{5.17}$$

where m_i^2 are the (possibly negative) field-dependent mass-squared values, n_i are their associated number of degrees of freedom, Λ is the renormalization scale, and $c = \frac{1}{2}$ for the transverse polarizations of gauge bosons while $c = \frac{3}{2}$ for their longitudinal polarizations and for all other particles. The plus and minus signs are for bosons and fermions, respectively. The sum over the relevant particles i include all standard model particles (although we ignore fermions lighter than the bottom quark), the physical Higgs and other scalar particles, their associated Goldstone bosons, the neutralinos and the charginos. We work in Landau gauge where the ghost bosons decouple and need not be included in the spectrum. The one-loop potential contains explicit gauge-dependence which cancels with the implicit gauge-dependence of the vevs at every order in $\hbar$ (for recent discussions of gauge dependence in effective potentials, see e.g. Refs. [138, 141, 139, 142]). As is common practice, we do not consider the effects of the implicit gauge-dependence, and therefore our results will contain gauge artifacts. However, our primary purpose in examining the effective potential is to estimate whether or not a first-order phase transition is possible, and for this purpose a rough calculation with

160

gauge-dependence is acceptable.

We calculate the neutralino masses from Eq. (5.4) above. The scalar mass matrix is given by taking the second derivative of the tree-level potential, but including CP-odd and charged directions. This yields a block-diagonal 10×10 matrix, with blocks consisting of CP-even states (3 degrees of freedom), CP-odd states (3 degrees of freedom), and two blocks of charged Higgses (4 degrees of freedom).

The finite-temperature contributions are

$$V_1(T>0) = V_1(T=0) + \frac{T^2}{2\pi^2} \sum_i n_i J_\pm \left(\frac{m_i^2}{T^2} \right), \qquad (5.18)$$

where

$$J_\pm(x^2) \equiv \pm \int_0^\infty dy \, y^2 \log \left(1 \mp e^{-\sqrt{y^2+x^2}} \right) \qquad (5.19)$$

and again the upper (lower) signs correspond to bosons (fermions). At high temperature, the validity of the perturbative expansion of the effective potential breaks down. Quadratically divergent contributions from non-zero Matsubara modes must be re-summed through inclusion of thermal masses in the one-loop propagators [143, 144]. This amounts to adding thermal masses to the longitudinal gauge boson degrees of freedom and to all of the scalars.

The full one-loop effective potential is

$$V(h_u, h_d, s, T) = V_0(h_u, h_d, s) + V_1(T=0) + \frac{T^2}{2\pi^2} \sum_i n_i J_\pm \left(\frac{m_i^2}{T^2} \right) \qquad (5.20)$$

where the masses m_i^2 are field-dependent and include thermal mass corrections.

The important qualitative feature of the finite-temperature contribution is that it lowers the effective potential anywhere m_i^2/T^2 is small. To get a strongly first-order

phase transition, we need to sharply lower the potential near the symmetric phase without significantly lowering it in the broken phase so that the two phases may be degenerate with a sizable barrier. Therefore, a strongly first-order transition demands either numerous heavy field-dependent particles (such that they are massless in the symmetric phase and heavy in the broken phase), or a tree-level contribution to the barrier separating the two phases. In the standard model, the electroweak phase transition is not strongly first-order. There are no heavy bosons (relative to the Higgs, which sets the relevant scale), and at high temperature the contribution of heavy fermions (top quarks) does not increase the barrier since $J_-(x^2)$ does not contain any cubic terms.

The particle spectrum in the NMSSM may seem somewhat promising, since there are additional heavy masses in the Higgs sector and field-dependent neutralino masses, but these are not enough to guarantee a strong transition. Since many more particles couple to the Higgs than to the singlet, finite-temperature effects drive $\langle h_u \rangle$ and $\langle h_d \rangle$ to zero at temperatures well below the point at which they drive $\langle s \rangle$ to zero. Therefore, s can be large on either side of electroweak symmetry breaking, and some of the new particle masses that depend on s can be heavy even in the symmetric phase.

However, the NMSSM can succeed in producing a strongly first-order transition through its tree-level contributions. If the transition occurs both in the Higgs and singlet directions simultaneously, and if the singlet vev is non-zero in the electroweak symmetric phase just above the transition, then terms like $s^2 h^2$ and $s h^2$ both contribute effective cubic terms to the potential which can increase the barrier between the the symmetric and broken phases.

λ	0.75	m_{A_1} [GeV]	261.26
κ	0.45	$m_{\chi_1^0}$ [GeV]	130.72
$\tan\beta$	1.7	$\langle\sigma v\rangle_{b\bar{b}}$ $[cm^3/s]$	3.07×10^{-26}
A_λ [GeV]	545.0	$\langle\sigma v\rangle_{\gamma\gamma}$ $[cm^3/s]$	1.54×10^{-27}
A_κ [GeV]	-88. 0	$\sigma_P^{\rm SI}$ [pb]	2.8×10^{-9}
μ [GeV]	275.8	$\sigma_P^{\rm SD}$ [pb]	1.4×10^{-6}
M_1 [GeV]	143.5	EWPT Properties:	
M_2 [GeV]	635.5	T_c [GeV]	72.3
m_{h_1} [GeV]	126.4	$\varphi(T_c)/T_c$	1.14

Table 5.1: Benchmark Point in the NMSSM with a strongly first-order EWPT and a 130 GeV line. We use a renormalization scale of $\Lambda = 100$ GeV in the effective potential.

We calculate the phase transition using the software package `CosmoTransitions` [145]. We input the above definition of the effective potential, find the necessary soft-breaking masses that produce desired values for $\tan\beta$ and μ via a minimization procedure, and choose a renormalization scale Λ such that the one-loop minimum does not drastically differ from its tree-level value. This last point requires a certain amount of finesse since the top-quark contribution to the zero-temperature one-loop potential tends to be fairly large. The `CosmoTransitions` package traces the broken electroweak phase up in temperature until it disappears, and then traces the symmetric phase down and checks for an overlap. If there is one, it calculates the temperature of degeneracy (the critical temperature) and the separation between the phases. If there is no overlap, then the transition is necessarily second-order.

The region of the NMSSM consistent with the 130 GeV Fermi line can in fact accommodate a strongly first-order phase transition. The barrier has large tree-level contributions and in particular does not require an additional light scalar. As a proof of principle, we outline a benchmark point consistent with a 125 GeV Higgs, 130 GeV

Fermi line, and a strongly first-order electroweak phase transition in Table 5.1. This point has an EWPT at $T_c = 72.3$ GeV with order parameter $\varphi(T_c)/T_c = 1.14$ and is consistent with all other relevant phenomenological constraints [9]. The spin-dependent and –independent neutralino-proton scattering cross-section for the point in Table 5.1 is computed taking $\sigma_{\pi N} = 39$ MeV, $\sigma_0 = 43$ MeV for the strange quark content of the proton and is thus rather optimistic. Also, note that we do not show the relic density for the specified point. Since we are near a resonance, as discussed in Sec. 5.1.2, the relic density calculation should be performed to loop level – something which is not implemented in `MicrOmegas` [10]. However, the asymptotic values of Ωh^2 computed by `MicrOmegas` away from the resonance and the trend of the relic density approaching the pole give us confidence that the correct value of the relic density is achieved in the vicinity of the resonance. Simple analytic estimates also corroborate this conclusion. The total zero-temperature annihilation cross-section (at tree-level) for our benchmark point is $\langle \sigma v \rangle \sim 3 \times 10^{-26}$ cm^3/s, dominated by the resonant $A_1 \to b\bar{b}$ channel. The resonant peak is smoothed out and suppressed at $T_{\text{f.o.}}$ (see Eq. (5.14)), and so one may be concerned that the relic density for this point will be too large. However, we have computed the corresponding finite-temperature thermally-averaged cross-section, and found that adjusting the splitting $|m_{A_1} - 2m_{\chi_0}|$ can indeed provide $\mathcal{O}(10^{-26})$ cm^3/s

---

[9]As mentioned previously, we can invoke some higher-dimension operators to render λ perturbative below the GUT scale.

[10]We have also found a suspected numerical issue with the `MicrOmegas 2.4.5` calculation of the relic density near the resonance. There is a very sharp increase in the annihilation cross section right above $m_{A_1} = 2m_{\chi_1^0}$ which we believe is unphysical. Since the zero-temperature total-annihilation cross section is of order $\langle \sigma v \rangle \sim 10^{-26}$ cm^3/s, by the arguments in Sec. 5.1.2.1 the thermally averaged cross-section at freeze-out should be smaller than this since the resonance is effectively shifted. Instead, we find a drop of four orders of magnitude in the relic density which is quite suspect.
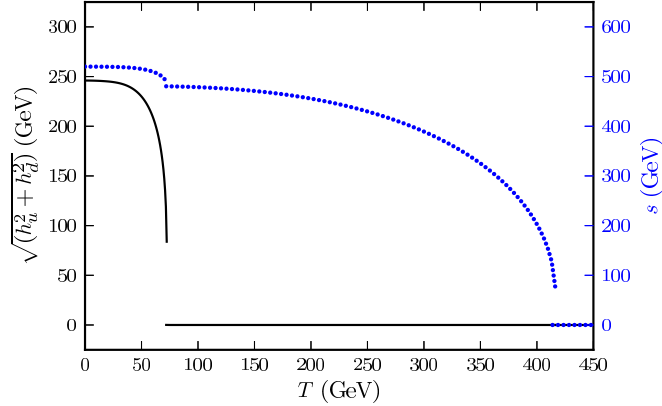
Figure 5.4: The phase structure for the benchmark point with first-order phase transitions. The dotted line gives the temperature-dependent singlet field values, and the solid line gives the temperature-dependent Higgs doublet field values.

contributions to $\langle \sigma v \rangle_{T=T_{\text{f.o.}}}$ while still conforming to indirect detection constraints. This adjustment should therefore be sufficient to dial in $\Omega h^2 = 0.11$. If, despite this tuning, the relic density remains too large, one can also introduce e.g. a moderately light stau with $M_{R_3} \sim 200\,\text{GeV}$ to reduce Ωh^2 to its canonical value through co-annihilation. Since $\tan \beta$ is small, the presence of such a light slepton will not affect the properties of the EWPT. Thus, we are confident that a proper one-loop calculation of the relic density for the benchmark point in Table 5.1 will yield a relic density compatible with observation, albeit with some possible minor changes to the parameters or the introduction of a co-annihilation channel which will not substantially affect the EWPT.

Fig. 5.4 shows the field evolution as a function of temperature for the benchmark point in Table 5.1. This makes the location of the phase transitions obvious: first-order phase transitions can happen anywhere there is a discontinuous jump in the vacuum expectation values. A second-order transition, if there were one, would be dis-
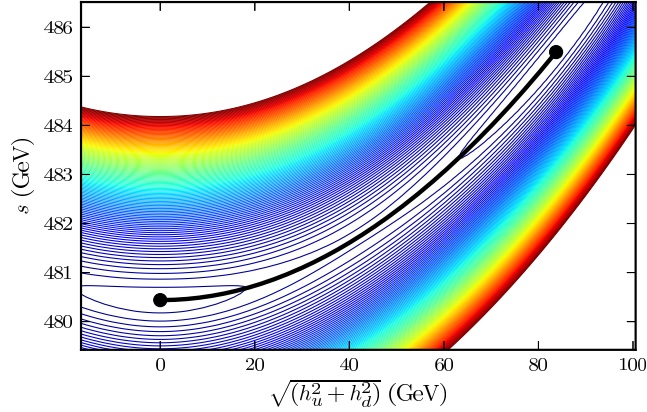
Figure 5.5: A contour plot of the effective potential just below the critical temperature. The electroweak broken minimum is represented by the dot on the upper-right, while the symmetric minimum is on the lower left. The actual tunneling happens along the curved solid black line.

tinguished by a continuous line of vacuum expectation values with discontinuous first derivatives.

Fig. 5.5 shows the field configuration at the critical temperature of electroweak symmetry breaking. All three fields — s, h_u and h_d — change values when tunneling from the high-temperature to the low-temperature minimum. We calculate the tunneling direction (denoted by a thick black line) using the `CosmoTransitions` package, where by "tunneling direction" we mean the path through field space that one would travel when crossing a bubble wall. The path is curved in the $s - h_u$ and $s - h_d$ planes, but is approximately straight in the $h_u - h_d$ plane ($\Delta\beta \ll 1$).

While we did not perform a systematic study of the NMSSM parameter space compatible with a strongly first-order transition (see e.g. Refs. [126, 61] for previous work in this direction), there are some common traits between the viable points we have found. Restricting ourselves to the case of positive λ, κ, μ, and A_λ, we find that

166

a strongly first-order phase transition typically requires $\lambda \gtrsim 0.6$, $\kappa \lesssim 0.6$, $A_\lambda \gtrsim 500$ GeV, and $\mu \lesssim 350$ GeV. This seems to be consistent with our intuition: increasing the strength of the cubic terms in the effective potential and decreasing the singlet vev tends to strengthen the transition. Note that, for all the points we considered, the transition tends to happen in two steps: the system transitions away from $\langle s \rangle = 0$ at a high temperature, around 300–400 GeV; while electroweak symmetry breaking happens much later, at a temperature around or below 100 GeV.

5.3 Computing the Baryon Asymmetry

The discussion in the previous section makes it clear that a strongly first-order EWPT can occur in the NMSSM region of parameter space compatible with the Fermi 130 GeV line. We now turn our attention to the CP-violating sources also required for electroweak baryogenesis, and to the detailed requirement of producing the correct amount of baryon asymmetry in the early universe, parametrized by the baryon-to-entropy ratio[11], $Y_B \sim 10^{-10}$. As we show in this section, CP-violating higgsino-gaugino sources can be very efficient in the NMSSM regions of interest and potentially source the observed baryon asymmetry of the universe.

In electroweak baryogenesis, the baryon asymmetry is produced by $SU(2)$ sphalerons acting on a net left-handed chiral density, n_L. To determine n_L, we must solve a set of quantum transport equations for each of the relevant particle densities contributing to the LH charge density. For each of these charge densities, n_i, the

---

[11]For concreteness and consistency with previous studies, we take $Y_B = 9.1 \times 10^{-11}$

Schwinger-Dyson equations yield the continuity equations [23]

$$\frac{\partial n_i}{\partial x_0} + \nabla \cdot j_i(x) = S_i(x). \tag{5.21}$$

The RHS of the above equation contains both CP-conserving and CP-violating contributions. For the case of Dirac fermions, the sources are given by

$$
\begin{aligned}
S_i(x) = \int d^3 z \int_{-\infty}^{x_0} dz_0 \, \text{Tr} \left[\Sigma^>(x,z) G^<(z,x) - G^>(x,z) \Sigma^<(z,x) \right. \\
\left. + G^<(x,z) \Sigma^>(z,x) - \Sigma^<(x,z) G^>(z,x) \right]
\end{aligned}
\tag{5.22}
$$

where $G^{<,>}$, $\Sigma^{<,>}$ are Green's functions and self-energies, respectively, in the closed time path formalism (see e.g. Ref. [23] for details). We focus here on the case of gaugino-higgsino sources, and compute the quantities $S_{\widetilde{H}^{0,\pm}}$ in the Higgs vev-insertion approximation, which we describe in more detail below (see e.g. Ref. [87] for a recent discussion on scalar sources in the MSSM).

5.3.1   The VEV-Insertion Approximation

The CP-violating interactions we consider involve the scattering of higgsinos and gauginos with the spacetime-dependent Higgs vevs in the bubble wall. In what follows we parallel the derivations for the corresponding quantities in the MSSM found in Ref. [23]. We will assume that the necessary CP-violating phase ϕ is that of the wino soft SUSY-breaking mass M_2 (in fact, the relevant phase is the relative phase between $M_{1,2}$ and μ, however as discussed previously we take μ, M_1 to be real to avoid large spontaneous CP-violating effects in the computation of the various dark matter properties). The part of the NMSSM Lagrangian giving rise to the relevant CP-violating

interactions is then given, in terms of four-component spinors, by:

$$\mathcal{L}_{\text{int}} \supset - \frac{g_2}{\sqrt{2}} \bar{\Psi}_{\widetilde{H}^0} \left[v_d(x) P_L + e^{i\phi} v_u(x) P_R \right] \Psi_{\widetilde{W}^0}$$

$$- g_2 \bar{\Psi}_{\widetilde{H}^+} \left[v_d(x) P_L + e^{i\phi} v_u(x) P_R \right] \Psi_{\widetilde{W}^+} + h.c.$$

(5.23)

where $P_{L,R}$ are the usual projection operators.

The spinors $\Psi_{\widetilde{H}^{0,\pm}}$ satisfy Dirac equations with a spacetime-varying mass $\mu(x)$. As discussed in Sec. 5.2, the profile $\mu(x)$ depends on the detailed properties of the phase transition at each point in parameter space. In the region of interest, however, the singlet vev does not change very significantly during the EWPT. Consequently, even though the variation of the singlet vev was crucial for achieving a strongly first-order phase transition, we ignore its space-dependence here[12] and approximate $\mu(x)$ by its value after the EWPT, $\mu(x) \simeq \mu$. Then the mode expansions for the operators in the Lagrangian Eq. (5.23) are the same as in the MSSM case and so the resulting source from Eq. (5.22) matches that of the MSSM in the vev-insertion approximation:

$$S_{\widetilde{H}^\pm}(x) = \int d^4 z \sum_{j=A,B} \left\{ [g_j(x,z) + g_j(z,x)] \right.$$

$$\times \text{Re Tr} \left[G^>_{\widetilde{W}^\pm}(x,z) G^<_{\widetilde{H}^\pm}(z,x) - G^<_{\widetilde{W}^\pm}(x,z) G^>_{\widetilde{H}^\pm}(z,x) \right]_j$$

$$\left. + i [g_j(x,z) - g_j(z,x)] \, \text{Im Tr} \left[G^>_{\widetilde{W}^\pm}(x,z) G^<_{\widetilde{H}^\pm}(z,x) - G^<_{\widetilde{W}^\pm}(x,z) G^>_{\widetilde{H}^\pm}(z,x) \right]_j \right\}$$

(5.24)

where the sum over A, B is over contributions arising from momentum and mass terms

---

[12]The spacetime-dependence of μ can introduce novel sources of CP-violation in the NMSSM; see e.g. Ref. [92]

169

in the spectral function, respectively, and where

$$g_A(x,y) \equiv \frac{g_2^2}{2} \left[v_d(x)v_d(y) + v_u(x)v_u(y) \right] \qquad (5.25)$$

$$g_B(x,y) \equiv \frac{g_2^2}{2} \left[v_d(x)e^{-i\phi}v_u(y) + e^{i\phi}v_u(x)v_d(y) \right]. \qquad (5.26)$$

The rest of the derivation proceeds as in the MSSM case, i.e. by performing a derivative expansion in $g_{A,B}(x,z)$ around $z = x$. The CP-conserving sources arise from the terms in Eq. (5.24) symmetric under the interchange of $x \leftrightarrow z$ and so appear at zeroth order in this expansion, while the CP-violating sources arise at first-order. In particular, performing the integration for the CP-violating contribution yields

$$S_{\widetilde{H}^\pm}^{\text{C\!P}} = \frac{g_2^2}{\pi^2} v(x)^2 \dot{\beta}(x) M_2 \mu \sin\phi \int_0^\infty \frac{dk k^2}{\omega_{\widetilde{H}} \omega_{\widetilde{W}}}$$
$$\times \text{Im} \left\{ \frac{n_F(\mathcal{E}_{\widetilde{W}}) - n_F(\mathcal{E}_{\widetilde{H}}^*)}{(\mathcal{E}_{\widetilde{W}} - \mathcal{E}_{\widetilde{H}}^*)^2} - \frac{n_F(\mathcal{E}_{\widetilde{W}}) + n_F(\mathcal{E}_{\widetilde{H}})}{(\mathcal{E}_{\widetilde{W}} + \mathcal{E}_{\widetilde{H}})^2} \right\} \qquad (5.27)$$

where $\omega_{\widetilde{H},\widetilde{W}}^2 \equiv |\mathbf{k}|^2 + M_{\widetilde{H},\widetilde{W}}^2$ (the masses here include thermal contributions, $\delta_{\widetilde{H},\widetilde{W}}$), $\mathcal{E}_{\widetilde{H},\widetilde{W}} \equiv \omega_{\widetilde{H},\widetilde{W}} - i\Gamma_{\widetilde{H},\widetilde{W}}$ (here the $\Gamma_{\widetilde{H},\widetilde{W}}$ are the thermal widths of the higgsinos and winos in the plasma), and n_F is the Fermi distribution function. The corresponding expressions for the CP-conserving (and neutral higgsino CP-violating) sources can be found in Ref. [23] with the appropriate replacements.

The CP-violating source in Eq. (5.27) exhibits several important properties. The first term of the integrand in Eq. (5.27) is resonant for $M_2 \sim \mu$ as can be appreciated by rewriting the denominator as

$$\mathcal{E}_{\widetilde{W}} - \mathcal{E}_{\widetilde{H}}^* = \sqrt{|\mathbf{k}|^2 + \mu^2 + \delta_{\widetilde{H}}^2} - \sqrt{|\mathbf{k}|^2 + (\mu + \Delta)^2 + \delta_{\widetilde{W}}^2} - i(\Gamma_{\widetilde{W}} + \Gamma_{\widetilde{H}}). \qquad (5.28)$$

Thus for a given choice of μ the parameter Δ determines the strength of the resonance,

and hence the resulting baryon asymmetry. At finite temperature, $\mu(T)$ will generally be different from $\mu(T = 0)$, since the singlet vev varies with temperature. This can be thought of as providing a finite temperature correction to Δ; we neglect this effect in calculating the baryon asymmetry across the parameter space, as this difference depends sensitively on the finite-temperature effective potential at each point. Note also that the Fermi distribution functions in the numerator result in a suppression of the baryon asymmetry for masses much larger than the electroweak phase transition temperature. As an optimistic estimate, we take $T_c = 140$ GeV in calculating the BAU across the parameter space; the $SU(2)$ sphaleron rate (and hence the overall baryon asymmetry) decreases for lower temperatures. For example, taking $T_c = 100$ GeV will decrease the overall baryon asymmetry by a factor of about 0.7 across the parameter space (i.e. the CP-violating phase $\sin\phi$ at each point would increase by a factor of about 1.4). For our particular benchmark point in Table 5.1, we found a transition around $T_c = 72$ GeV, but the phase transition temperature generally depends quite sensitively on the parameter space point in question and so we do not believe it is necessary for all points to have such low transition temperatures. We encourage the Reader to bear this in mind while interpreting our results.

Other important quantities determining the strength of the CP-violating source are the bubble wall width (L_w), velocity (v_w), and the variation of Higgs vevs across the wall ($\Delta\beta$). This can be seen by approximating the bubble wall profile by a step-function, whence $\dot\beta \approx \Delta\beta v_w / L_w$. For the wall width and velocity we choose the canonical MSSM values $L_w = 10/T$ and $v_w = .05$. Previous studies of the bubble wall in singlet ex-

tensions of the MSSM suggest typically thinner walls [92], and so we expect that this choice for L_w is a conservative one. Additionally, these parameters will vary depending on the particular point in the parameter space under consideration. Uncertainties in v_w and L_w are generally expected to induce $\mathcal{O}(1)$ uncertainties in the calculation of the baryon asymmetry [90], which we encourage the Reader to bear in mind. Regarding the quantity $\Delta\beta$, since there is only a small degree of mixing between A_1 and A_2 in our current set-up, we expect $\Delta\beta$ to scale approximately as in the MSSM, i.e. roughly $\Delta\beta \propto 1/m_{A_2}^2$ (in our calculation of $\Delta\beta$ we use the full two-loop results of Ref. [47]). Since m_{A_2} will vary across the parameter space, $\Delta\beta$ will have an important effect on the parameter space available for EWB. For the values of m_{A_2} we consider, $\Delta\beta$ falls in the range $\Delta\beta \sim 10^{-3} - 10^{-4}$. A more detailed study of the bubble wall profile in the NMSSM is required to go beyond the approximations and assumptions here, which we leave for future work.

The other relevant particle number-changing processes (including the triscalar, Yukawa, and CP-conserving relaxation interactions) are also computed in the vev-insertion approximation; expressions for these rates can be found in Refs. [23, 24, 21, 22, 25]. In addition to these MSSM processes, there are new interactions in the NMSSM arising from the singlet and singlino degrees of freedom. In particular, there is a resonant relaxation term (and possible CP-violating source [127]) arising from higgsino-singlino interactions with the Higgs vevs. The relevant part of the Lagrangian is

$$\mathcal{L}_{\text{int}}^{\widetilde{S}} = \lambda \left[v_u(x)\widetilde{H}_d^0 \widetilde{S} + v_d(x)\widetilde{H}_u^0 \widetilde{S} \right] + h.c. \tag{5.29}$$

172

where $\widetilde{H}^0_{u,d}$ and $\widetilde{S}$ correspond to the two-component higgsino and singlino fields. We can rewrite Eq. (5.29) in terms of four-component spinors as

$$\mathcal{L}^{\widetilde{S}}_{\text{int}} = \lambda \bar{\Psi}_{\widetilde{H}^0} \left[v_u(x) P_L - v_d(x) P_R \right] \Psi_{\widetilde{S}} \; + \; h.c.. \tag{5.30}$$

and follow the methods of Ref. [23] to compute the source. Since we assume that there is no CP-violation in the singlino sector, Eq. (5.30) results in a resonant chiral relaxation rate for the higgsino chemical potential $\Gamma_{\widetilde{H}^0\widetilde{S}} \equiv \Gamma^+_{\widetilde{H}^0\widetilde{S}} + \Gamma^-_{\widetilde{H}^0\widetilde{S}}$ where

$$
\begin{aligned}
\Gamma^\pm_{\widetilde{H}^0\widetilde{S}} = \frac{1}{T} \frac{\lambda^2}{2\pi^2} v(x)^2 \int_0^\infty \frac{dk k^2}{\omega_{\widetilde{H}} \omega_{\widetilde{S}}} \, \text{Im} \Bigg\{ & \left[\mathcal{E}_{\widetilde{S}} \mathcal{E}_{\widetilde{H}}^* - k^2 - M_{\widetilde{S}} |\mu| \sin 2\beta \right] \frac{h_F(\mathcal{E}_{\widetilde{S}}) \mp h_F(\mathcal{E}_{\widetilde{H}}^*)}{\mathcal{E}_{\widetilde{S}} - \mathcal{E}_{\widetilde{H}}^*} \\
& + \left[\mathcal{E}_{\widetilde{S}} \mathcal{E}_{\widetilde{H}} + k^2 + M_{\widetilde{S}} |\mu| \sin 2\beta \right] \frac{h_F(\mathcal{E}_{\widetilde{S}}) \mp h_F(\mathcal{E}_{\widetilde{H}})}{\mathcal{E}_{\widetilde{S}} + \mathcal{E}_{\widetilde{H}}} \Bigg\}
\end{aligned}
\tag{5.31}
$$

and where the various quantities are defined analogously to those in Eq. (5.27). The singlino mass given by

$$M^2_{\widetilde{S}} = 4\kappa^2 \mu^2 / \lambda^2 + \delta^2_{\widetilde{S}} \tag{5.32}$$

(here $\delta_{\widetilde{S}}$ is the singlino thermal mass), and the quantity h_F is defined as

$$h_F(x) = \frac{e^{x/T}}{\left(e^{x/T} + 1 \right)^2}. \tag{5.33}$$

Since we consider moderate values of λ, we take $\Gamma_{\widetilde{S}} \simeq 0.001T$ for the singlino width. The denominator of the first term in Eq. (5.31) has the same resonant structure as in Eq. (5.28) and is the most significant contribution to the transport equations from the singlino, tending to reduce the resulting charge density. Given our choices for λ and κ in Fig. 5.3, the relaxation rate $\Gamma_{\widetilde{H}^0\widetilde{S}}$ is near resonance in this region since $M_{\widetilde{S}} \sim \mu$. We account for this higgsino-singlino resonant relaxation in our computation of the baryon

173

asymmetry, but do not consider the other non-resonant singlet/singlino interactions, as they are subdominant.

5.3.2 Solving the Transport Equations

With the sources contributing to the RHS of Eq. (5.21) for the various charged current densities in place, we compute the baryon asymmetry point-by-point across the 130 GeV line parameter space described in Sec. 5.1.1 for $\lambda = 0.6$, $\kappa = 0.32$, and $\tan \beta = 1.8$ as an example. We do so by solving the system of transport equations to determine the LH charge density n_L, assuming a strongly first-order EWPT and that the $SU(2)$ sphaleron rate Γ_{ws} is slow compared to the other particle number-changing rates. Then, given $n_L(z)$, the baryon number density results from the integral of n_L over the unbroken phase,

$$n_B = \frac{-3\Gamma_{ws}}{v_w} \int_{-\infty}^{0} dz \ n_L(z) e^{\frac{15\Gamma_{ws}}{4v_w}z}, \tag{5.34}$$

where z is the comoving distance away from the bubble wall (neglecting the curvature of the wall and taking $z < 0$ to be the symmetric phase).

To determine n_L, we work under the set of assumptions detailed in Refs. [23, 90], and in particular assuming "super-equilibrium" (i.e. the equality of the chemical potentials) for the Higgs and higgsino densities [22], allowing us to define a common charge density for both. Given the condition of Higgs-higgsino super-equilibrium and assuming that the sfermions are heavy, one can show that the relevant charge densities we must keep track of are those corresponding to the Higgs/higgsinos (H), the

174

right-handed tops (T), and the left-handed third-generation quarks (Q). The transport equations then read

$$\partial_\mu Q^\mu = -\,\Gamma_{yt}\left(\frac{Q}{k_Q} - \frac{T}{k_T} + \frac{H}{k_H}\right) - \Gamma_{mt}\left(\frac{Q}{k_Q} - \frac{T}{k_T}\right) - 2\Gamma_{ss}\left(2\frac{Q}{k_Q} - \frac{T}{k_T} + 9\frac{Q+T}{k_B}\right)$$
(5.35)

$$\partial_\mu T^\mu = \Gamma_{yt}\left(\frac{Q}{k_Q} - \frac{T}{k_T} + \frac{H}{k_H}\right) + \Gamma_{mt}\left(\frac{Q}{k_Q} - \frac{T}{k_T}\right) + \Gamma_{ss}\left(2\frac{Q}{k_Q} - \frac{T}{k_T} + 9\frac{Q+T}{k_B}\right)$$
(5.36)

$$\partial_\mu H^\mu = -\,\Gamma_{yt}\left(\frac{Q}{k_Q} - \frac{T}{k_T} + \frac{H}{k_H}\right) - \Gamma_h\frac{H}{k_H} + S_{\widetilde{H}}^{C\!\!\!/P}.$$
(5.37)

Here, $\Gamma_{mt,h}$ are chiral relaxation rates (including the contribution from the higgsino-singlino-vev interaction), active only in the bubble wall[13] and broken EW phase, Γ_{yt} are Yukawa interaction rates [25], Γ_{ss} is the $SU(3)$ sphaleron rate (responsible for generating densities of first- and second-generation quarks), and the k_is are statistical factors relating the charge densities n_i to the corresponding chemical potential μ_i. We solve Eqs. (5.35)-(5.37) utilizing the diffusion approximation discussed in Ref. [23]. The LH charge density entering into Eq. (5.34) is then given to good approximation by the relation

$$n_L(z) = 5Q(z) + 4T(z).$$
(5.38)

While we are primarily concerned with heavy sfermions to avoid large EDM contributions, in solving the transport equations numerically we take the RH stop to be moderately light ($\sim$ 200 GeV, and hence also in super-equilibrium) to show the maximum extent of the compatible parameter space before encountering a sizable "Sha-

---

[13]For simplicity, in solving the transport equations we assume a step-function profile for the Higgs vevs in the bubble wall.

poshnikov suppression" [40] that arises from the $SU(3)$ sphalerons when both T and Q correspond entirely to densities of SM fermions (see Refs. [30, 90, 146] for previous work also implementing this strategy). As long as it is not too light, the RH stop mass is not crucial to the phenomenology (in fact, Ref. [125] assumed a RH stop around 300 GeV), whereas this suppression depends quite sensitively on the mass of the stops. In calculating the EDM limits below, however, we assume both stops are heavy, again to show the maximal extent of the parameter space under consideration. Of course a light stop would introduce sizable one-loop contributions to the various EDMs and so one cannot take the stop to be too light without also significantly reducing the CP-violating phase in M_2, or without relying on cancellations. This means that our results for the baryon asymmetry and EDMs will be idealized, while a more realistic stop spectrum will likely tighten the EDM constraints, either by increasing the one-loop stop contribution to the EDMs or by increasing the CP-violating phase to account for the suppressed baryon asymmetry.

We show contours corresponding to the observed value of the baryon-to-entropy ratio across the 130 GeV line parameter space on the resonance ($\Delta = 0$) for different values of the CP-violating phase ϕ in Fig. 5.3, calculated as described above. We have checked that even in solving the transport equations with both stops heavy (~ 1.5 TeV), and hence substantial Shaposhnikov suppression, there remain regions compatible with the observed baryon asymmetry of the universe, a 130 GeV gamma-ray line, and all other relevant constraints.

In interpreting our results, the reader should bear in mind that there are

176

several uncertainties present in our calculation of the baryon asymmetry. As mentioned, the microphysical properties of the EW bubble wall and details of the electroweak phase transition (L_w, v_w, $\Delta\beta$, T_c, etc) can significantly affect the calculation of n_L and Y_B (see e.g. Ref. [90] and references therein for a more detailed discussion of these effects). Also, there are several other frameworks for calculating the baryon asymmetry [44, 43, 46, 41, 88, 89], with results that can differ by up to an order of magnitude from one another (for a review of these different approaches, see Ref. [10]). Additionally, there are other possible sources of CP-violation in the NMSSM that could contribute to the BAU in this scenario. For example, allowing a relative phase between λ and κ would allow resonant CP-violating singlino sources arising from Eq. (5.30) which in fact would be close to resonant (see Ref.[127] for a discussion of singlino-driven EWB in the NMSSM).

Despite these issues and caveats, Fig. 5.3 suggests that resonant CP-violating higgsino-gaugino sources can be very efficient in the region of the NMSSM consistent with a 130 GeV gamma-ray line. Even if we had over-estimated the baryon asymmetry by an order of magnitude, there could still be regions consistent with both the Fermi line, the observed BAU, constraints from electric dipole moments (which we discuss below), and DM direct detection, provided more optimistic choices for the strange quark content of the proton or the local distribution of dark matter. For example, taking the values of σ_0, $\sigma_{\pi N}$ we considered for the EWPT benchmark point pushes out the allowed values of M_1 in Fig. 5.3 out to about 145 GeV, which would allow a factor of ten over-estimation of the BAU consistent with EDM constraints.

5.3.3   EDM Constraints

The NMSSM contains several possible sources of CP-violation beyond those in the MSSM: CP-violation in tree-level parameters λ, κ, and μ; CP-violation in soft-breaking terms A_λ and A_κ; and additional effects coming from the mixing between the two CP-odd eigenstates A_1 and A_2. However, in our setup we assume no CP-violation in the tree-level Higgs sector and very little mixing between A_1 and A_2 (A_1 must be mostly singlet-like, as explained above). Therefore, the electric dipole moment calculations reduce to those in the MSSM.

We use the package `CPSuperH` [71] to calculate the electric dipole moments of the electron, the neutron, and the mercury atom, which have current experimental limits of $|d_e| < 1.05 \times 10^{-27} e$ cm [67] (via the YbF molecule), $|d_n| < 2.9 \times 10^{-26} e$ cm [68], and $|d_{Hg}| < 3 \times 10^{-29} e$ cm [60]. The neutron and the Mercury atom generally provide extremely strong limits on CP-violating physics, but they are most sensitive to chromo-EDMs and CP-violation involving colored particles. We have no chromo-EDMs in this model, so the electron EDM provides, here, the strongest constraint. All one-loop EDMs are suppressed by the heavy sfermion masses. The dominant two-loop contribution comes from the Barr–Zee diagram containing a chargino loop.

For each point in the parameter space of Fig. 5.3, we calculate the EDMs using the value of ϕ that produces the proper baryon abundance. Except for ϕ, most of the parameters necessary for calculating the EDMs vary little over the plotted region, so the EDMs are most sensitive to ϕ and the corresponding iso-level curves follow

similar trajectories. The small region in the upper-left with $\sin\phi \gtrsim 0.37$ has $|d_e| > 1.05 \times 10^{-27} e$ cm, and is thus ruled out by experiment. The smallest EDM in this region, corresponding to $\sin\phi \approx \frac{1}{6}$, is $|d_e| = 5.1 \times 10^{-28}$. This is well within the anticipated sensitivity of next-generation EDM experiments (for a review, see, *e.g.*, Ref. [70]), which have the potential to either rule out or lend credence to this baryogenesis scenario.

5.4 Discussion and Summary

The present study reaffirms that the NMSSM framework (and indeed other singlet-extensions of the Higgs sector [147]) can provide a viable explanation of the 130 GeV Fermi gamma-ray line in terms of resonant neutralino annihilation through a pseudoscalar into photons. Agreement with observation and with the relevant constraints is realized in the NMSSM for a bino-like LSP (dictating that $M_1 \sim 130$ GeV), with relatively large λ, moderate μ, and with A_1 predominantly singlet-like to avoid indirect detection constraints on continuum photons. While there are many independent constraints on this scenario, currently there remains a substantial amount of parameter space consistent with the gamma-ray line and in agreement with the various dark matter and particle physics constraints.

Here we have shown that the parameter space consistent with the Fermi line in the NMSSM is also promising for electroweak baryogenesis. In particular, the relatively large values of λ typically considered tend to bolster the cubic term in the finite-temperature effective potential in the direction of electroweak symmetry break-

ing, leading to a strongly first-order electroweak phase transition in parts of the parameter space. Additionally, the moderate values of μ ensure that the singlet vev is not too far from the EW scale, again tending towards a strongly first-order transition. We illustrated this in Sec. 5.2 by providing a benchmark point consistent with the 130 GeV line and a strongly first-order EWPT, and in agreement with all other relevant phenomenological constraints. While we only studied in detail one particular point as a proof of principle, we expect a more systematic study of the NMSSM parameter space to uncover many other regions consistent with the line and a strongly first-order EWPT.

Not only does the parameter space consistent with the line support the possibility of a strongly first-order transition, it can also provide an efficient source for CP-violation that gives rise to the observed baryon-to-entropy ratio of the universe. Resonant higgsino-gaugino sources can be very efficient here due to the moderate values of $M_{1,2}$ and μ required to produce the line. In particular, allowing for a CP-violating phase in M_2 does not strongly affect the line or the dark matter phenomenology, but it can produce the observed BAU with $\sin\phi$ small enough to be consistent with electric dipole measurements, as shown in Sec. 5.3 and Fig. 5.3. While we focused on the higgsino-wino sources in the present study for the sake of illustration, similar resonant CP-violating sources arising from other interactions can be active in the same regions of parameter space by similar reasoning. For example, if one allows for M_1 to carry a complex phase, resonant bino-higgsino sources can be very efficient as well. This may be of particular interest in the case of negative μ whereby $|\mu|$ can be taken as low as 140 – 150 GeV (and thus potentially very close to this resonance) while in agreement with

direct detection constraints [128]. A careful study of the effect of a CP-violating phase in M_1 on the line and dark matter properties would be necessary to assess whether such a scenario is possible, but we expect it is since EDM measurements dictate that the CP-violating phase is necessarily small. Also, singlino-higgsino sources can in principle be efficient in this region as well, provided a relative phase between λ and κ [127], again due to the moderate values of the singlino mass (see Eq. (5.32)) and μ in this scenario. These other sources would be especially important for points such as our EWPT benchmark which features a rather heavy wino but lighter bino and singlino[14].

An interesting feature of our scenario is that the relevant parameter space will be conclusively tested in the near future by modest improvements in various experimental efforts. The moderate values of μ we consider result in rather large spin-independent neutralino-nucleon cross-sections which continue to be probed by direct detection experiments. The relatively large values of λ, as required for a large $\langle \sigma v \rangle_{\gamma\gamma}$, combined with the large A_λ and moderate values of κ necessary for a strongly first-order EWPT, tend towards a significant coupling of A_1 to e.g. $b\bar{b}$ and so will be tested by modest improvements in indirect detection experiments. Additionally, the CP-violating phase(s), required to source the left-handed charge density for the $SU(2)$ sphalerons, will be well within reach of various future EDM experiments (see e.g. Ref. [87] for a related discussion). The whole scenario will also continue to be tested by ongoing measurements of Higgs couplings and searches for other particles at the LHC.

Of course the viability of the 130 GeV line scenario in the NMSSM or any

---

[14]Note that non-resonant wino-higgsino sources, such as those considered in Refs. [44, 43, 146] can also potentially provide the necessary CP-violation for our particular EWPT benchmark point.

other SM extension hinges on the persistence of the line in the Fermi data and on a dark matter interpretation of these results. If the line is indeed due to resonant dark matter annihilation, this work shows that the NMSSM framework can potentially explain the origin of both the baryonic and dark matter in our universe.

6

Conclusion

In this dissertation, I have explored the possibility of baryogenesis at the electroweak phase transition in the context of supersymmetry, taking into account current constraints from particle physics, astrophysics, and cosmology. In particular, I have shown that:

- Electroweak baryogenesis sourced by the MSSM Higgsino-gaugino sector is tightly constrained. For resonant Higgsino-gaugino sources, dark matter direct- and indirect-detection experiments rule out large portions of the parameter space for EWB as shown in Chapter 3. This is because the CP-violating sources are strongest near the resonance, occurring for $\mu \sim M_{1,2}$ where both μ and $M_{1,2}$ must be moderately light to avoid thermal suppression. This in turn implies a significant Higgsino component in the lightest neutralino, especially if its dominant component drives the injection of the chiral current into the symmetric phase during the phase transition. Collider searches for light neutralinos and charginos also

constrain the parameter space, but not as significantly as dark matter searches. These conclusions are independent of the nature of the phase transition.

- CP-violating scalar sources for electroweak baryogenesis are also largely ruled out in the MSSM. This is because of the strong limits set by the non-observation of a permanent electric dipole moment of ^{199}Hg. The lack of superpartners found at the LHC is also telling. The one possibility remaining in the sfermion sector is a resonant stau source, since CP-violation in the slepton sector does not contribute to the chromo-EDM of mercury. The soft SUSY-breaking stau masses in this case have to be nearly degenerate as a result of the narrow thermal widths of the ($SU(3)$ singlet) staus in the plasma. With resonant stau sources it is possible to achieve a 125 GeV Higgs by appropriately tuning the MSSM stop sector, or potentially a light stop to provide a strongly first order electroweak phase transition, but likely not both. This was discussed in the latter half of Chapter 3.

- Accidental superymmetry provides a good framework for achieving electroweak baryogenesis beyond the MSSM. Previous work had suggested that the radion, which governs the separation between the branes in the Randall-Sundrum space-time, enters into the effective potential and can effectively supercool the electroweak phase transition. Chapter 4 showed that the accidental SUSY spectrum typically also provides viable candidates for CP-violating sources in the Higgsino-gaugino sector. In particular, resonant Higgsino-wino sources can be consistent with a well-tempered bino-like neutralino and be clear of all dark matter search

null results and EDM constraints. Non-resonant sources not appearing to lowest order in the Higgs VEV-insertion approximation were also considered, and the parameter space for successful EWB was outlined. These results could also apply to less exotic models without warped extra dimensions such as "split supersymmetry", since the spectra are similar, but in this case one would need another mechanism to provide a strongly first-order phase transition.

- Electroweak baryogenesis can be successfully accomplished in the NMSSM with a 125 GeV Higgs, 130 GeV gamma-ray line as seen by the Fermi space telescope, and consistent with all other phenomenological constraints. This scenario was outlined in Chapter 5 and was motivated by recent results from indirect searches for dark matter annihilating in the center of the galaxy. In this picture, higgsino-gaugino sources can once again provide a sufficient amount of CP-violation to source the chiral current in the symmetric phase, while the singlet contribution to the effective potential can supply a strongly first order electroweak phase transition without requiring a light stop. If the dark matter signal from the center of the galaxy is confirmed, then this scenario would arguably be one of the most plausible candidates for generating the observed baryon asymmetry at the electroweak phase transition in our universe.

As the exploration of the electroweak scale moves forward, the picture I have outlined here will inevitably change. However, if electroweak baryogenesis is in fact responsible for the baryon asymmetry we observe today and if supersymmetry is realized

in nature, the ideas presented here may fill in a piece of the puzzle explaining why the universe is not empty, and why we are able to sit here and mull over these questions in the first place.

Bibliography

[1] J. Kozaczuk and A. Aguirre, Phys. Rev. D **87**, 023506 (2013) [arXiv:1206.5038 [hep-th]].

[2] A. Silbergleit, J. Conklin, D. DeBra, M. Dolphin, G. Keiser, J. Kozaczuk, D. Santiago and M. Salomon *et al.*, Space Sci. Rev. **148**, 397 (2009).

[3] M. Salomon, J. W. Conklin, J. Kozaczuk, J. E. Berberian, D. I. Santiago, G. M. Keiser, A. S. Silbergleit and P. Worden, Rev. Sci. Instrum. **82**, 125110 (2011) [arXiv:1111.4521 [physics.ins-det]].

[4] E. Komatsu *et al.* [WMAP Collaboration], Astrophys. J. Suppl. **192**, 18 (2011) [arXiv:1001.4538 [astro-ph.CO]].

[5] J. M. Cline, hep-ph/0609145.

[6] S. Davidson, E. Nardi and Y. Nir, Phys. Rept. **466**, 105 (2008) [arXiv:0802.2962 [hep-ph]].

[7] A. D. Sakharov, Pisma Zh. Eksp. Teor. Fiz. **5**, 32 (1967) [JETP Lett. **5**, 24 (1967)] [Sov. Phys. Usp. **34**, 392 (1991)] [Usp. Fiz. Nauk **161**, 61 (1991)].

[8] A. G. Cohen, D. B. Kaplan and A. E. Nelson, Ann. Rev. Nucl. Part. Sci. **43**, 27 (1993) [hep-ph/9302210].

[9] K. Funakubo, Prog. Theor. Phys. **96**, 475 (1996) [hep-ph/9608358].

[10] D. E. Morrissey and M. J. Ramsey-Musolf, arXiv:1206.2942 [hep-ph].

[11] A. E. Nelson, D. B. Kaplan and A. G. Cohen, Nucl. Phys. B **373**, 453 (1992).

[12] C. Jarlskog, Phys. Rev. Lett. **55**, 1039 (1985).

[13] G. W. Anderson and L. J. Hall, Phys. Rev. D **45**, 2685 (1992).

[14] S. Chatrchyan *et al.* [CMS Collaboration], Phys. Lett. B **716**, 30 (2012) [arXiv:1207.7235 [hep-ex]].

[15] G. Aad *et al.* [ATLAS Collaboration], Phys. Lett. B **716**, 1 (2012) [arXiv:1207.7214 [hep-ex]].

[16] S. P. Martin, In *Kane, G.L. (ed.): Perspectives on supersymmetry II* 1-153 [hep-ph/9709356].

[17] M. Dine. *Supersymmetry and String Theory*. Cambridge University Press, 2007. Cambridge Books Online. http://dx.doi.org/10.1017/CBO9780511618482

[18] M. S. Carena, M. Quiros and C. E. M. Wagner, Phys. Lett. B **380**, 81 (1996) [hep-ph/9603420].

[19] M. Carena, G. Nardini, M. Quiros, C. E. M. Wagner, Nucl. Phys. **B812**, 243-263 (2009). [arXiv:0809.3760 [hep-ph]].

[20] M. Carena, G. Nardini, M. Quiros and C. E. M. Wagner, JHEP **1302**, 001 (2013) [arXiv:1207.6330 [hep-ph]].

[21] D. J. H. Chung, B. Garbrecht, M. J. Ramsey-Musolf and S. Tulin, Phys. Rev. D **81**, 063506 (2010) [arXiv:0905.4509 [hep-ph]].

[22] D. J. H. Chung, B. Garbrecht, M. .J. Ramsey-Musolf and S. Tulin, JHEP **0912**, 067 (2009) [arXiv:0908.2187 [hep-ph]].

[23] C. Lee, V. Cirigliano and M. J. Ramsey-Musolf, Phys. Rev. D **71**, 075010 (2005) [arXiv:hep-ph/0412354].

[24] D. J. H. Chung, B. Garbrecht, M. J. Ramsey-Musolf, S. Tulin, Phys. Rev. Lett. **102**, 061301 (2009). [arXiv:0808.1144 [hep-ph]].

[25] V. Cirigliano, M. J. Ramsey-Musolf, S. Tulin and C. Lee, Phys. Rev. D **73**, 115009 (2006) [arXiv:hep-ph/0603058].

[26] V. Cirigliano, C. Lee and S. Tulin, Phys. Rev. D **84**, 056006 (2011) [arXiv:1106.0747 [hep-ph]].

[27] P. Huet, A. E. Nelson, Phys. Rev. **D53**, 4578-4597 (1996). [hep-ph/9506477].

[28] V. Cirigliano, Y. Li, S. Profumo and M. J. Ramsey-Musolf, JHEP **1001**, 002 (2010) [arXiv:0910.4589 [hep-ph]].

[29] C. Amsler *et al.* [Particle Data Group], Phys. Lett. B **667**, 1 (2008).

[30] V. Cirigliano, S. Profumo and M. J. Ramsey-Musolf, JHEP **0607**, 002 (2006) [arXiv:hep-ph/0603246].

[31] H. Baer, M. A. Diaz, P. Quintana and X. Tata, JHEP **0004**, 016 (2000) [arXiv:hep-ph/0002245].

[32] A. Riotto, Phys. Rev. D **58**, 095009 (1998) [arXiv:hep-ph/9803357].

[33] C. Balazs, M. S. Carena, A. Menon, D. E. Morrissey, C. E. M. Wagner, Phys. Rev. **D71**, 075002 (2005). [hep-ph/0412264].

[34] M. Laine and K. Rummukainen, Nucl. Phys. B **535**, 423 (1998) [arXiv:hep-lat/9804019].

[35] M. Laine, arXiv:hep-ph/0010275.

[36] M. Carena, G. Nardini, M. Quiros, C. E. M. Wagner, JHEP **0810**, 062 (2008). [arXiv:0806.4297 [hep-ph]].

[37] See e.g. R. Fok and G. D. Kribs, Phys. Rev. D **78**, 075023 (2008) [arXiv:0803.4207 [hep-ph]]. and references therein; J. Shu, T. M. P. Tait and C. E. M. Wagner, Phys. Rev. D **75**, 063510 (2007) [arXiv:hep-ph/0610375]. and references therein; P. Fileviez Perez, T. Han, G. y. Huang, T. Li and K. Wang, Phys. Rev. D **78**, 015018 (2008) [arXiv:0805.3536 [hep-ph]].

[38] S. Profumo, M. J. Ramsey-Musolf, G. Shaughnessy, JHEP **0708**, 010 (2007). [arXiv:0705.2425 [hep-ph]].

[39] A. De Simone, G. Nardini, M. Quiros and A. Riotto, arXiv:1107.4317 [hep-ph].

[40] G. F. Giudice, M. E. Shaposhnikov, Phys. Lett. **B326**, 118-124 (1994). [hep-ph/9311367].

[41] S. J. Huber, P. John, M. G. Schmidt, Eur. Phys. J. **C20**, 695-711 (2001). [hep-ph/0101249].

[42] E. Carmona [ANTARES Collaboration], Nucl. Phys. Proc. Suppl. **95**, 161 (2001). M. S. Carena, M. Quiros and C. E. M. Wagner, Nucl. Phys. B **524**, 3 (1998) [arXiv:hep-ph/9710401]. J. M. Cline, M. Joyce and K. Kainulainen, Phys. Lett. B **417**, 79 (1998) [Erratum-ibid. B **448**, 321 (1999)] [arXiv:hep-ph/9708393].

[43] M. S. Carena, M. Quiros, M. Seco, C. E. M. Wagner, Nucl. Phys. **B650**, 24-42 (2003). [hep-ph/0208043].

[44] M. S. Carena, J. M. Moreno, M. Quiros, M. Seco and C. E. M. Wagner, Nucl. Phys. B **599**, 158 (2001) [arXiv:hep-ph/0011055].

[45] G. D. Moore, JHEP **0003**, 006 (2000) [arXiv:hep-ph/0001274]. P. John and M. G. Schmidt, Nucl. Phys. B **598**, 291 (2001) [Erratum-ibid. B **648**, 449 (2003)] [arXiv:hep-ph/0002050]. P. John and M. G. Schmidt, arXiv:hep-ph/0012077. A. Megevand and A. D. Sanchez, Nucl. Phys. B **825**, 151 (2010) [arXiv:0908.3663 [hep-ph]].

[46] J. M. Cline and K. Kainulainen, Phys. Rev. Lett. **85**, 5519 (2000) [arXiv:hep-ph/0002272].

[47] J. M. Moreno, M. Quiros and M. Seco, Nucl. Phys. B **526**, 489 (1998) [arXiv:hep-ph/9801272].

[48] Y. Li, S. Profumo, M. Ramsey-Musolf, Phys. Lett. **B673**, 95-100 (2009). [arXiv:0811.1987 [hep-ph]].

[49] S. Bornhauser, M. Drees, S. Grab, J. S. Kim, Phys. Rev. **D83**, 035008 (2011). [arXiv:1011.5508 [hep-ph]].

[50] E. Aprile *et al.* [XENON100 Collaboration], [arXiv:1104.2549 [astro-ph.CO]].

[51] E. Aprile, private communication.

[52] A. M. Brown and o. b. o. Collaboration, arXiv:1012.1633 [astro-ph.HE]; R. Abbasi *et al.* [ICECUBE Collaboration], Phys. Rev. Lett. **102**, 201302 (2009). [arXiv:0902.2460 [astro-ph.CO]].

[53] A. A. Abdo, M. Ackermann, M. Ajello, W. B. Atwood, L. Baldini, J. Ballet, G. Barbiellini, D. Bastieri *et al.*, Astrophys. J. **712**, 147-158 (2010). [arXiv:1001.4531 [astro-ph.CO]].

[54] A. Pomarol, R. Rattazzi, JHEP **9905**, 013 (1999). [hep-ph/9903448]; J. L. Feng, T. Moroi, Phys. Rev. **D61**, 095004 (2000). [hep-ph/9907319]; T. Moroi, L. Randall, Nucl. Phys. **B570**, 455-472 (2000). [hep-ph/9906527].

[55] S. Profumo, P. Ullio, JCAP **0311**, 006 (2003). [hep-ph/0309220].

[56] W. Beenakker, M. Klasen, M. Kramer, T. Plehn, M. Spira and P. M. Zerwas,

Phys. Rev. Lett. **83**, 3780 (1999) [Erratum-ibid. **100**, 029901 (2008)] [arXiv:hep-ph/9906298].

[57] H. Baer, T. Krupovnickas, S. Profumo, P. Ullio, JHEP **0510**, 020 (2005). [hep-ph/0507282].

[58] H. Baer, C. h. Chen, F. Paige and X. Tata, Phys. Rev. D **50** (1994) 4508 [arXiv:hep-ph/9404212].

[59] M. Carena, S. Gori, N. R. Shah and C. E. M. Wagner, arXiv:1112.3336 [hep-ph].

[60] W. C. Griffith, M. D. Swallows, T. H. Loftus, M. V. Romalis, B. R. Heckel and E. N. Fortson, Phys. Rev. Lett. **102**, 101601 (2009).

[61] M. Pietroni, Nucl. Phys. B **402**, 27 (1993) [hep-ph/9207227].

[62] K. Nakamura *et. al* (Particle Data Group) J. Phys. G **37**, 075021 (2010)

[63] M. Frank, T. Hahn, S. Heinemeyer, W. Hollik, H. Rzehak and G. Weiglein, JHEP **0702**, 047 (2007) [hep-ph/0611326]. G. Degrassi, S. Heinemeyer, W. Hollik, P. Slavich and G. Weiglein, Eur. Phys. J. C **28**, 133 (2003) [hep-ph/0212020]. S. Heinemeyer, W. Hollik and G. Weiglein, Eur. Phys. J. C **9**, 343 (1999) [hep-ph/9812472]. S. Heinemeyer, W. Hollik and G. Weiglein, Comput. Phys. Commun. **124**, 76 (2000) [hep-ph/9812320].

[64] S. Schael *et al.* [ALEPH and DELPHI and L3 and OPAL and LEP Working Group for Higgs Boson Searches Collaborations], Eur. Phys. J. C **47**, 547 (2006) [hep-ex/0602042].

[65] G. Aad *et al.* [ATLAS Collaboration], Phys. Lett. B **710**, 49 (2012) [arXiv:1202.1408 [hep-ex]].

[66] [ATLAS Collaboration], arXiv:1202.1408 [hep-ex]; [ATLAS Collaboration], arXiv:1202.1414 [hep-ex]; [ATLAS Collaboration], arXiv:1202.1415 [hep-ex]; S. Chatrchyan *et al.* [CMS Collaboration], arXiv:1202.1487 [hep-ex]; S. Chatrchyan *et al.* [CMS Collaboration], arXiv:1202.1416 [hep-ex]; S. Chatrchyan *et al.* [CMS Collaboration], arXiv:1202.1488 [hep-ex].

[67] J. J. Hudson, D. M. Kara, I. J. Smallman, B. E. Sauer, M. R. Tarbutt and E. A. Hinds, Nature **473**, 493 (2011).

[68] C. A. Baker, D. D. Doyle, P. Geltenbort, K. Green, M. G. D. van der Grinten, P. G. Harris, P. Iaydjiev and S. N. Ivanov *et al.*, Phys. Rev. Lett. **97**, 131801 (2006) [hep-ex/0602020].

[69] Y. Li, S. Profumo and M. Ramsey-Musolf, Phys. Rev. D **78**, 075009 (2008) [arXiv:0806.2693 [hep-ph]].

[70] J. L. Hewett, H. Weerts, R. Brock, J. N. Butler, B. C. K. Casey, J. Collar, A. de Govea and R. Essig *et al.*, arXiv:1205.2671 [hep-ex].

[71] J. R. Ellis, J. S. Lee and A. Pilaftsis, JHEP **0810**, 049 (2008) [arXiv:0808.1819 [hep-ph]].

[72] M. Pospelov and A. Ritz, Annals Phys. **318**, 119 (2005) [hep-ph/0504231].

[73] J. Hisano, J. Y. Lee, N. Nagata and Y. Shimizu, arXiv:1204.2653 [hep-ph].

[74] S. Ban, J. Dobaczewski, J. Engel and A. Shukla, Phys. Rev. C **82**, 015501 (2010) [arXiv:1003.2598 [nucl-th]].

[75] D. Curtin, P. Jaiswal and P. Meade, arXiv:1203.2932 [hep-ph].

[76] L. Randall and R. Sundrum, Phys. Rev. Lett. **83**, 3370 (1999) [hep-ph/9905221].

[77] T. Gherghetta and A. Pomarol, Nucl. Phys. B **586**, 141 (2000) [hep-ph/0003129].

[78] K. Agashe, G. Perez and A. Soni, Phys. Rev. D **71**, 016002 (2005) [hep-ph/0408134].

[79] T. Gherghetta and A. Pomarol, Phys. Rev. D **67**, 085018 (2003) [hep-ph/0302001].

[80] R. Sundrum, JHEP **1101**, 062 (2011) [arXiv:0909.5430 [hep-th]].

[81] T. Gherghetta, B. von Harling and N. Setzer, JHEP **1107**, 011 (2011) [arXiv:1104.3171 [hep-ph]].

[82] G. Nardini, M. Quiros and A. Wulzer, JHEP **0709**, 077 (2007) [arXiv:0706.3388 [hep-ph]].

[83] P. Creminelli, A. Nicolis and R. Rattazzi, JHEP **0203**, 051 (2002) [hep-th/0107141].

[84] L. Randall and G. Servant, JHEP **0705**, 054 (2007) [hep-ph/0607158].

[85] J. Kaplan, P. C. Schuster and N. Toro, hep-ph/0609012.

[86] W. D. Goldberger and M. B. Wise, Phys. Rev. Lett. **83**, 4922 (1999) [hep-ph/9907447].

[87] J. Kozaczuk, S. Profumo, M. J. Ramsey-Musolf and C. L. Wainwright, Phys. Rev. D **86**, 096001 (2012) [arXiv:1206.4100 [hep-ph]].

[88] T. Konstandin, T. Prokopec and M. G. Schmidt, Nucl. Phys. B **679**, 246 (2004) [arXiv:hep-ph/0309291].

[89] T. Konstandin, T. Prokopec, M. G. Schmidt, Nucl. Phys. **B716**, 373-400 (2005). [hep-ph/0410135].

[90] J. Kozaczuk and S. Profumo, JCAP **1111**, 031 (2011) [arXiv:1108.0393 [hep-ph]].

[91] A. Menon, D. E. Morrissey and C. E. M. Wagner, Phys. Rev. D **70**, 035005 (2004) [hep-ph/0404184].

[92] S. J. Huber, T. Konstandin, T. Prokopec and M. G. Schmidt, Nucl. Phys. B **757**, 172 (2006) [hep-ph/0606298].

[93] N. Arkani-Hamed, A. Delgado and G. F. Giudice, Nucl. Phys. B **741**, 108 (2006) [hep-ph/0601041].

[94] N. Arkani-Hamed and S. Dimopoulos, JHEP **0506**, 073 (2005) [hep-th/0405159].; G. F. Giudice and A. Romanino, Nucl. Phys. B **699**, 65 (2004) [Erratum-ibid. B **706**, 65 (2005)] [hep-ph/0406088]. N. Arkani-Hamed, S. Dimopoulos, G. F. Giudice and A. Romanino, Nucl. Phys. B **709**, 3 (2005) [hep-ph/0409232].

[95] J. A. Casas, J. R. Espinosa and I. Navarro, Nucl. Phys. B **620**, 195 (2002) [hep-ph/0109127].

[96] H. -S. Goh, M. A. Luty and S. -P. Ng, JHEP **0501**, 040 (2005) [hep-th/0309103].

[97] M. Chaichian, A. Datta, K. Huitu and Z. -h. Yu, Phys. Lett. B **524**, 161 (2002) [hep-ph/0110035]; V. Barger, M. Ishida and W. -Y. Keung, Phys. Rev. Lett. **108**, 101802 (2012) [arXiv:1111.4473 [hep-ph]]; H. de Sandes and R. Rosenfeld, Phys. Rev. D **85**, 053003 (2012) [arXiv:1111.2006 [hep-ph]]; B. Grzadkowski, J. F. Gunion and M. Toharia, Phys. Lett. B **712**, 70 (2012) [arXiv:1202.5017 [hep-ph]].

[98] A. Djouadi, Phys. Rept. **459**, 1 (2008) [hep-ph/0503173].

[99] J. L. Feng, K. T. Matchev and F. Wilczek, Phys. Lett. B **482**, 388 (2000) [hep-ph/0004043].

[100] H. Baer, A. Mustafayev, S. Profumo, A. Belyaev and X. Tata, JHEP **0507**, 065 (2005) [hep-ph/0504001].

[101] G. F. Giudice and A. Romanino, Nucl. Phys. B **699**, 65 (2004) [Erratum-ibid. B **706**, 65 (2005)] [hep-ph/0406088].

[102] A. Pierce, Phys. Rev. D **70**, 075006 (2004) [hep-ph/0406144].

[103] A. Masiero, S. Profumo and P. Ullio, Nucl. Phys. B **712**, 86 (2005) [hep-ph/0412058].

[104] H. Baer, A. Mustafayev, E. -K. Park and S. Profumo, JHEP **0507**, 046 (2005) [hep-ph/0505227]; H. Baer, T. Krupovnickas, A. Mustafayev, E. -K. Park, S. Profumo and X. Tata, JHEP **0512**, 011 (2005) [hep-ph/0511034].

[105] A. Birkedal-Hansen and B. D. Nelson, Phys. Rev. D **64**, 015008 (2001) [hep-ph/0102075]; A. Birkedal-Hansen and B. D. Nelson, Phys. Rev. D **67** (2003) 095006 [hep-ph/0211071].

[106] P. Gondolo, J. Edsjo, P. Ullio, L. Bergstrom, M. Schelke and E. A. Baltz, JCAP **0407**, 008 (2004) [astro-ph/0406204].

[107] G. D. Moore, Phys. Lett. B **412**, 359 (1997) [hep-ph/9705248].

[108] W. D. Goldberger and M. B. Wise, Phys. Lett. B **475**, 275 (2000) [hep-ph/9911457].

[109] C. Csaki, M. Graesser, L. Randall and J. Terning, Phys. Rev. D **62**, 045015 (2000) [hep-ph/9911406].

[110] M. S. Carena, M. Quiros, A. Riotto, I. Vilja and C. E. M. Wagner, Nucl. Phys. B **503**, 387 (1997) [hep-ph/9702409].

[111] Y. Li, S. Profumo and M. Ramsey-Musolf, JHEP **1008**, 062 (2010) [arXiv:1006.1440 [hep-ph]].

[112] S. M. Barr and A. Zee, Phys. Rev. Lett. **65**, 21 (1990) [Erratum-ibid. **65**, 2920 (1990)].

[113] E. April *et al.* [XENON100 Collaboration], arXiv:1207.5988 [astro-ph.CO].

[114] E. Aprile *et al.* [XENON100 Collaboration], [arXiv:1104.2549 [astro-ph.CO]].

[115] J. Gasser, H. Leutwyler and M. E. Sainio, Phys. Lett. B **253**, 252 (1991).

[116] M. Ackermann *et al.* [Fermi-LAT Collaboration], Phys. Rev. Lett. **107**, 241302 (2011) [arXiv:1108.3546 [astro-ph.HE]].

[117] M. Ackermann *et al.* [Fermi-LAT Collaboration], Phys. Rev. Lett. **107**, 241302 (2011) [arXiv:1108.3546 [astro-ph.HE]].

[118] A. A. Abdo, M. Ackermann, M. Ajello, W. B. Atwood, L. Baldini, J. Ballet, G. Barbiellini and D. Bastieri *et al.*, Phys. Rev. Lett. **104**, 091302 (2010) [arXiv:1001.4836 [astro-ph.HE]].

[119] `http://fermi.gsfc.nasa.gov/science/mtgs/symposia/2012/program/fri/AAlbert.pdf`

[120] C. Weniger, JCAP **1208**, 007 (2012) [arXiv:1204.2797 [hep-ph]].

[121] T. Bringmann, X. Huang, A. Ibarra, S. Vogl and C. Weniger, JCAP **1207**, 054 (2012) [arXiv:1203.1312 [hep-ph]].

[122] M. Su and D. P. Finkbeiner, arXiv:1206.1616 [astro-ph.HE].

[123] D. P. Finkbeiner, M. Su and C. Weniger, JCAP **1301**, 029 (2013) [arXiv:1209.4562 [astro-ph.HE]].

[124] L. Bergstrom and P. Ullio, Nucl. Phys. B **504**, 27 (1997) [hep-ph/9706232].

[125] D. Das, U. Ellwanger and P. Mitropoulos, JCAP **1208**, 003 (2012) [arXiv:1206.2639 [hep-ph]].

[126] K. Funakubo, S. Tao and F. Toyoda, Prog. Theor. Phys. **114**, 369 (2005) [hep-ph/0501052].

[127] K. Cheung, T. -J. Hou, J. S. Lee and E. Senaha, Phys. Lett. B **710**, 188 (2012) [arXiv:1201.3781 [hep-ph]].

[128] G. Chalons, M. J. Dolan and C. McCabe, arXiv:1211.5154 [hep-ph].

[129] U. Ellwanger, J. F. Gunion and C. Hugonie, JHEP **0502**, 066 (2005) [hep-ph/0406215].

[130] R. Harnik, G. D. Kribs, D. T. Larson and H. Murayama, Phys. Rev. D **70**, 015002 (2004) [hep-ph/0311349].

[131] E. Hardy, J. March-Russell and J. Unwin, JHEP **1210**, 072 (2012) [arXiv:1207.1435 [hep-ph]].

[132] U. Ellwanger, J. F. Gunion and C. Hugonie, JHEP **0502**, 066 (2005) [hep-ph/0406215]; U. Ellwanger and C. Hugonie, Comput. Phys. Commun. **175**, 290 (2006) [hep-ph/0508022]

[133] G. Belanger, F. Boudjema, C. Hugonie, A. Pukhov and A. Semenov, JCAP **0509**, 001 (2005) [hep-ph/0505142]; G. Belanger, F. Boudjema, P. Brun, A. Pukhov, S. Rosier-Lees, P. Salati and A. Semenov, Comput. Phys. Commun. **182**, 842 (2011) [arXiv:1004.1092 [hep-ph]].

[134] M. Ackermann *et al.* [LAT Collaboration], Phys. Rev. D **86**, 022002 (2012) [arXiv:1205.2739 [astro-ph.HE]].

[135] T. Cohen, M. Lisanti, T. R. Slatyer and J. G. Wacker, JHEP **1210**, 134 (2012) [arXiv:1207.0800 [hep-ph]].

[136] M. Carena, S. Gori, N. R. Shah, C. E. M. Wagner and L. -T. Wang, JHEP **1207**, 175 (2012) [arXiv:1205.5842 [hep-ph]].

[137] A. W. Thomas, P. E. Shanahan and R. D. Young, Nuovo Cim. C **035N04**, 3 (2012) [arXiv:1202.6407 [nucl-th]].

[138] H. H. Patel and M. J. Ramsey-Musolf, JHEP **1107**, 029 (2011) [arXiv:1101.4665 [hep-ph]].

[139] C. L. Wainwright, S. Profumo and M. J. Ramsey-Musolf, Phys. Rev. D **86**, 083537 (2012) [arXiv:1204.5464 [hep-ph]].

[140] C. Balazs, M. S. Carena and C. E. M. Wagner, Phys. Rev. D **70**, 015007 (2004) [hep-ph/0403224].

[141] C. Wainwright, S. Profumo and M. J. Ramsey-Musolf, Phys. Rev. D **84**, 023521 (2011) [arXiv:1104.5487 [hep-ph]].

[142] M. Garny and T. Konstandin, JHEP **1207**, 189 (2012) [arXiv:1205.3392 [hep-ph]].

[143] D. J. Gross, L. G. Yaffe, Rev. Mod. Phys. **53**, 43 (1981).

[144] R. Parwani, Phys. Rev. D **45**, 4695 (1992).

[145] C. L. Wainwright, Comput. Phys. Commun. **183**, 2006 (2012) [arXiv:1109.4189 [hep-ph]].

[146] J. Kozaczuk, S. Profumo and C. L. Wainwright, JCAP **1301**, 027 (2013) [arXiv:1208.5166 [hep-ph]].

[147] K. Schmidt-Hoberg, F. Staub and M. W. Winkler, JHEP **1301**, 124 (2013) [arXiv:1211.2835 [hep-ph]].